

**Rheological Modification of Polypropylene by  
Incorporation of Long Chain Branches Using UV  
Radiation**

by

Yasaman Amintowlieh

A thesis

presented to the University of Waterloo

in fulfillment of the

thesis requirement for the degree of

Doctor of philosophy

in

Chemical Engineering

Waterloo, Ontario, Canada, 2014

©Yasaman Amintowlieh 2014

## **AUTHOR'S DECLARATION**

I hereby declare that I am the sole author of this thesis. This is a true copy of the thesis, including any required final revisions, as accepted by my examiners.

I understand that my thesis may be made electronically available to the public.

## Abstract

Modification of polypropylene (PP) is important as it aims at changing the molecular structure of PP and synthesizing different grades of PP for different processing applications. These changes include narrowing of the PP's molecular weight distribution (MWD) by degradation via  $\beta$ -scission (controlled rheology PP) or formation of long chain branches (LCBs) in the PP backbone (via the formation of macroradicals). However,  $\beta$ -scission should be controlled to prevent severe degradation in the polymer. In addition to  $\beta$ -scission reactions, bimolecular chain combination reactions are necessary to form long chain branched PP (LCBPP). Thus, by adjusting reaction conditions, PP with different molecular structures can be generated.

In order to initiate any PP modification reaction, PP macroradicals should be formed first by abstracting hydrogens from the PP backbone. In this thesis, UV radiation was used along with photoinitiator (hence, UV photomodification) to abstract hydrogens from PP backbones and initiate their modification. The reaction was conducted in the solid state. It was found that the final PP molecular structure is affected by photoinitiator concentration, radiation time, UV lamp intensity, radiation temperature and type of photoinitiator used. Combinations of these variables that result in LCBPP with improved melt strength were identified.

In order to characterize the molecular structure of PP, rheological measurements were found to be versatile and reliable tools. Rheological techniques, along with GPC and gel content determination, were utilized in this thesis to characterize the molecular properties of the samples. Number of long chain branches (LCBs), crosslinked structures and strain hardening behavior of LCBPP and degraded PP were compared using these techniques.

After detailed analysis of the effects of different radiation variables on PP modification, high benzophenone (BPH) concentration and low lamp intensity were found to be necessary to form LCBs in PP in the solid state. It was also found that more than 5 min radiation time is required to form LCBPP rather than degraded PP, when the thickness of the samples is 1 mm.

One of the drawbacks in using UV radiation in polymer modification is its limited penetration depth. In order to investigate the effect of UV penetration depth along with UV radiation time, discs with thickness of 1, 2 and 3 mm were radiated for 5, 10 and 15 minutes. It was shown in this thesis that as sample thickness decreased and/or radiation time increased, more LCBs were formed. The limited UV penetration depth in PP solid samples was found to be below 1 mm.

Long radiation time (above 5 min), which is necessary to form LCBPP decreases the potential of this technique for commercialization. Thus, an attempt was made to decrease the required radiation time by using a coagent. Trimethylolpropane triacrylate (TMPTA) is a trifunctional acrylic monomer, which was used as a coagent to reduce degradation by stabilizing the radical center. The effects of coagent concentration, BPH concentration and radiation time on formation of LCBs were studied via rheological measurements and relaxation spectra analysis. Formation of LCBs in the runs was also confirmed by GPC. It was found that an increase in coagent concentration, BPH concentration and radiation time, led to formation of more branches; however, gel content of the samples also increased. Low gel content is required for certain applications, such as packaging; thus, it is important to optimize the conditions to minimize crosslinking in PP. Conditions that result in maximum long chain branching (LCB) in PP while gel content of the runs remained relatively low were found using a central composite design of experiments. Mechanisms were suggested to explain formation of LCBs or crosslinked structures under different processing conditions.

Finally, in order to assist in the commercialization and scale up of the PP photomodification, a method was developed to continuously radiate PP. The modification was carried out on the solidified strand after extrusion from a twin screw extruder. The strand was stretched and folded several times over two parallel rollers. UV radiation was carried out on stretched strands between rollers and radiated PP strands were then collected on a winder. Continuous photomodification was carried out both with and without coagent. By manipulating BPH concentration and radiation time, LCBPP was successfully produced both with and without coagent. In the continuous photomodification of PP, the radiation

time required for formation of LCBPP was significantly lower than in batch reactions due to low thickness of the strands. Moreover, post-extrusion stretching of the strands limits chain mobility and restricts  $\beta$ -scission reactions.

In general, the results obtained in this thesis show that UV radiation can easily be used to modify PP and form different PP grades, ranging from controlled rheology to long chain branched and crosslinked PP.

## Acknowledgements

I would like to express my deep and sincere gratitude to my co-supervisor, Professor Alexander Penlidis, whose critical opinions and feedback I appreciated throughout my work. During the past 4 years, I benefited from his guidance and mentorship as well as friendship. His influence in my life will go beyond my academic experience. I learned a lot from you, I sincerely thank you.

I truly appreciate the help, guidance and insight of my other co-supervisor, Professor Costas Tzoganakis. I have always admired his in-depth knowledge of polymer science and processing. Being able to work under his supervision and learn from him was one of the main reasons that kept me at the University of Waterloo for my PhD studies.

I would like to thank Profs Marianna Kontopoulou (my external, Queen's University ON), and Marianna Polak, Xianshe Feng and Boxin Zhao (my Waterloo PhD committee members), for providing useful comments that made the discussions in my thesis more accurate, and Dr. Guangjian He for all his help with this project.

I would like to thank all in the Chemical Engineering department at the University of Waterloo, especially Bert Habicher, for his technical help.

Many thanks to my friends and colleagues at the University of Waterloo for discussions we have had regarding different projects and for being such amazing and patient colleagues. This list includes (but is not limited to) Dr. Pouyan Sardashti, Dr. Hadi Izadi, Dr. Prashant Mutyala, Shouliang Nie and Alison Scott. In particular, I would like to acknowledge Dr. Shuihan Zhu for being so generous with his vast knowledge and for all training and useful discussions.

During my studies at UW, I have been fortunate to have very dear friends, roommates and neighbors; you enriched my life. I would like to especially thank Sara Ahmadian and Siavash Rahbar for gym sessions (only few!) and friendship (all the time!), and Sayeh Rajabi for our very productive Saturday discussions. I would like to thank Dr. Nima Rezaei, for educating me on Matlab simulations as well as being such an amazing friend.

Finally, I would like to thank my family for their kind support; the list includes Nahid, Vali, Ava, Aida, Simon, Charlie and dear Parya. Most importantly, I would like to thank Iman for being so kind, patient and supportive; I cannot thank you enough. Last but not least, I would like to thank my parents and my dear brother for all their love and support throughout my life.

To Monir Maleki, my very dear mother

# Table of Contents

LIST OF TABLES.....	XI
LIST OF FIGURES.....	XII
COMMON ABBREVIATIONS.....	XIV
<b>1 CHAPTER 1: MOTIVATION, OBJECTIVES AND THESIS OUTLINE .....</b>	<b>1</b>
1.1 MOTIVATION.....	1
1.2 OBJECTIVES.....	2
1.3 THESIS OUTLINE .....	3
<b>2 CHAPTER 2: OVERVIEW OF DIFFERENT METHODS FOR PP MELT STRENGTH MODIFICATION.....</b>	<b>5</b>
2.1 SYNTHESIS OF LONG CHAIN BRANCHED PP (LCBPP).....	6
2.2 POST-REACTOR MODIFICATION: CHEMICAL METHODS .....	7
2.2.1 <i>Decreasing MW of PP via peroxides</i> .....	7
2.2.2 <i>Increasing PP melt strength via peroxides</i> .....	8
2.2.3 <i>Utilizing supercritical fluid (SCF) for polypropylene modification</i> .....	11
2.3 POST-REACTOR MODIFICATION: RADIATION TECHNIQUES.....	12
2.3.1 <i>Electron beam radiation (EB)</i> .....	12
2.3.2 <i>Gamma ray radiation</i> .....	14
2.3.3 <i>UV radiation: photoinitiation reactions</i> .....	14
2.4 PHOTOMODIFICATION MECHANISMS .....	15
2.5 CONCLUDING REMARKS .....	18
<b>3 CHAPTER 3: CHARACTERIZATION OF LONG CHAIN BRANCHED PP (LCBPP).....</b>	<b>20</b>
3.1 RHEOMETRY.....	20
3.1.1 <i>Shear rheometry</i> .....	20
3.1.1 <i>Extensional rheometry</i> .....	27
3.2 GEL PERMEATION CHROMATOGRAPHY (GPC) .....	30
3.3 NUCLEAR MAGNETIC RESONANCE (NMR) .....	32
3.4 ELECTRON SPIN RESONANCE (ESR) .....	33
3.5 CONCLUDING REMARKS .....	34
<b>4 CHAPTER 4: DETERMINATION OF EFFECTS OF DIFFERENT PROCESSING VARIABLES IN PP PHOTOMODIFICATION .....</b>	<b>35</b>
4.1 INTRODUCTION .....	35
4.2 EXPERIMENTAL .....	38
4.2.1 <i>Design of experiments</i> .....	38
4.2.2 <i>Materials and sample preparation</i> .....	41
4.2.3 <i>Characterization</i> .....	41
4.3 RESULTS AND DISCUSSION .....	46
4.3.1 <i>Statistical analysis of LVE properties</i> .....	46
4.3.1 <i>Optimization of processing conditions for formation of LCBPP</i> .....	53
4.3.2 <i>LVE graphs of selected runs</i> .....	55

4.3.3	<i>Extensional rheometry</i> .....	59
4.3.4	<i>Gel content</i> .....	63
4.3.5	<i>GPC results</i> .....	64
4.3.6	<i>Differential scanning calorimetry (DSC)</i> .....	69
4.4	CONCLUDING REMARKS .....	70
<b>5</b>	<b>CHAPTER 5: EFFECT OF RADIATION TIME AND SAMPLE THICKNESS ON PHOTOMODIFICATION</b>	
	<b>REACTIONS</b> .....	<b>72</b>
5.1	INTRODUCTION .....	72
5.2	MATERIALS AND METHODS .....	74
5.2.1	<i>Materials</i> .....	74
5.2.2	<i>Design of experiments</i> .....	74
5.2.3	<i>Preparation method</i> .....	75
5.2.4	<i>Characterization</i> .....	75
5.3	RESULTS AND DISCUSSION .....	76
5.3.1	<i>Effect of radiation time and sample thickness on LVE properties</i> .....	79
5.3.2	<i>Effect on molecular weight and molecular weight distribution</i> .....	91
5.3.3	<i>Effect on gel content</i> .....	96
5.4	CONCLUDING REMARKS .....	99
<b>6</b>	<b>CHAPTER 6: COMBINATION OF COAGENT EFFECT AND PHOTOMODIFICATION</b> .....	<b>101</b>
6.1	INTRODUCTION .....	101
6.2	EXPERIMENTAL .....	104
6.2.1	<i>Materials</i> .....	104
6.2.2	<i>Design of experiments</i> .....	105
6.2.3	<i>Preparation method</i> .....	106
6.2.4	<i>Characterization</i> .....	106
6.3	RESULTS AND DISCUSSION .....	108
6.3.1	<i>Information from the viscoelastic measurements</i> .....	108
6.3.2	<i>Information from the relaxation spectrum</i> .....	112
6.3.3	<i>Information from the molecular weight distribution</i> .....	116
6.4	INFORMATION FROM FTIR SPECTROSCOPY .....	126
6.5	CONCLUDING REMARKS .....	128
<b>7</b>	<b>CHAPTER 7: CONTINUOUS PHOTOMODIFICATION OF PP</b> .....	<b>129</b>
7.1	INTRODUCTION .....	130
7.2	MATERIALS AND METHODS .....	132
7.2.1	<i>Materials</i> .....	132
7.2.2	<i>Design of experiments</i> .....	133
7.2.3	<i>Preparation method</i> .....	134
7.2.4	<i>Parallel plate rheometry</i> .....	136
7.2.5	<i>Gel permeation chromatography (GPC)</i> .....	136
7.2.6	<i>Determination of gel content</i> .....	137
7.3	RESULTS AND DISCUSSION .....	137

7.3.1	<i>Rheological properties</i>	137
7.3.2	<i>Gel content measurements</i>	147
7.3.3	<i>Conditions that result in long chain branched PP with minimum gel content</i>	149
7.3.4	<i>GPC measurements</i>	150
7.4	CONCLUDING REMARKS	152
<b>8</b>	<b>CHAPTER 8: OVERALL THESIS CONCLUSIONS, MAIN THESIS CONTRIBUTIONS AND RECOMMENDATIONS</b>	<b>153</b>
8.1	OVERALL THESIS CONCLUSIONS	153
8.2	CONTRIBUTIONS	154
8.3	RECOMMENDATIONS FOR FUTURE WORK	156
8.3.1	<i>Short-term recommendations</i>	156
8.3.2	<i>Long-term recommendations</i>	157
	<b>REFERENCES</b>	<b>159</b>
	<b>APPENDICES</b>	<b>167</b>
	APPENDIX A: JUSTIFICATION FOR USING RHEOLOGICAL POLYDISPERSITY INDICES	167
	APPENDIX B: PROCEDURES FOR CHOOSING SIGNIFICANT TERMS IN EMPIRICAL MODELS	168
	APPENDIX C: CRITERIA TO CHOOSE FACTORS IN EMPIRICAL MODELS	170
	APPENDIX D: CONFIRMING FORMATION OF LONG CHAIN BRANCHES IN A SAMPLE WITH HIGH GEL CONTENT	171

## List of Tables

TABLE 3-1: SUMMARY OF LITERATURE REMARKS FOR ASSESSING LCB OR DEGRADATION IN THE RUNS .....	27
TABLE 4-1: SELECTED FACTORS AND RANGES.....	38
TABLE 4-2: DESIGN OF EXPERIMENTS FOR D-OPTIMAL DESIGN.....	40
TABLE 4-3: LVE RESPONSES ALONG WITH RHEOLOGICAL POLYDISPERSITY DATA FOR EXPERIMENTAL RUNS .....	47
TABLE 4-4: POSSIBLE MOLECULAR STRUCTURE (RELATIVE TO PARENT PP) OF THE DIFFERENT RUNS BASED ON LVE DATA .....	49
TABLE 4-5: SPECIFICATIONS CHOSEN FOR EACH RESPONSE VARIABLE TO FIND OPTIMAL CONDITIONS.....	54
TABLE 4-6: GPC ANALYSIS RESULTS .....	64
TABLE 4-7: MELTING, CRYSTALLIZATION TEMPERATURE, HEAT FUSION OF MELTING FOR RUNS 9, 10, 11, 13, 29 AND THE PARENT PP .....	70
TABLE 4-8: SUMMARY OF INDICATORS FOR DIFFERENT RUNS, RELATIVE TO PARENT PP.....	71
TABLE 5-1: DESIGN OF EXPERIMENTS FOR 3-LEVEL FACTORIAL DESIGN .....	75
TABLE 5-2: LINEAR VISCOELASTIC PROPERTIES OF THE RUNS .....	87
TABLE 5-3: EMPIRICAL MODELS FOR LVE PROPERTIES.....	88
TABLE 5-4: MOLECULAR WEIGHT AVERAGES AND PDI OF THE RADIATED RUNS ALONG WITH MELT MIXED AND PARENT PP .....	93
TABLE 5-5: EMPIRICAL MODEL FOR GEL CONTENT IN THE RADIATED RUNS .....	98
TABLE 6-1: DESIGN OF EXPERIMENTS (CCD DESIGN) .....	105
TABLE 6-2: VISCOELASTIC PROPERTIES, RHEOLOGICAL POLYDISPERSITY (ER), RSI AND RSS MEASUREMENTS, GEL CONTENT AND FTIR MEASUREMENTS FOR THE EXPERIMENTAL RUNS .....	109
TABLE 6-3: EMPIRICAL MODELS FITTED ON VISCOELASTIC PROPERTIES AND GEL CONTENT.....	110
TABLE 6-4: MOLECULAR WEIGHT AVERAGES AND PDI OF SELECTED RUNS ALONG WITH THE PARENT PP .....	118
TABLE 6-5: RESPONSE VARIABLES AND SPECS TO FIND OPTIMIZED PROCESSING CONDITION REGION.....	125
TABLE 7-1: EXPERIMENTS FOR 2 <sup>3</sup> FULL FACTORIAL DESIGN .....	134
TABLE 7-2: VISCOELASTIC PROPERTIES ( $\eta_0$ , $\lambda$ AND N), RHEOLOGICAL POLYDISPERSITY INDICES (PI, MODSEP AND ER) AND GEL CONTENT OF THE EXPERIMENTAL RUNS .....	138
TABLE 7-3: EMPIRICAL MODELS FOR VISCOELASTIC PROPERTIES AND GEL CONTENT BASED ON CODED VARIABLES .....	143
TABLE 7-4: RESPONSE VARIABLES AND THEIR SPECS FOR LOCATING THE OPTIMAL PROCESSING CONDITION REGION .....	149
TABLE 7-5: MOLECULAR WEIGHT AVERAGES AND PDI OF THE SELECTED RADIATED RUNS ALONG WITH THE PARENT PP .....	152
TABLE B: BEST EMPIRICAL MODELS FOR EACH RESPONSE VARIABLE .....	169
TABLE C: EMPIRICAL MODELS FOR VISCOELASTIC PROPERTIES AND GEL CONTENT BASED ON CODED VARIABLES.....	170

## List of Figures

FIGURE 2-1: DEPENDENCE OF GRAFTING, BRANCHING AND CHAIN SCISSION REACTION ON TEMPERATURE COPIED FROM [10] .....	6
FIGURE 2-2: ELECTRON LOCATION AND SPIN DURING SINGLET AND TRIPLET EXCITED STATES; COPIED FROM [21] .....	16
FIGURE 2-3: REACTION MECHANISM FOR BENZOPHENONE PHOTOINITIATION; COPIED FROM [20] .....	16
FIGURE 2-4: DIFFERENT METHODS FOR PRODUCING LONG CHAIN BRANCHED PP .....	19
FIGURE 3-1: WEIGHTED RELAXATION SPECTRUM FOR VIRGIN AND LCB PP; COPIED FROM [30] .....	25
FIGURE 3-2: SCHEMATIC FIGURE OF MEISSNER EXTENSIONAL RHEOMETER; COPIED FROM [36] .....	28
FIGURE 3-3: SCHEMATIC FIGURE OF THE MÜNSTEDT DESIGN [38].....	29
FIGURE 3-4: SENTEMANAT EXTENTIONAL RHEOMETER; COPIED FROM [40].....	30
FIGURE 3-5: <sup>13</sup> CNMR SPECTRA FOR LCBPP; THE STARS ARE CHEMICAL SHIFTS CORRESPONDING TO LCBs IN PP; COPIED FROM [45] .....	33
FIGURE 4-1: PARALLEL PLATE, FREQUENCY SWEEP DATA ( $H^*-\Omega$ ) ALONG WITH CAPILLARY SHEAR VISCOSITY VERSUS SHEAR RATE DATA FOR A) PARENT PP, B) RUN 9 AND C) RUN 13 .....	43
FIGURE 4-2: 3D RESPONSE SURFACE FOR $\eta_0$ (A) AND ER (B) WHEN BPH IS USED.....	51
FIGURE 4-3: 3D RESPONSE SURFACE FOR $\eta_0$ (A) AND ER (B) WHEN DEBPH IS USED .....	53
FIGURE 4-4: PROCESSING WINDOW THAT MAXIMIZES DEGREE OF LCB USING BPH .....	54
FIGURE 4-5: PROCESSING WINDOW THAT MAXIMIZES DEGREE OF LCB USING DEBPH .....	55
FIGURE 4-6: STORAGE MODULUS ( $G'$ ) VERSUS ANGULAR FREQUENCY FOR RUNS 9, 10, 11, 13, 29 AND PARENT PP .....	56
FIGURE 4-7: COMPLEX VISCOSITY ( $\eta^*$ ) VERSUS ANGULAR FREQUENCY FOR RUNS 9, 10, 11, 13, 29 AND PARENT PP .....	57
FIGURE 4-8: COLE-COLE PLOTS FOR RUNS 9, 10, 11, 13, 29 AND PARENT PP .....	58
FIGURE 4-9: TAN ( $\delta$ ) VERSUS COMPLEX MODULUS ( $G^*$ ) FOR RUNS 9, 10, 11, 13, 29 AND PARENT PP.....	59
FIGURE 4-10: UNIAXIAL TENSILE STRESS GROWTH COEFFICIENT ( $\eta^+_{\epsilon}$ ) VS. TIME FOR SELECTED RUNS AND PARENT PP AT HENCKY STRAIN RATES OF 0.01, 0.1, 1, AND 10 $s^{-1}$ .....	61
FIGURE 4-11: SHC VERSUS HENCKY STRAIN RATE FOR RUNS 9, 10, 11, 13, 29, AND PP (LINES ARE SIMPLY VISUAL GUIDES) .....	62
FIGURE 4-12: GEL FRACTION OF RUNS 9, 10, 11, 13, 29 AND PARENT PP .....	63
FIGURE 4-13: MWDs FOR RUNS 9, 10, 11, 13, 29 AND PARENT PP.....	66
FIGURE 4-14: COMPARISON BETWEEN MARK-HOUWINK PLOTS FOR RUNS 10, 11, 29 AND PARENT PP.....	68
FIGURE 4-15: MARK-HOUWINK PLOTS FOR RUNS 9, 13 AND PARENT PP .....	68
FIGURE 4-16: DSC GRAPHS OF RUNS 9, 10, 11, 13, 29 AND THE PARENT PP.....	69
FIGURE 5-1: SCHEMATIC MECHANISM FOR PP DEGRADATION .....	73
FIGURE 5-2: $G'$ (A) AND $\eta^*$ (B) VS. $\omega$ FOR 1 MM THICK SAMPLES WHICH WERE RADIATED BETWEEN 1 AND 5 MIN .....	77
FIGURE 5-3: SCHEMATIC MECHANISM FOR FORMATION OF LCB IN THE PP BACKBONE .....	78
FIGURE 5-4: COMPARISON BETWEEN LVE PROPERTIES OF THE RUNS WITH DIFFERENT THICKNESS AFTER 15 MIN RADIATION A) $G'-\omega$ , B) $\eta^*-\omega$ , C) COLE-COLE PLOTS AND D) TAN ( $\delta$ )- $G^*$ .....	80
FIGURE 5-5: COMPARISON BETWEEN LVE PROPERTIES OF THE RUNS WITH 1 MM THICKNESS WITH DIFFERENT RADIATION TIMES A) $G'-\omega$ , B) $\eta^*-\omega$ , C) COLE-COLE PLOTS AND D) TAN ( $\delta$ )- $G^*$ .....	82
FIGURE 5-6: COMPARISON BETWEEN RELAXATION SPECTRA OF THE RUNS WITH THE SAME THICKNESS A) 1 MIN, B) 2 MM C) 3 MM .....	84
FIGURE 5-7: COMPARISON BETWEEN RELAXATION SPECTRA OF THE RUNS WITH THE SAME RADIATION TIME A) 5 MIN, B) 10 MIN C) 15 MIN .....	86
FIGURE 5-8: EFFECT OF THE TIME-THICKNESS INTERACTION ON ZERO SHEAR VISCOSITY ( $\eta_0$ ) .....	89
FIGURE 5-9: EFFECT OF THE TIME-THICKNESS INTERACTION ON RELAXATION TIME ( $\lambda$ ) .....	89
FIGURE 5-10: EFFECT OF THE TIME-THICKNESS INTERACTION ON RHEOLOGICAL POLYDISPERSITY INDEX (PI).....	90
FIGURE 5-11: EFFECT OF THE TIME-THICKNESS INTERACTION ON MODSEP.....	90

FIGURE 5-12: COMPARISON BETWEEN CALCULATED (LINEAR REFERENCE) AND MEASURED $H_0$ .....	92
FIGURE 5-13: MWDs OF THE RUNS A) WITH 1 MM THICKNESS AT DIFFERENT EXPOSURE TIMES TO UV B) WITH DIFFERENT THICKNESS AFTER 15 MIN RADIATION .....	94
FIGURE 5-14: INTRINSIC VISCOSITY $[\eta]$ vs. $\log(M_i)$ A) WITH 1 MM THICKNESS AT DIFFERENT EXPOSURE TIMES TO UV B) WITH DIFFERENT THICKNESS AFTER 15 MIN RADIATION .....	96
FIGURE 5-15: GEL CONTENT OF THE RUNS WITH DIFFERENT THICKNESS AT DIFFERENT RADIATION TIMES .....	97
FIGURE 5-16: SCHEMATIC OF MECHANISM THAT LEADS TO CROSSLINKING OF LONG CHAIN BRANCHED POLYMERS .....	98
FIGURE 5-17: EFFECT OF THE TIME-THICKNESS INTERACTION ON GEL CONTENT .....	99
FIGURE 6-1: SCHEMATIC MECHANISM OF A) PHOTOINITIATION AND B-SCISSION, B) TMPTA REACTIONS WITH MACRORADICALS.....	103
FIGURE 6-2: EFFECT OF COAGENT CONCENTRATION-IRRADIATION TIME INTERACTION ON $H_0$ .....	111
FIGURE 6-3: EFFECT OF COAGENT CONCENTRATION-IRRADIATION TIME INTERACTION ON ER.....	111
FIGURE 6-4: COMPARISON BETWEEN VISCOELASTIC PROPERTIES OF RUNS 3, 4, 5, 7, 8 AND PP A) $\eta^*-\omega$ , B) $G'-\omega$ , C) $\tan \delta-G^*$ D) COLE-COLE PLOT ( $G'-G''$ ) .....	114
FIGURE 6-5: COMPARISON BETWEEN RELAXATION SPECTRUM OF RUNS 3, 4, 5, 7, 8 AND PP .....	116
FIGURE 6-6: MWD OF SELECTED RUNS ALONG WITH THE PARENT PP .....	117
FIGURE 6-7: COMPARISON BETWEEN CALCULATED (LINEAR REFERENCE) AND MEASURED $H_0$ FROM PARALLEL PLATE RHEOMETRY.....	119
FIGURE 6-8: A) INTRINSIC VISCOSITY AND B) WEIGHT AVERAGE OF NUMBER BRANCHES PER POLYMER CHAINS .....	120
FIGURE 6-9: THE EFFECT OF COAGENT CONCENTRATION-IRRADIATION TIME INTERACTION ON GEL CONTENT .....	122
FIGURE 6-10: SCHEMATIC MECHANISM OF POSSIBLE REACTIONS AT HIGH CONCENTRATION OF TMPTA .....	123
FIGURE 6-11: THE EFFECT OF BPH CONCENTRATION-IRRADIATION TIME INTERACTION ON GEL CONTENT .....	124
FIGURE 6-12: EFFECT OF INCREASING BPH CONCENTRATION ON FORMATION OF LCB IN PP IN PRESENCE OF TMPTA.....	125
FIGURE 6-13: CONDITIONS THAT YIELD HIGH DEGREE OF LCB WITHOUT SIGNIFICANT GEL CONTENT .....	126
FIGURE 6-14: FTIR SPECTRA OF A) PP/0.75 WT-% TMPTA/0.5 WT-% BPH BEFORE AND AFTER WASHING WITH XYLENE B) RUN 8 BEFORE AND AFTER WASHING WITH XYLENE .....	127
FIGURE 7-1: TWIN SCREW EXTRUDER SCREW COMBINATION AND TEMPERATURE OF THE ZONES .....	135
FIGURE 7-2: THE EXPERIMENTAL SETUP FOR CONTINUOUS MODIFICATION OF POLYPROPYLENE VIA UV RADIATION .....	136
FIGURE 7-3: COMPARISON BETWEEN VISCOELASTIC PROPERTIES OF THE RUNS WITHOUT COAGENT A) $\eta^*-\omega$ , B) $G'-\omega$ , C) $\tan \delta-G^*$ AND D) COLE-COLE PLOTS .....	140
FIGURE 7-4: COMPARISON BETWEEN VISCOELASTIC PROPERTIES OF THE RUNS WITH COAGENT A) $\eta^*-\omega$ , B) $G'-\omega$ , C) $\tan \delta-G^*$ AND D) COLE-COLE PLOTS.....	142
FIGURE 7-5: 3D INTERACTION PLOTS FOR $H_0$ (A), $\lambda$ (B) AND $N$ (C); THE PLOTS ON THE LEFT ARE WITHOUT COAGENT, WHEREAS THE PLOTS ON THE RIGHT ARE WITH COAGENT.....	145
FIGURE 7-6: 3D INTERACTION PLOTS FOR MODSEP (A), ER (B) AND PI (C); THE PLOTS ON THE LEFT ARE WITHOUT COAGENT, WHEREAS THE PLOTS ON THE RIGHT ARE WITH COAGENT .....	146
FIGURE 7-7: 3D INTERACTION PLOTS FOR GEL CONTENT A) WITHOUT COAGENT B) WITH COAGENT .....	149
FIGURE 7-8: CONDITIONS THAT YIELD HIGH DEGREE OF LCB WITHOUT SIGNIFICANT GEL CONTENT A) WITHOUT TMPTA, B) WITH TMPTA.....	150
FIGURE 7-9: MWDs AND $\log [H]$ vs. $\log M$ FOR RUNS 4, 6, 8 AND THE PARENT PP .....	151
FIGURE D: COMPARISON BETWEEN $\eta^*-\omega$ PLOTS OF RUN 8 AND PARENT PP, BEFORE AND AFTER GEL EXCLUSION.....	172

## COMMON ABBREVIATIONS

$\overline{M}_n$	Number average molecular weight	MW	Molecular weight
$\overline{M}_w$	Weight average molecular weight	MWD	Molecular weight distribution
$\overline{M}_z$	Z average molecular weight	n	Power law index
Bw	Weight Average number of long chain branches in polymer chains		Shear thinning index
CL	Crosslinking	$N_{LCB}$	Number of long chain branches per 1000 monomer units
CRPP	controlled rheology polypropylene	NMR	Nuclear magnetic resonance
EB	Electron beam	PDI	Polydispersity index
ER	Rheological polydispersity index of high molecular weight chains	PE	Polyethylene
ESR	Electron spin resonance	PI	Rheological polydispersity index
$G''$	Loss modulus	PP	Polypropylene
$G'$	Storage modulus	$R_g$	Radius of gyration
$G_c$	Crossover modulus	S	Photoinitiator
GPC	Gel permeation chromatography	SCF	Supercritical fluid
$I_t$	Intensity of transmitted UV	TAM	Triallyl trimesate
$J_e^0$	Steady state compliance	$\tan \delta$	Loss tangent
LCB	Long chain branching	TAP	Triallyl phosphate
LCBPP	Long chain branched polypropylene	TMPTA	Trimethylolpropane triacrylate
LCBs	Long chain branches	Z-N	Ziegler-Natta
LPP	Linear polypropylene	$\epsilon$	Molar extinction coefficient
MFI	Melt flow index	$\dot{\epsilon}$	Hencky strain rate
MFR	Melt flow rate	$\eta^*$	Complex viscosity
ModSep	Separation modulus	$\eta_0$	Zero shear viscosity
		$\eta_E$	Extensional viscosity

$\lambda$

Relaxation time

$\omega$

Angular frequency

$\Phi$

Quantum yield of photoinitiator disappearance

# **1 CHAPTER 1: MOTIVATION, OBJECTIVES AND THESIS OUTLINE**

## **1.1 MOTIVATION**

Polypropylene (PP) is one of the most common thermoplastics in the plastics industry with numerous applications ranging from household appliances to automotive interior. Each application requires a specific PP grade with a specific molecular structure, molecular weight (MW) and molecular weight distribution (MWD). PP molecular weight and polydispersity index (PDI) affect the melt flow behaviour, processing characteristics and eventually the final applications of PP.

A commercial way to synthesize PP with specific stereo-regularity is by using Ziegler-Natta (Z-N) catalysts. The molecular weight (MW) of PP which is produced by this method is in the range of  $3 \cdot 10^5$  to  $7 \cdot 10^5$ . The corresponding PDI is within the range of 5 to 20 for heterogeneous and 2 to 5 for homogenous Z-N catalysts [1]. Industries synthesizing PP are mainly utilizing heterogeneous Ziegler-Natta catalysts [2]. Control over MWD of the PP which is produced by this synthesis method is difficult [1]. Since 1990, alternative catalysts called metallocenes have been used for producing isotactic PP. PP produced by a metallocene catalyst has a narrower molecular weight distribution [3].

The MWD is an important molecular property, which determines flow behaviour of a polymer melt. The polymer melt behaviour dictates the processing conditions and method. Due to the variety of PP applications in different industries, it is important to utilize a method to modify its MWD and consequently its melt rheology. Efforts have been made to decrease the polydispersity and MW of PP to fit the wide applications range. This grade of modified PP, whose melt flow rate (MFR) has been reduced via degradation, is called controlled rheology PP (CRPP). Chemical initiators, electron beam (EB) and gamma radiation have all been employed to produce PP with lower molecular weight and narrow the molecular weight distribution of PP by degradation. Despite developments made for

synthesizing narrow molecular weight distribution PP by metallocene catalysts, these post-production modification methods remain popular due to the extremely cost-efficient and straightforward steps and equipment used for PP degradation.

In spite of the large market of polypropylene, poor rheological properties such as lack of melt strength, limit its processing in certain applications. Thus, by modifying the rheology and enhancing strain hardening of the PP melt, PP can be processed via different methods such as foaming, thermoforming, extrusion coating and blow moulding [4]. The high melt strength of a polymer is either due to long chain branching (LCB) or high molecular weight [5]. Formation of long chain branches (LCBs) in PP structure is found to be the most efficient method to increase its melt strength. Thus, attempts were made to introduce long chain branches (LCBs) to the PP chains in order to provide some balance with respect to the commonly occurring degradation reactions. Methods such as EB and gamma beam radiation, and/or peroxide use along with the presence of appropriate coagents, such as styrene or allylic and acrylic multi-functional chemicals, have been utilized to produce LCBPP [6-8].

However, all these methods have potential drawbacks and commercial production of long chain branched PP (LCBPP) is still limited [9]. In this thesis, UV radiation is suggested as a novel method for PP rheological modification. Possible drawbacks for commercialization of this technique are investigated and effects of potential solutions are studied.

## **1.2 OBJECTIVES**

The first general objective of this thesis is to identify the significant processing variables and their effects on PP photomodification.

The second objective is to find the processing window that results in the maximum amount of long chain branching in the samples.

The third objective is to identify UV modification limitations and verify the effect of possible solutions.

The fourth and final objective of this thesis is to develop a technique to scale up PP photomodification for commercial purposes.

### **1.3 THESIS OUTLINE**

The thesis will begin with a literature review, followed by a detailed description of characterization techniques and data analysis methodologies, which have been introduced in the literature to identify PP molecular structure.

In the literature and background section (Chapter 2), we first start with introducing methods that have been presented in the literature for rheological modification of PP either through degradation (CRPP) or introduction of LCBs to PP linear chains. At the end of this chapter, the kinetics of UV-initiated systems are explained.

Then, in Chapter 3, a summary is presented of different characterization techniques that have been utilized to determine important aspects of the micromolecular structure of PP.

Since materials, equipment and processing techniques were not necessarily the same for all of the results presented in Chapters 4 to 7, specific experimental procedures are discussed in each chapter individually. That is why there is no separate materials/methods chapter in this thesis.

The focus of Chapter 4 is on identifying the effect of photomodification variables on PP molecular structure and determining the significant variables. Optimal processing conditions for the formation of LCBPP are also presented in Chapter 4.

Chapter 5 discusses the effect of UV penetration depth and radiation time on the formation of long chain branches (LCBs). These two factors were found to be the main limitations of photomodification reactions. The effects of these two variables are studied in Chapter 5 by preparing samples with different thickness and radiating them for different durations.

In order to minimize the radiation time required to form LCBPP, an appropriate coagent can be used. The focus of Chapter 6 is on explaining the effect of trimethylolpropane triacrylate (TMPTA), which was used as coagent for formation of LCBs by suggesting

mechanisms for the reactions involved. The effects of coagent concentration, photoinitiator concentration and radiation time on formation of LCBs are also discussed in this chapter.

A setup for continuous photomodification of PP was finally developed. This setup, along with conditions that result in LCB under the continuous modification of PP, are discussed in Chapter 7. The conditions for producing LCBPP with minimum gel content are explained in this chapter as well.

Chapter 8 contains overall thesis conclusions and recommendations for the future for research in this field. The main contributions of the thesis are also summarized in this chapter.

Finally, several appendices complementary to the thesis chapters are cited. Appendix A includes justifications for using rheological polydispersity measurements throughout the thesis. Appendix B and C contain details on the statistical analysis of the responses in Chapters 4 and 7, respectively. And Appendix D (complementary to Chapter 7, but also applicable to other chapters in the thesis) includes the results of additional experiments that confirm formation of long chain branches in the sol fraction of the modified samples with high gel content.

## **2 CHAPTER 2: OVERVIEW OF DIFFERENT METHODS FOR PP MELT STRENGTH MODIFICATION**

PP post-reactor modification has been practised with two objectives: to reduce its polydispersity or to introduce long chain branches (LCBs) to its backbone. Both these modifications involve hydrogen abstraction from the PP main chains and formation of tertiary carbon radicals. Tertiary radicals in PP chains are unstable and undergo  $\beta$ -scission reactions that lead to the formation of a macroradical and a PP chain with an unsaturated end. It is worth noting that although this reaction ( $\beta$ -scission) is necessary for most PP post-reactor modifications, it should be carried out in a controlled manner to avoid severe degradation.

It is well-known that  $\beta$ -scission is more pronounced at elevated temperatures. Figure 2-1 shows the relative rates of possible reactions during PP modification with respect to temperature [10]. Figure 2-1 shows that  $\beta$ -scission reactions become dominant as the temperature increases. Thus, modification temperature is the key factor affecting the molecular structure of the modified PP.

In this chapter the aim is to discuss different techniques that have been introduced in the literature for PP rheological modification. Although the main aim of this thesis is formation of LCBs in PP, both degradation and chain combination reactions are discussed. The reason is that degradation is part of reactions responsible for eventual formation of LCBs in PP.

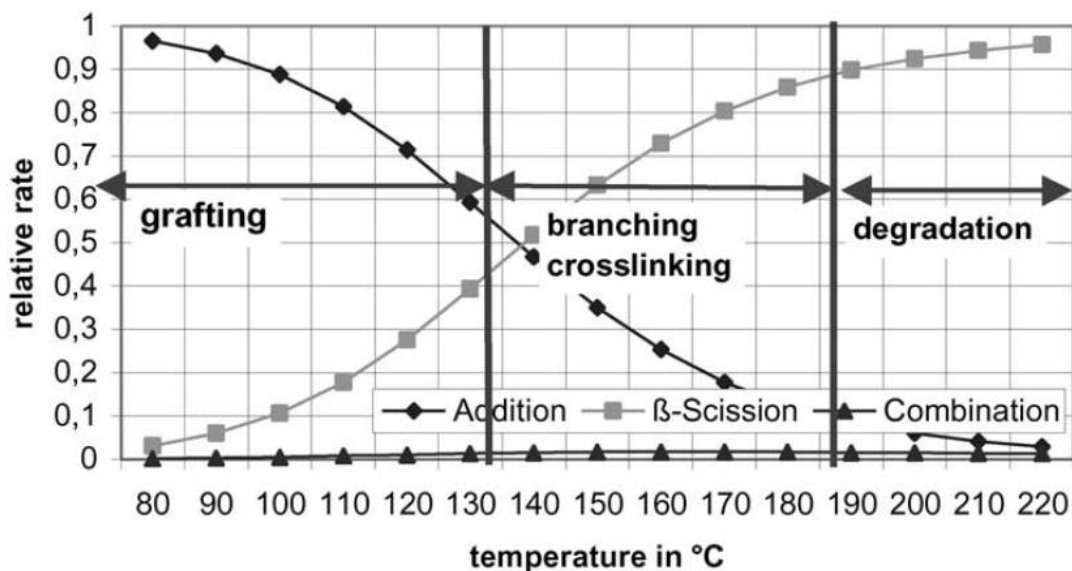


Figure 2-1: Dependence of grafting, branching and chain scission reaction on temperature copied from [10]

## 2.1 SYNTHESIS OF LONG CHAIN BRANCHED PP (LCBPP)

Long chain branched PP (LCBPP) can be formed via two different strategies: Synthesis of LCBPP or post-reactor modification of PP. Synthesizing LCBPP has been done using different techniques. One of these techniques includes incorporation of unconjugated units in the PP chain backbone during PP polymerization. In this technique, branches were later added to the unconjugated sites. One of the most versatile techniques, which has been recently introduced in the literature, is synthesizing LCBPP via T-reagents and metallocene catalysis. Langstone et al. [11] synthesized PP with a well-defined branching structure using metallocene reagent catalysts and T-agents.

However, in general, metallocene catalysts were not successful in capturing much of the polypropylene market. In 2010, only 2 to 3% of the world's polypropylene demand was provided from metallocene catalysis since the industry does not have the tendency to switch from current Z-N catalyst plants [12]. Due to the high production load of Z-N PP, the demand for post-reactor modification of PP is still significantly high.

## **2.2 POST-REACTOR MODIFICATION: CHEMICAL METHODS**

Several methods have been introduced in the literature for post-reactor modification of PP rheological properties, either through controlled degradation or introduction of LCBs. Methods presented in the literature for hydrogen abstraction from the PP backbone can be divided into two categories: methods using thermo-chemical initiators and methods using high energy radiation. The use of peroxides that can be activated by heat falls into the former, while gamma and electron beam (EB) radiation belong to the latter category. Photoinitiators can also be used for macroradical generation and they can be activated using UV energy. This method can also fall into the second category as high energy UV radiation causes excitation of the photoinitiator and subsequent hydrogen abstraction.

As mentioned before, in order to produce LCBPP, degradation should be controlled; thus, multi-functional monomers can be used to discourage further degradation by stabilizing the radical centre. The efficiency of different comonomers to control  $\beta$ -scission depends on their ability to maintain resonance stability (stabilizing the radical center). Thus, the experimental results from different peroxide systems that were used for hydrogen abstraction, and different comonomers used for macroradical stabilization are explained in the following sections. Then systems utilizing high energy radiation are discussed in more detail.

Different peroxides can react with PP and initiate the modification reaction. Peroxides have been used both in melt and solid state reactions.

### **2.2.1 DECREASING MW OF PP VIA PEROXIDES**

Tzoganakis et al. [1] used peroxide derivatives to modify rheological properties of PP by increasing its MFI and narrowing its molecular weight distribution (MWD). The reaction between 2, 5-bis (tert-butylperoxy) hexane and PP was carried out in both ampoules and single screw extruder. They conducted the experiments in ampoules both in the presence

and absence of oxygen and at two different temperatures. It was found that as the reaction temperature increased, MFI could increase further. It was also shown that in the presence of oxygen the rate of the reaction increased due to formation of more reactive peroxide radicals. However, it was suggested to eliminate the oxygen during the reaction as the color of the final PP was affected by its presence. This change in the product color was attributed to interference of oxygen with peroxide degradation reactions. In the presence of oxygen,  $\overline{M}_w$  decreases in a more severe manner and higher MFI results. The effects of peroxide degradation on flow rate in the extruder, die pressure and die swell were also studied. It was found that an increase in peroxide concentration causes an increase in the mass flow rate, while die pressure and die swell decrease due to a decrease in  $\overline{M}_z$  of PP. The authors concluded that peroxide will attack longer polymer chains preferentially and break them to smaller chains by  $\beta$ -scission. This leads to reduced PP melt elasticity.

Attempts were also made by this group [1] to simulate the peroxide degradation process both in the extruder and in the ampoules. The molecular weight averages and PDI of the PP after the degradation process were predicted. Their simulation results for MW averages ( $\overline{M}_n$ ,  $\overline{M}_w$  and  $\overline{M}_z$ ) were in good agreement with the experimental results obtained from the ampoules. However, while simulation results for  $\overline{M}_n$  and  $\overline{M}_w$  were satisfactory for the reaction inside the extruder, comparison between simulated  $\overline{M}_z$  and results recorded from GPC (experimental data) showed small deviations. It was suggested that this deviation was due to the probability of branching and crosslinking at the high molecular weight tail of the distribution or inaccuracies in GPC results at high molecular weights.

### **2.2.2 INCREASING PP MELT STRENGTH VIA PEROXIDES**

In an attempt to form LCBPP using peroxide initiator, Parent et al. [6] utilized peroxide initiators along with coagents such as triallyl trimesate (TAM), trimethylpropane triacrylate (TMPTA) and triallyl phosphate (TAP) to modify the rheology of PP by introducing LCB. The modification was conducted in the melt state and the effects of allylic and acrylic coagents on molecular weight and branching distribution were studied by comparing shear and elongation viscosities. The modified PP contains both degraded

chains, slightly branched polymer chains and hyper-branched chains, which can only be formed after the gel point. The modifications were done in a batch mixer at 200 °C. The PP was pre-impregnated with coagents and peroxide initiators. They found that the final PP structure is a function of the yield and the selectivity of the peroxide in the degradation reaction and the coagent that assists the crosslinking. Moreover, addition of initiator with no coagent will reduce the polydispersity of PP due to degradation of the high molecular weight chains.  $\eta^*$  vs. frequency plots showed that the zero shear viscosity and complex viscosities will decrease as a result of chain scission. They also observed from these plots that the shear thinning behaviour was delayed in degraded samples to higher frequencies. The degraded samples had a linear molecular structure with no signs of strain hardening, as expected, from linear PP (LPP) chains.

In contrast, in the presence of coagents, the length of the Newtonian plateau region in  $\eta^*$  vs. frequency graphs was reduced and at 0.2 wt-% of TAM, this region completely disappeared as a sign of LCB. However, none of the samples reached the zero shear viscosity and complex viscosity of the linear parent PP.

Their results also showed that TMPTA has faster kinetics compared to the other coagents and it has more of a pronounced effect on shear and extensional rheology. Isolated gel regions were formed due to addition of TMPTA and it was found that TMPTA is the only coagent among these three that shows hyper-branching at low percentages. On the other hand, TAP has higher crosslinking efficiency compared to TMPTA, which results in a higher shear and extensional viscosity, and strain hardening.

This group suggested a mechanism for the reaction between PP, initiator and coagent. They stated that after PP macroradicals are formed as a result of the presence of the chemical initiator, they will attack the carbon-carbon double bond on the coagent and then a stable radical adduct will be formed, which is protected from  $\beta$ -scission. The hydrogen on this intermediate radical adduct should be able to react with other degraded polymer chains with a terminal double bond to terminate the radicals and to make crosslinks or long chain branches.

Yu and Zho [13] compared peroxide degradation and crosslinking kinetics of isotactic and syndiotactic polypropylene. They found that despite the same chemical structure of the two grades used, stereoregularity can affect the concentration of the radicals that were generated using peroxide as initiator. Using electron spin resonance (ESR), they found that tertiary radicals will be produced for both PP grades after the peroxide attack, but the concentration of the radicals is higher for isotactic PP. This is due to steric hindrance in the case of syndiotactic PP that limits peroxide attack. Consequently, the crosslink efficiency of syndiotactic PP in the presence of coagent was lower. This is because the rate of bimolecular combination decreases when the concentration of radicals decreases.

Wong and Baker [7] used two different chemical initiators along with a grafting monomer as a coagent for PP modification. They observed that PP modified with an initiator with shorter decomposition time has a higher degree of grafting. They attributed this to formation of macroradicals at the solid surface of PP prior to mixing in the batch mixer. In the case of an initiator with low decomposition rate,  $\beta$ -scission can go on until the initiator is fully dispersed with PP in the batch mixer at high temperature, and hence PP chains undergo severe degradation. During this time, the coagent monomer can be consumed by homopolymerization and its accessibility becomes limited in the vicinity of the macroradicals. Consequently, lower molecular weight chains will result, which is reflected in the rheological properties as well. They observed that upon increasing the initiator concentration, the degree of grafting decreases, while further decreases in molecular weight were observed due to higher  $\beta$ -scission.

Styrene monomer was also used as a grafting agent for PP modification by peroxide [7]. An increase in batch mixer torque was detected, which was attributed to PP crosslinking (CL). An increase in the  $G'$  and  $\eta^*$  of the runs containing 6.5 wt-% or more of styrene compared to virgin PP was found. They also found that addition of 6.5 to 16.5 wt-% of styrene can result in 2.6 to 6.2 % grafting by weight. It was found that addition of a high concentration of styrene results in crosslinked structures in PP, while low styrene concentrations lead to degradation.

### **2.2.3 UTILIZING SUPERCRITICAL FLUID (SCF) FOR POLYPROPYLENE MODIFICATION**

Decreasing the processing temperature would increase the probability of branching reactions over degradation reactions. Thus, using supercritical fluid (SCF) is beneficial in the sense that it allows the processing to be carried out at lower temperatures.

The other beneficial effect of SCF is its capability to be used as a solvent during the reaction and promote better mixing. Better mixing will occur due to a decrease in the viscosity which is due to the presence of SCF as the reaction medium. Moreover, SCF can increase the free volume between polymer chains and act as a plasticizer. This behaviour leads to better mixing of reactive species within the polymer melt. Thus, grafting reactions can also be facilitated due to better mass transfer of reactive species.

Su and Huang [14] utilized supercritical CO<sub>2</sub> during PP modification for producing long chain branched PP (LCBPP). They used peroxide initiator and acrylic monomer as a functional group for branching. It has been found that by increasing the concentration of supercritical carbon dioxide, the extensional viscosity, melt strength and strain hardening will all increase. They suggest this is due to a higher efficiency of LCB. They have also found an increase in shear thinning behaviour as a result of a higher degree of LCB. Higher shear thinning behaviour was evidenced when the concentration of supercritical CO<sub>2</sub> was increased. Greater storage modulus ( $G'$ ) at low frequencies and a decrease in the terminal slope of the  $G'$ - $\omega$  curve are both indication of higher levels of LCB in PP. It was evidenced that the higher the supercritical CO<sub>2</sub> concentration the greater the  $G'$  is at lower frequencies, and the lower the slope is at higher frequencies.

## 2.3 POST-REACTOR MODIFICATION: RADIATION TECHNIQUES

### 2.3.1 ELECTRON BEAM RADIATION (EB)

In this method, linear PP pellets were irradiated in a vessel with electrons generated by an electron beam accelerator. In order to avoid an increase in the temperature while irradiating PP pellets with doses higher than 10 kGy, a “step-by-step” procedure was followed. This means that radiation was done in short time intervals [15].

Krause et al. [16] used this technique and irradiated PP samples under a nitrogen atmosphere. They used GPC, rheometry and elongation viscosity to characterize low amounts of LCB that would result. The GPC analysis showed that degradation was more pronounced for longer chains.

This group [16] also found the  $N_{LCB}$  (number of long chain branches per 1000 monomer units) for each irradiated PP chains. Then, they plotted  $N_{LCB}$  corresponding to each chain vs. its molar mass. They found that  $N_{LCB}$  will increase gradually with respect to molar mass of the chain up to 0.08 branches per 1000 repeating units. After reaching this value,  $N_{LCB}$  will stay constant for any larger chain length. They observed that these amounts of LCB are the same for the range of radiation dose employed (20-150 kGy). They also conducted rheological tests on the samples and found that zero shear viscosity increases with the dose of radiation up to 5 kGy. However, they observed a slight decrease in the zero shear viscosity of the samples irradiated with a 10 kGy radiation dose.

Results from elongation flow experiments on these samples also indicated that as the number of LCB increases the elongation viscosity and strain hardening will increase. Elongation viscosity measurements were found to be very sensitive for characterizing LCB qualitatively. Among three methods that they used for LCB characterization, the only way to quantify the number of the long chain branches was using size exclusion chromatography and the hydrodynamic volume of each fraction; however, the sensitivity of

this method is less than that of rheological instruments [16]. Quantifying the number of the long chain branches using size exclusion chromatography by GPC is elaborated in Section 3.2.

Mousavi et al. [17] compared rheological properties and gel content that could be obtained from electron beam radiation method and chemical modification. They used trimethylolpropane trimethacrylate (TMPTA) as a coagent in the chemical modification along with dicumyl peroxide (DCP) as an initiator. The chemical modifications were carried out in a mixer and in the melt state, while radiation was conducted under either air or nitrogen ( $N_2$ ) atmosphere and in the solid state. They found that the electron beam under air and in the presence of TMPTA gives higher yield of LCB. On the other hand, degradation through  $\beta$ -scission is more severe when no coagent is added. They also observed that by increasing the radiation dose at the same concentration of TMPTA, the probability of crosslinking and long chain branching reactions increases. This is evidenced from the presence of a shorter plateau region in complex viscosity ( $\eta^*$ ) versus  $\omega$  plots and decrease in slope of  $G'$  vs.  $\omega$  curves. In addition, at the same radiation dose, higher percentage of TMPTA leads to higher storage modulus and viscosity [17].

Rheological results that they obtained from chemical modification show that an increase in DCP level causes a decrease in zero shear viscosity and increase in MFI and even addition of more coagent cannot compensate for the severe degradation. They also conducted their experiments on PP copolymerized with 8% ethylene and reported lower degradation, greater gel fraction and LCB in PP-co-PE.

Basell [18] claims to have produced high melt strength PP using high energy electron beam radiation under  $N_2$  atmosphere in the solid state. This method consists of irradiation of PP in a fluidized bed under  $N_2$  atmosphere to decrease the chain scission as much as possible. Then, irradiated PP samples will be heated at elevated temperature to bring the entrapped radicals in the crystalline domains into the interface of crystalline and amorphous regions. This is done to encourage termination of the trapped radicals via bimolecular termination which leads to formation of long chain branches [18].

Finally, Rätzsch et al. [5] suggested using low-energy EB in the solid state for further control on the degradation, while Lugao et al. [19] used medium to high energy radiation to enhance electron penetration.

### **2.3.2 GAMMA RAY RADIATION**

Another common radiation technique for rheological modification and increasing the melt strength of PP is using gamma radiation. In this method, energetic ions and excited states are produced using Cobalt 60 as a gamma ray source. Gamma irradiation can abstract hydrogens from the PP backbones and cause  $\beta$ -scission. [18].

Lugao et al. [18, 19] used this method under an acetylene atmosphere. The procedure they followed includes a final step at high temperatures. They found out that upon using gamma radiation, the melt strength of the modified PP decreases with increase in the MFI. They indicated that the acetylene atmosphere helps control the degradation and facilitates crosslinking of PP chains to each other due to the bifunctionality of acetylene [18, 19]. They stated that the modification reaction is controlled by acetylene diffusion into PP; as a result, low dose rates of typical Gamma radiation give enough time for diffusion, combination and termination reactions. They observed higher melt strength in PP chains that were modified using Gamma radiation in acetylene atmosphere compared to PP chains that were modified using electron beam radiation under N<sub>2</sub> atmosphere.

### **2.3.3 UV RADIATION: PHOTOINITIATION REACTIONS**

Chemical initiators, such as different peroxides, are known to have a toxic nature. Also controlling degradation of PP when peroxides are used is difficult. This is because mixing PP and initiator happens above the PP melting temperature. This temperature is well above the initiator activation temperature; hence, excessive and inhomogeneous degradation occurs in the polymer. UV radiation offers good controllability over the process since the initiation step is independent of temperature. Moreover, high energy radiation techniques such as gamma or EB are not available to all industries due to high cost and certain safety

concerns. Hence, UV radiation can be adopted since it is a relatively safe and low cost technique.

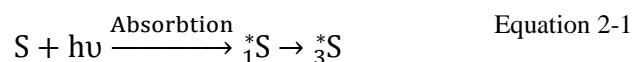
In this project, benzophenone (BPH) was used as a photoinitiator, which absorbs the UV energy to produce free radicals. The process of modification of PP via photoinitiator along with UV irradiation is referred as photomodification. PP photomodification was chosen in this research above all other techniques introduced in this chapter due to the above mentioned advantages (safety, costs, availability and controllability).

He and Tzoganakis [20] utilized a photoinitiator to decrease the polydispersity of PP and produce controlled rheology PP. The photoinitiator (BPH) generated free radicals in the PP chain. BPH absorbs UV light and becomes excited. At this stage, it can abstract hydrogens from the PP chains. The photoinitiation mechanism is elaborated further shortly in this section. This method has been utilized both in the solid and melt states to modify PP.

## 2.4 PHOTOMODIFICATION MECHANISMS

The main difference of utilizing UV in PP modification compared to the other techniques is the initiation step. This section explains how reactive initiator radicals can be formed (i.e., the photoinitiation mechanism). It is important to get an insight of the initiation mechanism in order to be able to develop rate expressions for photoinitiation during PP modification.

Photoinitiation reactions are those that occur by activating an initiator molecule by UV irradiation (Equation 2-1).



In this reaction, the photoinitiator (S) absorbs UV light and generates an electronically excited state. This excited stage can be either a Singlet ( ${}^1S$ ) or a Triplet ( ${}^3S$ ) state (Figure 2-2).

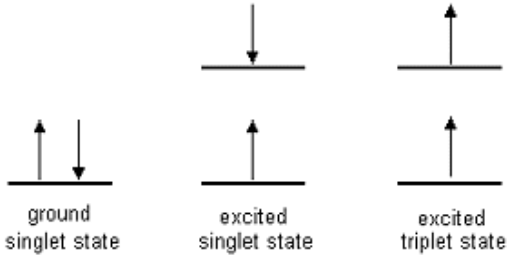


Figure 2-2: Electron location and spin during Singlet and Triplet excited states; copied from [21]

A Singlet excited state ( $^1S$ ) is formed when an electron from ground energy level transfers to upper levels of energy (a spin favoured conversion that occurs by UV energy absorption). Conversion to Triplet state ( $^3S$ ) is usually a radiationless transition and it is called intersystem crossing, where electron transfers to upper level orbitals despite of the spin-forbidden nature of the transition (Figure 2-2 and ISC transition in Figure 2-3) [22].

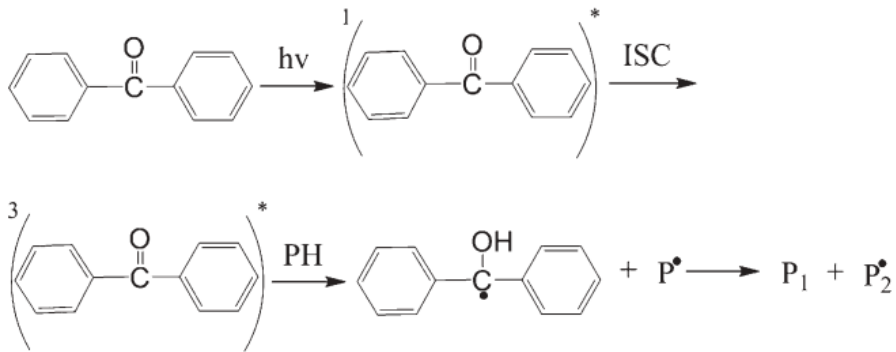


Figure 2-3: Reaction mechanism for benzophenone photoinitiation; copied from [20]

The rate of absorption stage in a photochemical reaction can be expressed by Equation 2-2:

$$I_a = -\frac{d[S]}{dt} = \frac{d[{}^1S]}{dt} \quad \text{Equation 2-2}$$

In Equation 2-2,  $I_a$  is the intensity of absorbed light per volume of the sample per unit of time.  $I_a$  can be found according to Beer-Lambert law (Equation 2-3).

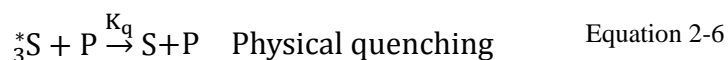
$$\frac{I_t}{I_0} = 10^{-\epsilon l [S]} \quad \text{Equation 2-3}$$

In Equation 2-3,  $I_t$  is the intensity of transmitted UV light, which is the intensity of the light that passes through the initiator.  $I_0$  is the incident light intensity,  $l$  is the sample thickness and  $[S]$  is the photoinitiator concentration.  $\epsilon$  is the amount of irradiation that the photoinitiator absorbs at a certain wavelength and it is referred to as molar extinction coefficient (or molar absorption coefficient).

Equation 2-4 correlates the incident and transmitted light intensity to the intensity of the light absorbed by the initiator.

$$I_a = I_0 - I_t = I_0(1 - 10^{-\epsilon l [S]}) \quad \text{Equation 2-4}$$

The reaction expressed in Equation 2-1 is not the only reaction that happens. The following reactions are probable during photoinitiation.



In the reaction Equation 2-6 and Equation 2-7,  $P$  and  $P^*$  represent polymer chains and polymer radicals, respectively. From the reaction in Equation 2-7, the rate of initiation can be expressed by Equation 2-8.

$$\frac{d[S]}{dt} = K_a [P] [{}^3S] \quad \text{Equation 2-8}$$

At steady state,  $\frac{d[{}^3S]}{dt} = 0$  and Equation 2-9 will result.

$$\frac{d[{}^*_3S]}{dt} = 0 = I_a - (K_0 + K_q[P] + K_a[P])[{}^*_3S] \quad \text{Equation 2-9}$$

By substituting  $[{}^*_3S]$  from Equation 2-9 into Equation 2-8, Equation 2-10 is obtained.

$$\frac{d[S]}{dt} = \frac{K_a[P]I_0(1 - 10^{-\epsilon I[S]})}{(K_0 + K_q[P] + K_a[P])} \quad \text{Equation 2-10}$$

The quantum yield of photoinitiator disappearance ( $\Phi$ ) is a constant that can be defined by Equation 2-11.

$$\Phi = \frac{K_a[P]}{(K_0 + K_q[P] + K_a[P])} \quad \text{Equation 2-11}$$

Using this concept ( $\Phi$ ) and a mathematical approximation, Equation 2-10 can be rewritten as Equation 2-12 [23].

$$\frac{d[S]}{dt} = 2300\Phi\epsilon[S]I_0 \quad \text{Equation 2-12}$$

After integrating Equation 2-12, Equation 2-13 is obtained.

$$\ln\left(\frac{S}{S_0}\right) = 2300\Phi\epsilon I_0 t \quad \text{Equation 2-13}$$

In Equation 2-13,  $S_0$  is the initial concentration of the photoinitiator and  $S$  is the concentration of photoinitiator at time  $t$ .

## 2.5 CONCLUDING REMARKS

In this chapter, different methods that have been introduced in the literature for production of long chain branched PP have been overviewed. Figure 2-4 categorizes all these techniques. Among all these methods, UV radiation was chosen to form LCBPP since it is an easy, affordable and relatively safe technique for PP rheological modification.

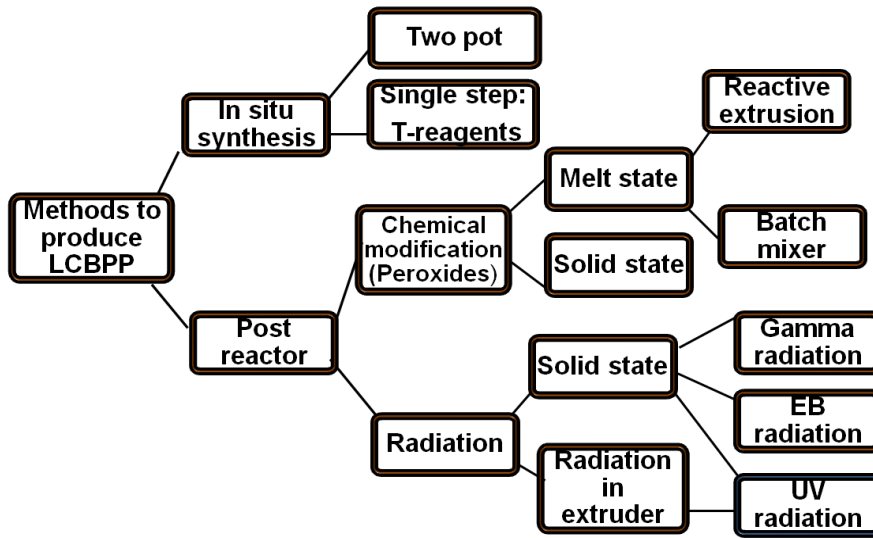


Figure 2-4: Different methods for producing long chain branched PP

## **3 CHAPTER 3: CHARACTERIZATION OF LONG CHAIN BRANCHED PP (LCBPP)**

The molecular structure of polymers can be studied by different characterization techniques. UV radiation can affect the molecular properties of PP in different ways (such as degradation, long chain branching or crosslinking). Depending on the radiation conditions, one, two or all of these structures can be found in photomodified PP. Hence, it is necessary to confirm formation of each molecular structure via different characterization techniques.

Among all characterization methods used to determine PP molecular properties, shear rheometry and GPC are discussed in more detail, since these two are commonly used for PP micromolecular characterization. Other complementary methods, such as nuclear magnetic resonance (NMR), electron spin resonance (ESR) and extensional rheometry, are also introduced in this chapter. These methods have been utilized in research to detect LCB in PP, studying LCB reactions or determine the effect of LCBs on viscosity. Note that not all of these methods have been employed for PP characterization in the analysis conducted in this thesis.

### **3.1 RHEOMETRY**

#### **3.1.1 SHEAR RHEOMETRY**

Rheological properties are affected by the molecular structure of the polymer [24-26]. A simple shear rheometer can be used to characterize the degree of long chain branching, qualitatively. The success in PP characterization is due to differences in the melt behavior of degraded and long chain branched polymers [27, 28]. For convenience, rheological characterizations are mostly performed using small amplitude oscillatory shear devices, such as a parallel plate or cone and plate rheometer. In these experiments, an oscillatory

sinusoidal strain is applied to the polymer. Equation 3-1 shows shear strain as a function of time.

$$\gamma(t) = \gamma_0 \sin(\omega t) \quad \text{Equation 3-1}$$

In Equation 3-1,  $\gamma_0$  is the amplitude of the strain and  $\omega$  is the angular frequency. Having the strain, the resultant stress  $\sigma(t)$  in the polymer can be obtained by measuring the torque imposed on the top plate. Equation 3-2 shows the time-dependent behavior of the corresponding stress.

$$\sigma(t) = \sigma_0 \sin(\omega t + \delta) \quad \text{Equation 3-2}$$

In Equation 3-2,  $\delta$  is the phase shift between applied strain and stress response, which happens due to the viscoelastic nature of the polymer. It is customary to write Equation 3-2 in the form of Equation 3-3.

$$\sigma(t) = \gamma_0 [G'(\omega) \sin(\omega t) + G'' \cos(\omega t)] \quad \text{Equation 3-3}$$

In Equation 3-3,  $G'$  is the storage modulus and  $G''$  is the loss modulus.  $G'$  and  $G''$  can be calculated using Equation 3-4 and Equation 3-5. The loss tangent ( $\tan \delta$ ) can be calculated using Equation 3-6.

$$G' = \frac{\sigma_0}{\gamma_0} \cos \delta \quad \text{Equation 3-4}$$

$$G'' = \frac{\sigma_0}{\gamma_0} \sin \delta \quad \text{Equation 3-5}$$

$$\tan \delta = \frac{G''}{G'} \quad \text{Equation 3-6}$$

The response of the material at very low frequencies (terminal region) is dominated by its viscous behavior and Equation 3-7 is valid at this limiting condition.

$$\eta_0 = \lim_{\omega \rightarrow 0} \frac{G''(\omega)}{\omega} \quad \text{Equation 3-7}$$

According to Equation 3-7, at the terminal condition (very low frequencies),  $G''$  is proportional to  $\omega$  and  $\eta_0$  is the proportionality constant.  $\eta_0$  is the zero shear viscosity and will be discussed shortly in this section. On the other hand, the storage modulus of a

viscoelastic liquid is proportional to  $\omega^2$  in the terminal region, since Equation 3-8 is valid at very low frequencies.

$$J_e^0 = \frac{1}{\eta_0^2} \lim_{\omega \rightarrow 0} \frac{G'(\omega)}{\omega^2} \quad \text{Equation 3-8}$$

In Equation 3-8,  $J_e^0$  is the steady state compliance and it represents the elastic energy stored in the polymer.

Having  $G'$  and  $G''$  at different frequencies, the relaxation spectrum of the material can be calculated using Equation 3-9 and Equation 3-10. Nonlinear regression algorithms were used to solve Equation 3-9 and Equation 3-10. A broader relaxation spectrum is expected from LCBPP [16].

$$G'(\omega) = \sum_{i=1}^N H(\lambda_i) * \frac{(\omega\lambda_i)^2}{1 + (\omega\lambda_i)^2} \quad \text{Equation 3-9}$$

$$G''(\omega) = \sum_{i=1}^N H(\lambda_i) * \frac{(\omega\lambda_i)}{1 + (\omega\lambda_i)^2} \quad \text{Equation 3-10}$$

Using data points acquired from oscillatory shear rheometry, the complex viscosity ( $\eta^*$ ) versus frequency ( $\omega$ ) can be obtained. Rheological models were used to fit these data points and estimate the zero shear viscosity. The Cross model (Equation 3-11) can be fitted on  $\eta^*$ - $\omega$  data to calculate the parameters that characterize rheological behaviour of the linear and the long chain branched polymers [29, 30].

$$\eta^*(\omega) = \frac{\eta_0}{1 + (\lambda\omega)^n} \quad \text{Equation 3-11}$$

In Equation 3-11,  $\eta_0$  is the zero shear viscosity,  $\lambda$  is the relaxation time whose reciprocal accounts for the onset of non-Newtonian or shear thinning behaviour, and  $n$  is the power-law index describing shear thinning behaviour.

$\eta_0$  is the Newtonian viscosity which is the limiting value of the complex viscosity at very low shear rates where the polymer melt behaves in a Newtonian way. It is known that the zero shear viscosity of the linear PP depends on  $\overline{M}_w$  according to Equation 3-12 [16].

$$\log \eta_0 = \log (K) + a \log \overline{M}_w \quad \text{Equation 3-12}$$

In Equation 3-12, K and a are constants; for linear PP,  $\log K = -15.4$  and  $a = 3.5$  at 190 °C. However, it was found that LCBPP deviates from Equation 3-12 with the factor of  $\eta_{0(\text{branch})}/\eta_{0(\text{linear})}$  at the same molecular weight. Thus, as the LCB increases, this deviation increases [16]. The magnitude of the deviation can also be used to compare structural differences due to the presence of long chain branches. For example, a tree-like branching structure results in lower  $\eta_0$  values than what Equation 3-12 predicts at the same molecular weight ( $\overline{M}_w$ ), while a star-shape branching structure results in  $\eta_0$  values that are larger than what Equation 3-12 predicts for the same  $\overline{M}_w$  [5, 16].

Nam et al. [29] used shear and elongation rheometry to quantify the effect of long chain branches on the behaviour of different grades of PP, having the same  $\overline{M}_w$  and PDI with different degrees of LCB. It was found that long chain branched PP (LCBPP) has higher zero shear viscosity ( $\eta_0$ ) than the linear one. On the other hand, longer Newtonian plateau and less shear thinning behavior in the complex viscosity versus frequency graphs of the linear PP were evidenced. Their observations indicated that large efficiency of long chain branching results in greater amounts of storage modulus ( $G'$ ) at lower frequencies when compared to linear PP. But this trend changes at high frequencies because at this range of frequencies the polymer molecular weight is more critical than its topology (degree and structure of branching) [29]. Also, according to Equation 3-7 and Equation 3-8 a certain relation is expected for  $G'$  or  $G''$  versus angular frequency at the terminal region. For linear PP (LPP), the dependency of  $G'$  on angular frequency is quadratic, while  $G''$  has a linear relation with the angular frequency. Deviation from this trend to lower slopes is expected for the LCBPP.

Another way for characterizing the presence of LCB is through Cole-Cole plots ( $G'$  vs.  $G''$ ). By forming Cole-Cole plots for different PP grades, the amount of LCB can be compared qualitatively by looking at the separation of the curves at lower frequencies.

Tian et al. [30] used parallel plate rheometry to quantify the number of long chain branches in the PP. The modified PP was prepared by the addition of polyfunctional monomers as grafting agents using peroxide initiators. They stated that GPC is not sensitive to high molecular weight species at low concentrations and long chain branched molecules are within this slice of the molecular weight distribution. They first monitored the batch mixer torque and concluded that after the addition of the additives and after complete melting, the torque stayed constant for a while. However, an increase in the torque was observed due to the reaction in the runs with the grafting agents. It was also evidenced that the runs that contained grafting agents had higher torque compared to the runs that contained only PP and peroxide.

After preparing long chain branched PP with different levels of the grafting agent, they used parallel plate rheometry to quantify the number of long chain branches. They used the Cross model (Equation 3-11) and again observed that the long chain branched PP has a higher relaxation time, a lower “ $n$ ” and a greater value for  $\eta_0$  compared to the linear PP. They also found lower values of the loss angle ( $\tan \delta$ ) for the long chain branched PP. It was also found that the  $\tan \delta$  will stay constant with respect to the angular frequency. This is because the long chain branched polymer, like the crosslinked polymer, behaves more as a viscoelastic solid material and has less damping and viscous-like behaviour.

By plotting  $\eta''$ - $\eta'$ , Tian et al. [30] observed that samples containing LCB in their structure show a deviation from the virgin PP and the degraded PP.  $\eta''$ - $\eta'$  plots of the long chain branched PP yielded curves (responses) higher than the linear PP.

They also plotted the weighted relaxation spectrum ( $\log(\lambda H(\lambda))$  vs.  $\lambda$ ) of the linear, the degraded and the long chain branched PP. Figure 3-1, shows the weighted relaxation spectrum for different PP grades. The star shaped and the full bullet data points in Figure 3-1 show the relaxation time for the virgin and the degraded PP samples. These two samples only have one relaxation time called linear relaxation time ( $\tau_L$ ). It can be seen that

all other runs show another longer relaxation time besides the linear relaxation time due to the presence of long chain branched molecules. This second relaxation time is called characteristic relaxation time, and is due to the presence of long chain branches ( $\tau_B$ ). While the linear relaxation time is the same for runs D0 to D5, the characteristic relaxation time depends on the degree of the LCB. Therefore, samples with a higher degree of LCB show a longer characteristic relaxation time [30].

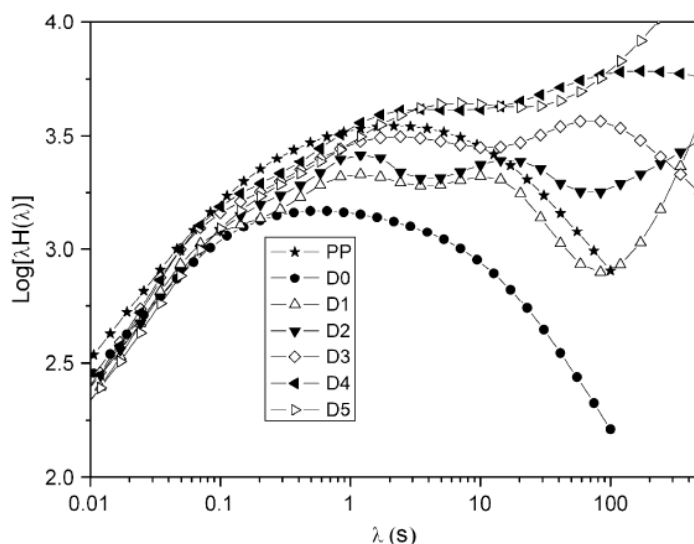


Figure 3-1: Weighted relaxation spectrum for virgin and LCB PP; copied from [30]

Determining rheological polydispersity indices is another method to assess the molecular properties of polymers via rheology [31]. The most useful indices for characterization of the modified PP MWD distribution are PI, separation modulus (ModSep) and ER. These indices can be obtained using Equation 3-13, Equation 3-14 and Equation 3-15 [32].

$$PI = \frac{10^5}{G_c(\text{Pa})} \quad \text{Equation 3-13}$$

$$ModSep = \frac{\omega'}{\omega''} \quad \text{Equation 3-14}$$

$$ER = C_1 G' \text{ at } G'' = 500 \text{ Pa} \quad \text{Equation 3-15}$$

PI is the so-called rheological "polydispersity index", ModSep stands for "Modulus Separation" and ER is another polydispersity index, more indicative of the high molecular weight end, as introduced by Shroff and Mavridis [32]. These useful rheological polydispersity indices relate to MWD breadth and branching.  $G_c$  in Equation 3-13 is the crossover modulus, which is the modulus at which  $G'$  and  $G''$  are equal. In Equation 3-14,  $\omega'$  and  $\omega''$  are the angular frequencies when  $G'$  and  $G''$  are equal to 1000 Pa. In Equation 3-15,  $C_1$  is the slope of the  $\log(G')$  versus  $\log(G'')$  curve.

In Equation 3-13 and Equation 3-14, PI correlates inversely with  $G_c$  and ModSep shows the  $G'$  and  $G''$  distance from each other at a specific modulus (1000 Pa). It is expected that the values of PI and ModSep reflect the MWD of the runs, while ER is only sensitive to the high MW end of the MWD (essentially, it is the polydispersity of the high molecular weight chains) [32]. Justifications for using these indices to correlate polymer rheology to MWD are given in Appendix A.

Finally, in order to summarize the main literature remarks on the correlation between polymer molecular structure and different rheological indicators, Table 3-1 has been constructed. Table 3-1 compares the rheological behavior expected from linear PP (degraded) with LCBPP.

Table 3-1: Summary of literature remarks for assessing LCB or degradation in the runs

Response	Polymer conformation	References
n	Increase in n: narrowing MWD along with degradation Decrease in n: LCB and/or broadening MWD	[30]
$\eta_0$	Increase in $\eta_0$ : increase in MW and/or LCB Decrease in $\eta_0$ : decrease in MW (degradation)	[4, 24]
$\lambda$	Increase in $\lambda$ : broader MWD and/or LCB Decrease in $\lambda$ : narrower MWD	[4, 24]
PI	Increase: broader MWD Decrease: narrower MWD	[32]
ModSep	Increase: narrower MWD Decrease: broader MWD	[32]
ER	Increase: broader distribution of the high molecular weight chains and/or LCB Decrease: narrower distribution of the high molecular weight chains and/or degradation	[32]
$G' - \omega$	The slope of Log $G'$ -Log $\omega$ graph at terminal region is 2 for linear polymer Deviation to lower slopes is an indication of LCB Larger $G'$ at low $\omega$ : LCB and/or CL	[4, 24, 30]
$G'' - \omega$	The slope of Log $G''$ -Log $\omega$ graph at terminal region is 1 for linear polymer Deviation to lower slopes is an indication of LCB	[4, 24, 30]
Cole-Cole plot ( $G'-G''$ )	Above the linear reference sample: high MWD and/or LCB Below the linear reference sample: lower MWD	[32]
$\tan\delta - G^*$	Above the linear reference sample: high MWD and/or LCB Below the linear reference sample: lower MWD	[15, 32, 33]

### 3.1.1 EXTENSIONAL RHEOMETRY

In order to observe the effect of the presence of long chain branches on all aspects of viscoelastic properties, extensional rheometry is needed to be conducted along with shear rheometry [34, 35]. The reason is that the strain hardening behavior, expected from LCBPP, is reflected in the extensional melt viscosity of the polymers. During extensional rheometry, the polymer melt is stretched via a uniform, extensional strain rate called

Hencky strain rate ( $\dot{\epsilon}$ ). The resulted deformation (Hencky strain) is the ratio of final to initial length of the stretched polymer melt.

$$\epsilon_H = \frac{l(t)}{l_0} \quad \text{Equation 3-16}$$

Extensional viscosity ( $\eta_E$ ) can be found using the ratio of extensional stress to the Hencky strain rate.

Different instruments were developed to evaluate the extensional viscosity of the polymers. The common concept among all these techniques is stretching of a polymer melt at constant elongation rates. Meissner [36] developed horizontal rotary clamps, which stretch a rod-like polymer melt in a silicon oil bath (Figure 3-2). Since rotary clamps transfer the material continuously, no necking will be developed in the samples [36, 37].

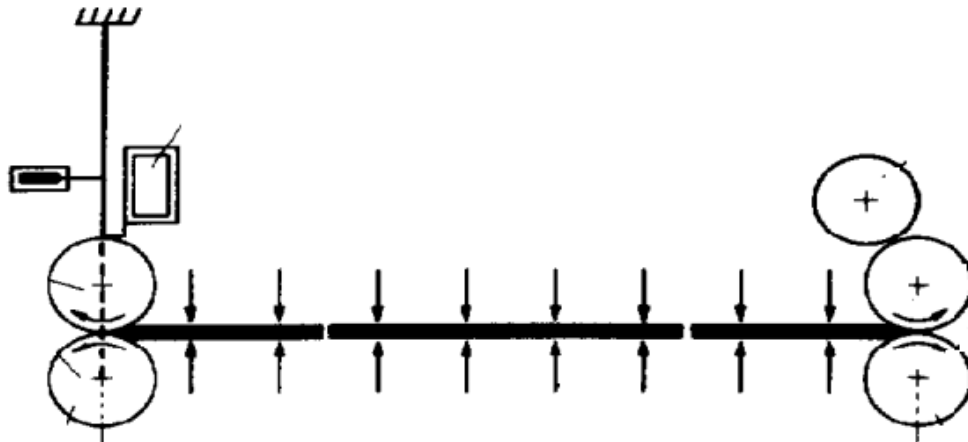


Figure 3-2: Schematic figure of Meissner extensional rheometer; copied from [36]

Münstedt [38] designed another piece of equipment which stretches the polymer melt during a vertical suspension (the sample is heated up in an oil bath). The advantage of this technique compared to the Meissner horizontal stretch equipment is that the effect of friction of the pulleys will be minimized and smaller sample size is required. Münstedt extensional rheometer is shown in Figure 3-3.

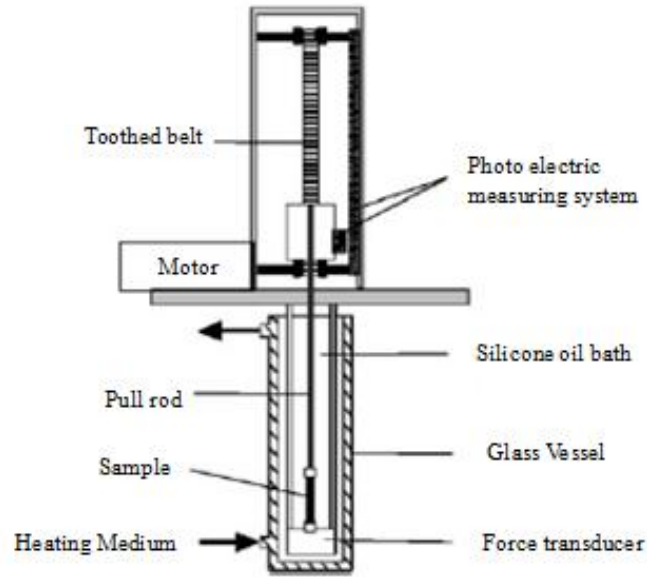


Figure 3-3: Schematic figure of the Münstedt design [38]

The other technique for measuring extensional flow properties, which is also based on the Meissner uniaxial extensional rheometer, is the Sentmanat extensional rheometer (SER) (Figure 3-4). It has two parallel drums which draw a rectangular molten polymer sample and the uniaxial stress growth coefficient or transient extensional viscosity ( $\eta_E^+$ ) is measured over time using Equation 3-17 [39].

$$\eta_E^+ = \frac{T(t)}{2A(t)R\dot{\epsilon}} \quad \text{Equation 3-17}$$

In Equation 3-17,  $T(t)$  is the time dependent torque of the cylinder rotating with rotational rate of  $\Omega$ .  $R$  is the cylinder radius and  $A(t)$  is the cross-section area of the sample. In the Sentmanat setup,  $\dot{\epsilon}$  (Hencky strain rate) can be calculated via Equation 3-18.

$$\dot{\epsilon} = \frac{2\pi R}{L_0} \quad \text{Equation 3-18}$$

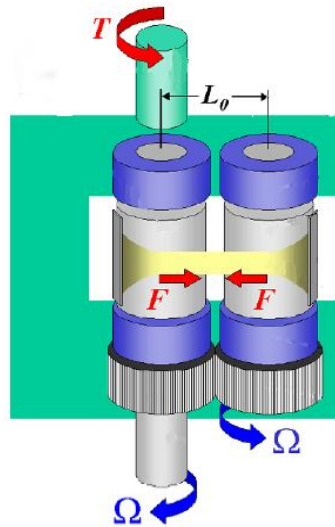


Figure 3-4: Sentemanat extentional rheometer; copied from [40]

### 3.2 GEL PERMEATION CHROMATOGRAPHY (GPC)

A polymer consists of chains with different chain lengths and hence molecular weights. GPC is a technique that fractionates polymer chains into slices (slices of the overall chromatogram) based on their hydrodynamic volume, which for linear chains corresponds to a specific molecular weight. The molecular weight and other properties of each slice can be determined using different detectors. For example, a laser light scattering can measure the absolute weight average molecular weight of each slice of polymer chains. Differential viscometers are other common detectors for GPC which can be used for measuring intrinsic viscosity of the (slices of the) chromatograms.

It is well known that GPC is not the most reliable tool for determining low degrees of long chain branching in PP [30]. However, one can still compare intrinsic viscosities of linear and branched PP and make qualitative (and some approximate quantitative) conclusions about the presence of long chain branches [41].

The mean squared radius of gyration  $R_g$ , is related to the intrinsic viscosity  $[\eta]$  of a polymer of molecular weight  $M$  in solution via Equation 3-19.

$$[\eta] \propto \frac{R_g}{M} \quad \text{Equation 3-19}$$

It is known that the presence of LCB leads to a lower end-to-end distance of a polymer chain and hence to a denser polymer coil. Thus, a lower intrinsic viscosity  $[\eta]$  and radius of gyration  $R_g$  will result for a long chain branched polymer compared to its linear counterpart of the same molecular weight. Therefore, in a plot of  $R_g$  or  $[\eta]$  versus  $M$ , the linear samples will show linear behaviour, whereas a branched polymer will start deviating from the linear behaviour (towards smaller values) at higher molecular weights. One can use these plots for each slice of the GPC chromatogram, thus creating a contrast between linear and branched structures [16, 42, 43].

For a more quantitative measure, the Zimm-Stockmayer branching parameter is used to determine number of branches in the polymer. This parameter represents the ratio of the mean squared radius of gyration of branched to linear polymer. The Zimm-Stockmayer branching parameter,  $g$ , can also be obtained from the ratio of intrinsic viscosity of branched to linear polymer (Equation 3-20) [41].

$$g = \frac{R_{g \text{ branch}}}{R_{g \text{ linear}}} = (g')^{1/\varepsilon} = \left( \frac{[\eta]_{\text{branch}}}{[\eta]_{\text{linear}}} \right)^{1/\varepsilon} \quad \text{Equation 3-20}$$

In Equation 3-20,  $\varepsilon$  is a constant between 0.5-1.5 for different branching configurations. Scoria et al. [43] presented theoretical functions for  $\varepsilon$  of different branching structures. This value is equal to 0.75 for randomly branched polymers. In Equation 3-20,  $g$  becomes lower than 1 for branched PP. Zimm and Stockmayer [44] suggested Equation 3-21 for the evaluation of the weight average number of long chain branches in a polymer ( $B_w$ ). This equation for a trifunctional randomly branched polymer is [44]:

$$g = \frac{6}{Bw} \left[ 0.5 \left( \frac{Bw}{7} \right)^{0.5} + \ln \left( \frac{(2 + Bw)^{0.5} + Bw^{0.5}}{(2 + Bw)^{0.5} - Bw^{0.5}} \right) - 1 \right] \quad \text{Equation 3-21}$$

By obtaining the Zimm-Stockmayer branching parameter  $g$  (Equation 3-20) first from GPC measurements, the weight average number of long chain branches is evaluated using Equation 3-21. The number of long chain branches per 1000 repeating units is subsequently obtained by Equation 3-22 [16].

$$N_{LCB} = 1000 * M_m * \frac{Bw}{M} \quad \text{Equation 3-22}$$

In Equation 3-22,  $M_m$  is the molar mass of the monomer unit and  $M$  is the molar mass of the branched molecules.

Using Equation 3-22 one can calculate  $N_{LCB}$  for each slice of the molecular weight distribution and plot it versus molar mass to find the degree of branching at each molecular weight slice.

### 3.3 NUCLEAR MAGNETIC RESONANCE (NMR)

$^{13}\text{C}$ NMR is another experimental technique, which has been used to determine number of branches, especially when the amount of branching is low. By using NMR not only number of branches could be found but also distribution and frequency of branching points in the polymer chain can be determined. These can be concluded from the difference between the chemical shift of LCBPP compared to the linear PP. Weng et al. [45] used  $^{13}\text{C}$ -NMR for PP characterization and attributed 4 peaks (starred peaks in Figure 3-5) to the presence of long chain braches in PP.

However, the main limitation of this technique is that  $^{13}\text{C}$ -NMR cannot distinguish between branches that have more than 6 carbon atoms. However, the effective length of long chain branches in PP (the length that affects rheological properties) is larger than 2000 g/mol [46]. Moreover, in order to distinguish a branch point from the other carbon atoms in the chain, long detection time is required. Thus, evaluating low amounts of LCB might be impossible due to detection limits. Despite these limitations, attempts were made to utilize

NMR in characterization of PP. In the very special cases where special chemical groups were incorporated in the branched structures, H-NMR was utilized to characterize number and distribution of long chain branches in PP [46].

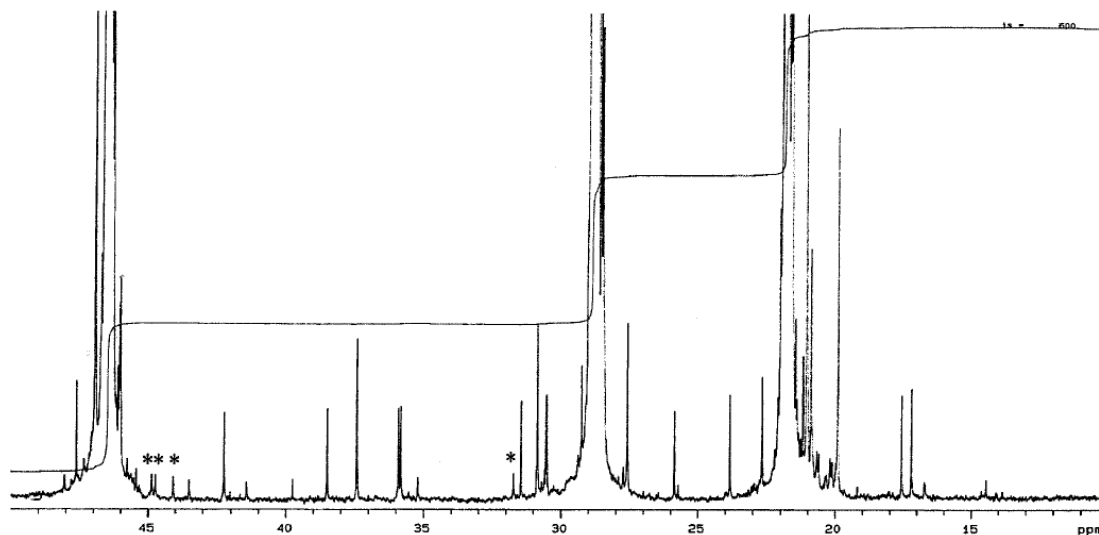


Figure 3-5:  $^{13}\text{C}$ NMR spectra for LCBPP; the stars are chemical shifts corresponding to LCBs in PP; copied from [45]

### 3.4 ELECTRON SPIN RESONANCE (ESR)

This technique can be used to investigate radical types, radical concentration, and the changes of the radical concentration with time in the system. Zhou and Zhu [47] used this technique to obtain radical concentrations during degradation of PP using peroxide initiators. They conducted their experiments at different temperatures and estimated the rate constant for radical termination and its dependence on temperature. The main limitation of this technique is that it is not sensitive to low radical concentrations. Zhou and Zhu [47] calibrated ESR signal amplitudes with a reference (inhibitor) chemical with a known concentration of radicals. Then, they measured radical concentrations during the decay of the signal. They used the rate of radical consumption equation (Equation 3-23) to estimate

the rate constant for radical termination ( $K_t$ ) by substituting the radical concentration ( $[P^*]$ ) in Equation 3-23.

$$\frac{d[P^*]}{dt} = 2fK_d[s] - K_t[P^*]^2 \quad \text{Equation 3-23}$$

In this equation,  $K_d$  is the rate constant of initiator decomposition,  $f$  is the peroxide decomposition efficiency factor and  $[s]$  is the initiator concentration [47].

Qu et al. [48] used spin-traps during polyethylene (PE) crosslinking to stabilize the radicals with a short lifetime. They used nitroso-compounds as spin traps to stabilize the radical intermediates. A photoinitiator was used to generate free radicals for PE modification. Nitroso-compounds were mixed with PE and photoinitiator and loaded into the ESR cell. They irradiated the samples inside the ESR using a UV lamp and finally characterized the radical intermediates that were detected during and after irradiation [48].

### 3.5 CONCLUDING REMARKS

Rheological measurements are found to be one of the most efficient and reliable techniques for PP characterization. However, since most indications of formation of long chain branches overlap with a broadening in the MWD, it is necessary to use at least one additional characterization technique to confirm formation of long chain branches. A multiple detector GPC is another characterization technique, which can be used for characterization of PP. The radius of gyration of LCBPP is smaller than that of linear PP at the same molecular weight. Hence, the amount of deviation from the linear reference can be used to calculate the number of branch points in the chains.

Another effective method is utilizing extensional rheology measurements and finding extensional viscosity. Presence of even small number of branches can lead to significant increase in the extensional viscosity and strain hardening behavior.

## **4 CHAPTER 4: DETERMINATION OF EFFECTS OF DIFFERENT PROCESSING VARIABLES IN PP PHOTOMODIFICATION**

In this chapter, a technique has been developed to modify the melt properties of polypropylene (PP). Photoinitiators along with UV irradiation were employed to introduce long chain branching (LCB) and/or crosslinking (CL). Statistically designed experiments were carried out to study the effect of processing conditions, such as photoinitiator concentration, duration of irradiation, UV lamp intensity, cooling air pressure, and photoinitiator type, on rheological properties, molecular weight characteristics and branching level. Samples were evaluated through linear viscoelastic (LVE) measurements, extensional rheometry, gel content, gel permeation chromatography (GPC), and differential scanning calorimetry (DSC). Results clearly indicated that PP can be successfully modified in order to enhance strain hardening behavior without significant gel formation.

The results presented in this chapter have led to the submission of a provisional patent application [52].

### **4.1 INTRODUCTION**

Polypropylene (PP) is one of the most common thermoplastics in the plastics industry with numerous applications ranging from household appliances to automotive interiors. Each application requires a specific PP grade with a specific average molecular weight (MW) and polydispersity index (PDI). PP molecular weight and PDI affect the melt flow behaviour, processing characteristics and eventually the final applications of PP.

However, its use is limited in applications requiring significant melt strength. Thus, modifying the molecular structure and enhancing strain hardening of PP melt, can lead to uses in areas such as foaming, thermoforming, extrusion coating and blow moulding [4]. The high melt strength of a polymer is either due to long chain branching (LCB) or high MW [5].

Hence, attempts have been made over the years to introduce LCB to PP chains. Methods such as electron beam radiation, gamma radiation or utilizing peroxides in the presence of coagents (like styrene or allylic and acrylic multi-functional monomers) have been utilized to impart LCB and increase the number of long chain branches in the PP chains.

Electron beam radiation of PP has been used extensively to modify its melt strength. Linear PP pellets are irradiated in a vessel with electrons generated by an electron beam accelerator [10, 16-18]. Irradiation of PP is carried out under N<sub>2</sub> atmosphere to discourage chain scission as much as possible. Then, irradiated PP samples are heated at an elevated temperature to bring the entrapped radicals in the crystalline domains into the interface between crystalline and amorphous regions. This is done to encourage bimolecular termination of the trapped radicals, which leads to formation of long chain branches [16, 18].

Another technique for rheology modification and increasing of the melt strength of PP is using gamma radiation. In this method, energetic ions and excited states are produced using Cobalt 60 as a gamma ray source. However, good control is lost due to the intensity of gamma radiation. As a result, gamma irradiation can also abstract hydrogens from the PP backbones and cause  $\beta$ -scission [18, 19].

Peroxide initiators have been used along with coagents such as triallyl trimesate (TAM), trimethylpropane triacrylate (TMPTA) and triallyl phosphate (TAP) to modify the rheology of PP by introducing LCB. This technique is popular since it is less expensive (and less energy intensive) than the previous radiation techniques. The effects of allylic and acrylic coagents on molecular weight and branching distribution were studied by comparing shear and elongation viscosities. It was found that a mix of degraded chains, slightly branched polymer chains and hyper-branched chains, which can only be formed after the gel point, were present in the polymer melt when coagents were used [6, 7].

The following mechanism has been suggested for the reaction between PP, peroxide and coagent. After PP macro-radicals are formed because of the presence of the peroxide initiator, they will attack the carbon double bond on the coagent, and then a stable radical adduct will be formed. This stable intermediate radical adduct is protected from  $\beta$ -scission.

In addition, the hydrogen on this intermediate adduct can react with other degraded polymer chains. These degraded polymer chains are produced from the initial  $\beta$ -scission reaction and contain a terminal double bond. These terminal double bonds react with the intermediate radical adducts, leading to the formation of long chain branches and/or crosslinks. Eventually, the final PP structure will be a function of the yield and the selectivity of the peroxide in the degradation reaction and the coagent that assists in the crosslinking (CL) step [6].

Yet another technique that can be employed is UV radiation. UV radiation is a cheaper and safer process for generating free radicals in PP and modifying its molecular structure. In this method, PP is mixed with photoinitiators and UV energy is utilized to activate the photoinitiator. After activation with UV radiation, these initiators can abstract hydrogens from the PP backbone. Hydrogen abstraction will be followed by scission and degradation of PP chains. Degradation of PP using UV energy along with photoinitiators was successful in a twin screw extruder to decrease the polydispersity index (PDI) of PP and produce controlled rheology PP [20]. In addition, in order to control the degradation level of PP in the melt state and form long chain branched PP (LCBPP) for foaming applications, multi-functional acrylic coagents were used along with photoinitiators. The radiation was carried out in the last two zones of a twin screw extruder by using a transparent barrel [49].

In other applications, Zamotaev et al. [50] investigated the effect of different photoinitiators and coagents on the amount of gel formed in PP films radiated with UV energy. Moreover, different photoinitiators along with coagents were used to introduce LCB to linear PP and increase its melts strength [51]. In our work [52] (Chapter 4), PP was modified by UV radiation without applying any coagents. Modification was done in the solid state and degradation was controlled by manipulating several variables: conditions such as photoinitiator concentration, duration of radiation, UV lamp intensity, cooling air pressure and type of photoinitiator all affected the formation of the long chain branches on the PP backbone.

In this chapter, we present results on the effects of the process operating conditions (photoinitiator concentration, duration of radiation, UV lamp intensity, cooling air pressure,

type of photoinitiator, and combinations thereof), in order to identify regions that maximize the LCB level in the PP structure. Since linear viscoelastic (LVE) properties are known to be affected significantly by changes in polymer molecular structure characteristics such as LCB, MW and molecular weight distribution (MWD), these properties are tracked in order to achieve the desired LCB balance. After an optimizing experimental design, extensional viscosity, gel content, MWD and crystallinity of these runs are discussed selectively in order to confirm the presence of LCB (and/or CL) in different samples.

## 4.2 EXPERIMENTAL

### 4.2.1 DESIGN OF EXPERIMENTS

The processing condition/variables chosen to be studied are given in Table 4-1, along with their selected levels. These factors will be referred to as A to E.

Table 4-1: Selected factors and ranges

Factor	Process variable (units)	Ranges
A	Photoinitiator concentration (wt %)	0.1-0.5 (with respect to polymer mixture)
B	Duration of radiation (s)	120-600
C	UV lamp intensity (%)	47-100 (with respect to total lamp intensity)
D	Cooling air pressure (%)	0-100 (with respect to total air flow pressure)
E	Type of photoinitiator (N/A)	BPH and DEBPH

In Table 4-1, factor A levels are with respect to total weight in the polymer mixture. These ranges for photoinitiator concentration are typically found in the literature [20] and chosen based on preliminary screening experiments. Factor C, the UV lamp intensity, was adjusted as a percentage of the total UV lamp intensity, which was  $1.42 \text{ W/m}^2$  at a distance of 1.3 cm from the lamp. Factor D, the cooling air pressure, was expressed as a percentage of the total available air flow (line) pressure (which was 8247 kPa), and adjusted via a pressure regulator. Cooling air pressure was used as a surrogate variable in order to control temperature during the radiation. Of course, an increase in lamp intensity (factor C) and

decrease in cooling air pressure (factor D) result in a higher temperature level. For all experimental trials, and within the putative range of factors C and D, the temperature level (of the environment) beneath the lamp varied between 35 to 146 °C. The average temperature levels during irradiation are cited in Table 4-2 for each experimental run. Finally, factor E, the photoinitiator type, included the choices of benzophenone (BPH) and 4,4' bis-diethylamino-benzophenone (DEBPH).

Based on the process variables and levels of Table 4-1, Design Expert 8 software (DesExp) was used to obtain the experimental runs (trials) of Table 4-2. The 32 runs of Table 4-2 are based on the D-optimal design option, which results eventually in models with minimum variance in their parameters with the minimum number of trials (D-optimality refers to the minimization of the determinant of the parameter variance-covariance matrix and is a standard criterion in statistical designs [53]). Of course, the experimental trials of Table 4-2 were conducted in a completely randomized order. The starred runs 6, 11, 18, and 22 are completely independent replicates of runs 7, 12, 19 and 23 respectively. The replicates were used to calculate pure error and construct empirical models based on the main factors and their interactions that significantly affect each response. These models were subsequently used to identify conditions which result in the highest LCB content.

The process response variables were the shear thinning index ( $n$ ), zero shear viscosity ( $\eta_0$ ), relaxation time ( $\lambda$ ) and rheological polydispersity indices (PI, ModSep and ER). These response variables, along with brief descriptions of sample preparation and other measurements, are discussed in the subsection below.

Table 4-2: Design of experiments for D-optimal design

Run ID	A	B	C	D	E	Temperature (°C)
1	0.5	120	47	0	BPH	74
2	0.25	300	47	0	BPH	74
3	0.1	600	47	0	BPH	73
4	0.1	120	100	0	BPH	126
5	0.1	120	100	0	BPH	126
6*	0.5	600	100	0	BPH	146
7	0.5	600	100	0	BPH	146
8	0.3	600	47	50	BPH	47
9	0.3	360	74	50	BPH	84
10	0.1	600	100	50	BPH	87
11*	0.1	120	47	100	BPH	35
12	0.1	120	47	100	BPH	36
13	0.5	600	47	100	BPH	41
14	0.26	600	79.2	100	BPH	59
15	0.5	120	100	100	BPH	62
16	0.1	378	100	100	BPH	55
17	0.5	120	47	100	DEBPH	34
18*	0.1	600	47	100	DEBPH	36
19	0.1	600	47	100	DEBPH	36
20	0.1	120	76	100	DEBPH	49
21	0.28	120	100	100	DEBPH	50
22*	0.5	600	100	100	DEBPH	50
23	0.5	600	100	100	DEBPH	50
24	0.1	120	47	0	DEBPH	60
25	0.5	600	47	0	DEBPH	61
26	0.1	402	69	0	DEBPH	97
27	0.5	302	67	0	DEBPH	96
28	0.35	422	100	0	DEBPH	128
29	0.1	600	100	0	DEBPH	128
30	0.5	120	100	0	DEBPH	128
31	0.3	360	74	50	DEBPH	93
32	0.1	120	100	50	DEBPH	93

## **4.2.2 MATERIALS AND SAMPLE PREPARATION**

PP homopolymer (Pro-fax PH 382M) from LyondellBasell with a melt flow rate (MFR) of 3.5g/10 min was used. Benzophenone (BPH), of 99% purity, was purchased from Sigma Aldrich and used as received. 4, 4'-bis-diethylamino-benzophenone (DEBPH), of 99% purity, was purchased from VWR and used as received. BPH and DEBPH were the two selected photoinitiators.

PP pellets along with photoinitiator were melt-mixed in a batch mixer at 190 °C and 100 rpm for 8 minutes. The samples were ground using a Wiley mill (model 1102, Arthur H. Thomas Co.). After grinding, PP-initiator blend granules were compression-moulded into discs with 25 mm diameter and 1 mm thickness at 190 °C under an applied force of 4,400 N for five minutes. The discs were subsequently irradiated using a mercury UV lamp (Versa Cure).

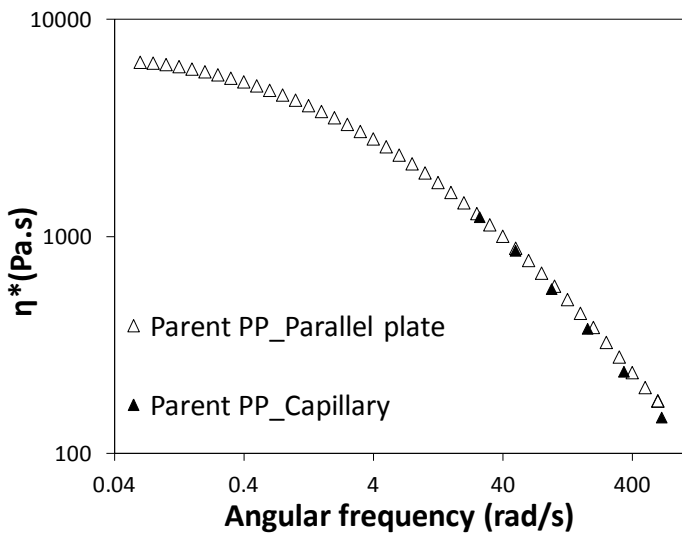
Prior to radiation of the samples, the lamp was turned on for two minutes so that a steady level of radiation intensity was achieved. During irradiation, pressurized air was used to cool down the area beneath the lamp.

## **4.2.3 CHARACTERIZATION**

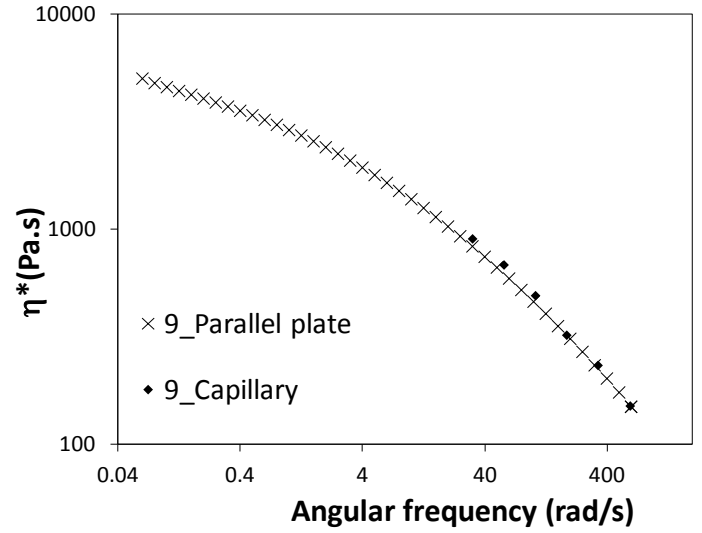
### **4.2.3.1 RHEOLOGICAL CHARACTERIZATION**

A stress-controlled parallel plate rheometer (AR2000, TA instruments) was used to measure the rheological properties of the irradiated samples at 190°C. Parallel plates with diameter of 25 mm were used for all shear tests. Strain sweeps were carried out to identify the linear viscoelastic region during the test (typically less than 1% strain over the whole frequency range). Frequency sweeps were subsequently performed in the range of 0.01-100 Hz at a constant strain of 0.9%. From these tests, storage modulus ( $G'$ ), loss modulus ( $G''$ ), complex modulus ( $G^*$ ), loss tangent ( $\tan \delta$ ), and complex viscosity ( $\eta^*$ ) were obtained at different angular frequencies ( $\omega$ ).

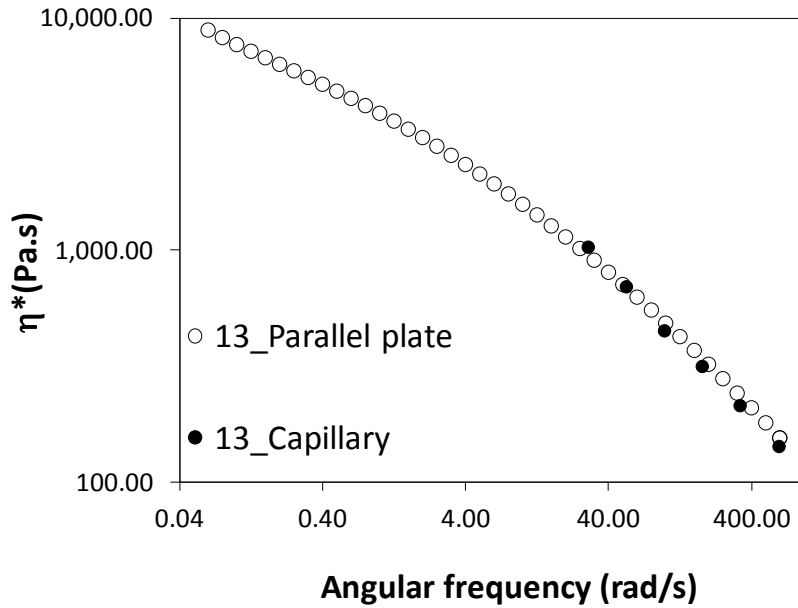
In order to check the validity of the Cox-Merz rule, capillary rheometry was conducted on runs 9, 13 and the parent PP (Figure 4-1 a, b and c). A bench top twin-bore Rosand capillary rheometer (RH2200 series) manufactured by Malvern was used to measure the shear viscosity. The validity of the Cox-Merz rule was confirmed, since parallel plate rheometry data ( $\eta^*$  vs.  $\omega$ ) were in agreement with capillary rheometry data (shear viscosity vs. shear rate). Figure 4-1 shows parallel plate, frequency sweep data ( $\eta^*$ - $\omega$ ), along with capillary shear viscosity versus shear rate data for runs 9, 13 and the parent PP. Thus, the Cross model (Equation 3-11) was fit on  $\eta^*$  vs.  $\omega$  data to determine the shear thinning index ( $n$ ), zero shear viscosity ( $\eta_0$ ) and relaxation time ( $\lambda$ ) of each sample.



a



b



c

Figure 4-1: parallel plate, frequency sweep data ( $\eta^*-\omega$ ) along with capillary shear viscosity versus shear rate data for a) parent PP, b) run 9 and c) run 13

PI, ModSep and ER were calculated using Equation 3-13, Equation 3-14 and Equation 3-15 for all of the runs and the results are presented and discussed in section 4.3.1.

The Sentmanat extensional rheometer (SER) universal testing platform (Xpansion instruments) was used to measure extensional flow properties in conjunction with a stress-

controlled rotational rheometer (MCR501 by Anton Paar). In this set-up, the uniaxial tensile stress growth coefficient ( $\eta^+_E$ ) is measured over time [39]. Experiments were performed at Hencky strain rates of 0.01, 0.1, 1 and 10 s<sup>-1</sup> at 180 °C. Linear viscoelastic (LVE) measurements were repeated at this temperature to find the linear viscoelastic envelope of ( $3\eta^+_0$ ) needed as a basis to identify strain hardening effects.. Strain hardening for long chain branched samples is exhibited by a positive deviation of  $\eta^+_E$  from ( $3\eta^+_0$ ).

#### **4.2.3.2 DETERMINATION OF GEL CONTENT**

The percent gel content of selected samples was found by extraction. The method followed is described in ASTM D2765-11. Approximately 0.3 g of a ground sample were placed in stainless steel 120 mesh pouches. The pouches were sealed and immersed in 350 ml of boiling xylene. 1 % antioxidant (Irganox 1010) was added to the solvent. After 12 hours, the stainless steel pouches were removed from the boiling solvent and dried out at 120 °C vacuum oven for 12 hours. The material remaining in the cage is the insoluble fraction (gel fraction) of the modified PP. The measurements were independently replicated at least once for each sample.

#### **4.2.3.3 GEL PERMEATION CHROMATOGRAPHY (GPC)**

High temperature GPC (Polymer CHAR (Spain)) was used to determine molecular weight (MW), molecular weight distribution (MWD), polydispersity index (PDI) and intrinsic viscosity [ $\eta$ ] of the runs. Refractive index, FTIR and viscometer detectors were employed to characterize each slice of the chromatogram. The GPC set-up had three columns in series (PLgel Olexis, mixed), and each column was 30 cm long with a diameter of 7.5 mm. 1, 2, 4-trichlorobenzene (TCB) was used as the GPC solvent at 135 °C. 13-15 mg of each sample was dissolved in 9 ml of TCB at 160 °C for 90 minutes. The solutions were inspected visually first for complete dissolution prior to injection. 250 mg/l Irganox 1010 was used as stabilizer. Each run was independently replicated once.

#### 4.2.3.4 THERMAL PROPERTIES

Differential scanning calorimetry (DSC) was used to determine the effect of UV treatment on the crystallinity of selective runs. Q2000 DSC controlled by a TA processor was used to conduct the DSC tests. The DSC conditions (sample size close to 5 mg) were as follows: Cycle 1: temperature sweep from 35 °C to 210 °C, heating rate of 20 °C min<sup>-1</sup>; Cycle 2: temperature sweep from 210 °C to 35 °C, cooling rate of 10 °C min<sup>-1</sup>; and finally, Cycle 3: temperature sweep from 35 °C to 210 °C, heating rate of 10 °C min<sup>-1</sup>. Cycle 1 is to erase the previous thermal history of the polymer, whereas Cycles 2 and 3 are used to determine crystallization and melting points. All cycles were done under 50 ml/min nitrogen. The DSC data were analyzed by Universal Analysis 2000 software (TA Instruments).

The percentage crystallinity of each sample was calculated as:

$$X_c = \frac{\Delta H_f}{\Delta H_f^{100\% \text{ crystalline PP}}} * 100 \quad \text{Equation 4-1}$$

In Equation 4-1,  $\Delta H_f$  is the melting enthalpy of the experimental sample in question, which is measured by integrating the area under the melting peak. The denominator represents the melting enthalpy of a 100% crystalline PP sample. This has been found to be 209 J/g for a 100% crystalline pure PP [54].

Melting temperature ( $T_m$ ), crystallization temperature ( $T_c$ ) and  $X_c$  were determined as complementary aids to study the effect of degradation and LCB on some of the modified samples and compare them with the parent PP.  $T_m$ ,  $T_c$  and  $X_c$  of the parent PP were 164 °C, 131 °C and 44.5%, respectively.

## **4.3 RESULTS AND DISCUSSION**

### **4.3.1 STATISTICAL ANALYSIS OF LVE PROPERTIES**

LVE properties such as  $n$ ,  $\eta_0$  and  $\lambda$  were determined by fitting Equation 3-11 to  $\eta^*$  vs.  $\omega$  data. In addition, rheology indices (PI, ModSep and ER) were determined using Equation 3-13, Equation 3-14 and Equation 3-15. These values are summarized in Table 4-3. Again, starred runs represent independent replicates of the runs below them, as per Table 4-2.

Table 4-3: LVE responses along with rheological polydispersity data for experimental runs

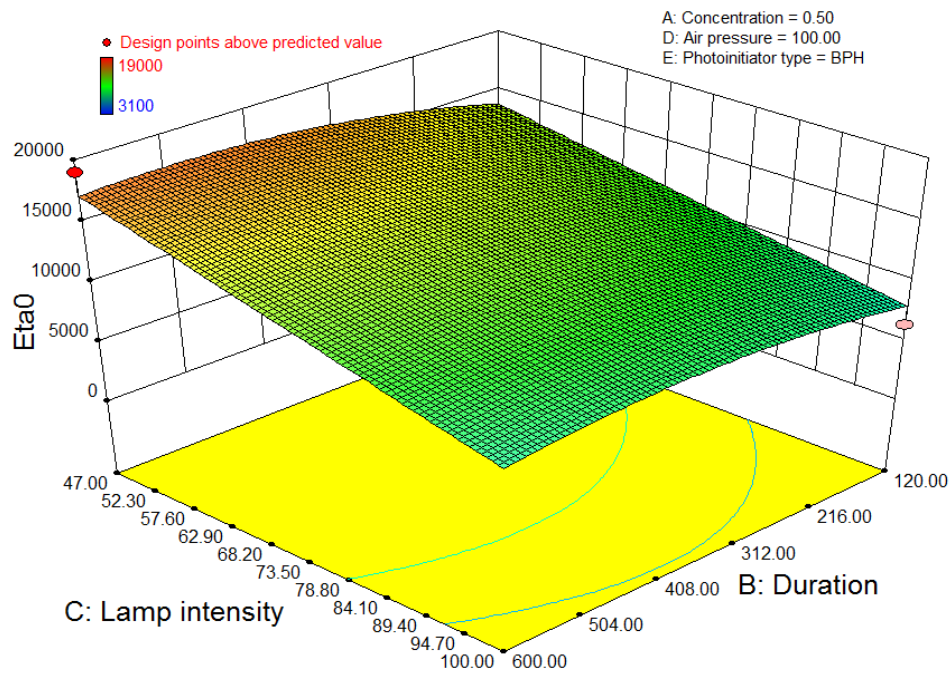
Run ID	n	$\eta_0$ (Pa.s)	$\lambda$ (s)	PI	ModSep	ER
1	0.51	5579	0.88	3.83	3.59	1.33
2	0.49	6430	2.03	4.30	3.19	1.78
3	0.50	5953	1.31	4.19	3.19	1.86
4	0.53	4491	0.59	4.03	3.46	1.52
5	0.55	3316	0.45	3.74	3.81	1.11
6*	0.50	6184	1.86	4.42	2.85	2.15
7	0.60	5800	0.70	4.80	2.87	1.88
8	0.48	8570	2.53	3.88	3.19	1.79
9	0.49	10000	14.87	5.19	2.71	2.89
10	0.58	3446	0.30	3.53	3.55	1.38
11*	0.54	4670	0.55	4.01	3.53	1.24
12	0.54	4871.5	0.48	3.66	3.74	1.16
13	0.46	19000	227.37	6.87	2.39	4.77
14	0.54	9079	2.40	4.87	2.83	2.18
15	0.52	6469	1.44	4.42	3.23	1.48
16	0.50	7479	1.99	3.97	3.45	1.36
17	0.59	5341	0.39	3.64	3.81	1.08
18*	0.60	3035	0.18	3.42	3.83	1.48
19	0.60	3191	0.19	3.30	4.04	1.35
20	0.58	5353	0.45	4.04	3.60	1.28
21	0.57	5251	0.42	3.77	3.72	1.12
22*	0.57	5902	0.53	3.70	3.60	1.21
23	0.58	6193	0.59	3.95	3.47	1.22
24	0.60	3819	0.33	4.84	3.48	1.31
25	0.56	5519	0.51	3.86	3.65	1.07
26	0.54	6456	0.69	3.58	3.59	1.26
27	0.57	5779	0.49	3.66	3.70	1.10
28	0.56	6802	0.88	4.65	3.37	1.66
29	0.54	10970	2.13	4.72	3.15	2.00
30	0.57	6652	0.59	3.86	3.59	1.25
31	0.56	5834	0.60	3.85	3.58	1.20
32	0.57	5613	0.46	3.68	3.68	1.11
PP	0.57	7828	0.67	3.58	3.68	1.19

Table 3-1 in section 3.1.1 of Chapter 3 summarizes literature remarks on the effect of LCB and degradation on LVE properties. This table was used as a road-map for qualitative analysis of the runs. By comparing the LVE properties of the experimental runs with the parent PP (designated as PP at the end of Table 4-3) and using Table 3-1, several diagnostic remarks can be made for each experimental trial (of Table 4-3). These remarks are cited in Table 4-4.

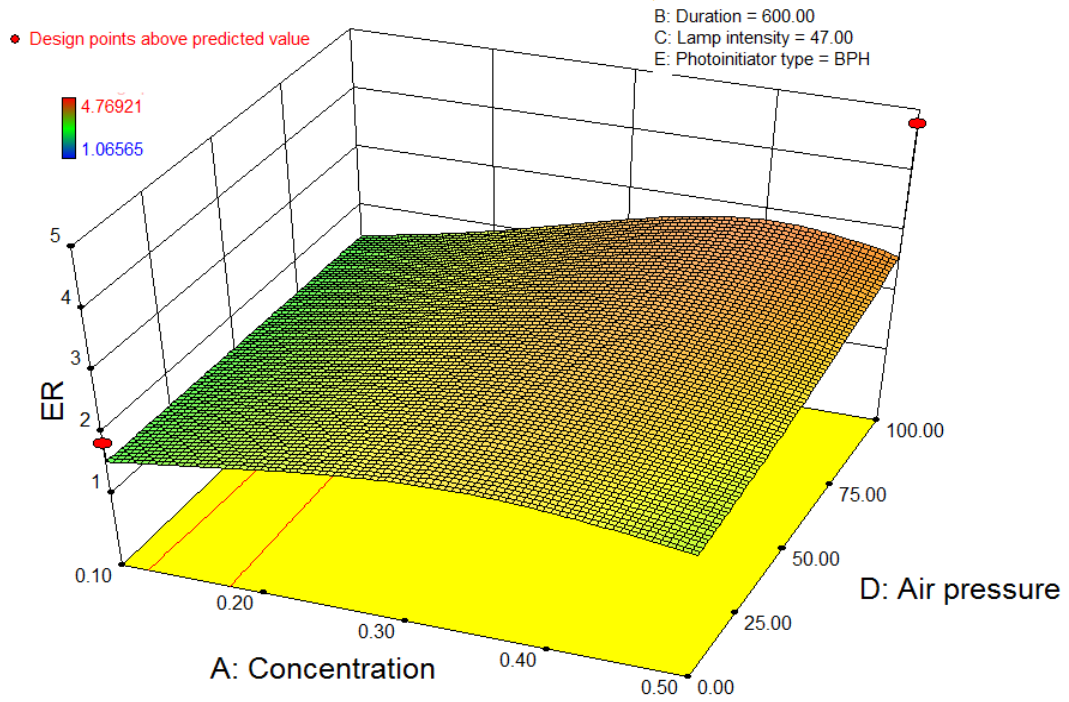
Table 4-4: Possible molecular structure (relative to parent PP) of the different runs based on LVE data

Run ID	Molecular structure
1	Possibility of very small amount of LCB and/or broadening MWD along with degradation, formation of shorter chains
2	Possibility of very small amount of LCB and/or broadening MWD along with degradation, formation of smaller chains
3	Possibility of very small amount of LCB and/or broadening MWD along with degradation, formation of shorter chains
4	Degradation, lower MW
5	Degradation, lower MW
6*	Possibility of very small amount of LCB and/or broadening MWD along with degradation, formation of shorter chains
7	
8	Possibility of LCB, crosslinking and/or broadening MWD
9	Possibility of LCB, crosslinking and/or broadening MWD
10	Degradation, lower MW
11*	Degradation, lower MW
12	
13	Possibility of LCB, crosslinking and/or broadening MWD
14	Possibility of LCB, crosslinking and/or broadening MWD
15	Possibility of very small amount of LCB and/or broadening MWD along with degradation, formation of shorter chains
16	Possibility of very small amount of LCB and/or broadening MWD along with degradation, formation of shorter chains
17	Degradation, lower MW
18*	Degradation, lower MW
19	
20	Degradation, lower MW
21	Degradation, lower MW
22*	Degradation, lower MW
23	
24	Degradation, lower MW
25	Degradation, lower MW
26	Degradation, lower MW
27	Degradation, lower MW
28	Possibility of very small amount of LCB and/or broadening MWD along with degradation, formation of shorter chains
29	Possibility of LCB, crosslinking and/or broadening MWD
30	Degradation, lower MW
31	Degradation, lower MW
32	Degradation, lower MW

Using Design Expert software, the best empirical fit was found via statistical analysis for each response variable. The empirical models and the procedure followed for choosing these models are summarized in Appendix B. Using these empirical models response surface graphs were constructed for each response variable. Figure 4-2 and Figure 4-3 show representative response surface graphs for  $\eta_0$  and ER. Other LVE properties such as  $n$  and  $\lambda$  show similar trends but are not shown here for the sake of brevity. In Figure 4-2 and Figure 4-3, red and pink (ellipsoid) dots correspond to the experimental values of the design points in Table 4-2. Pink dots correspond to the design points below the 3D empirical fit, while the red ones are the design points above the 3D empirical fit. Figure 4-2 (a) shows an example of factor levels for maximizing  $\eta_0$ . It can be seen that decreasing lamp intensity and increasing duration of radiation, when maximum cooling air pressure and the highest BPH concentration are applied, results in larger  $\eta_0$  values. The same conditions lead to a maximum ER value when BPH is used as photoinitiator (Figure 4-2 (b)). In order to confirm formation of long chain branches under the above mentioned conditions, runs 9 and 13 were chosen for complementary characterization tests. Run 13 (red dot) represents the maximum of the  $\eta_0$  and ER graphs (Figure 4-2 a and b). Run 9 (not shown in the processing window of Figure 4-2 a and b) also showed indications of LCB at the conditions close to the above mentioned maximum. In contrast, runs 10 (low concentration of BPH, radiated for long time with high intensity and low cooling air pressure) and 11 (low concentration of BPH, radiated for short time with low lamp intensity and high cooling air pressure) were chosen from the runs that exhibited dominant degradation for more characterization tests.



a

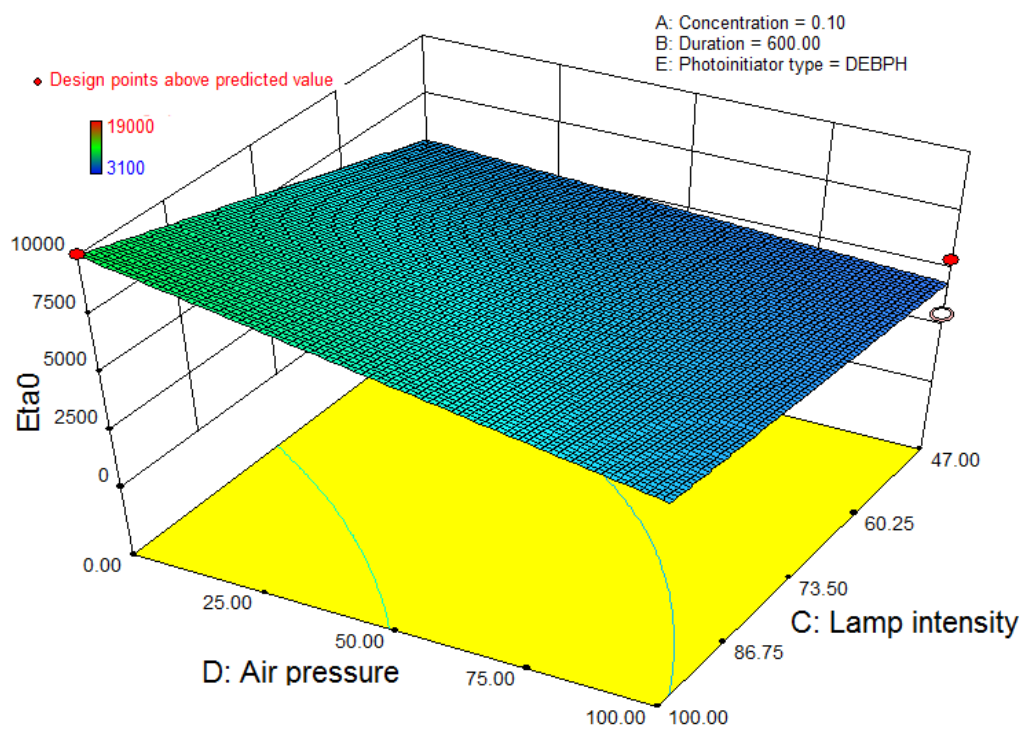


b

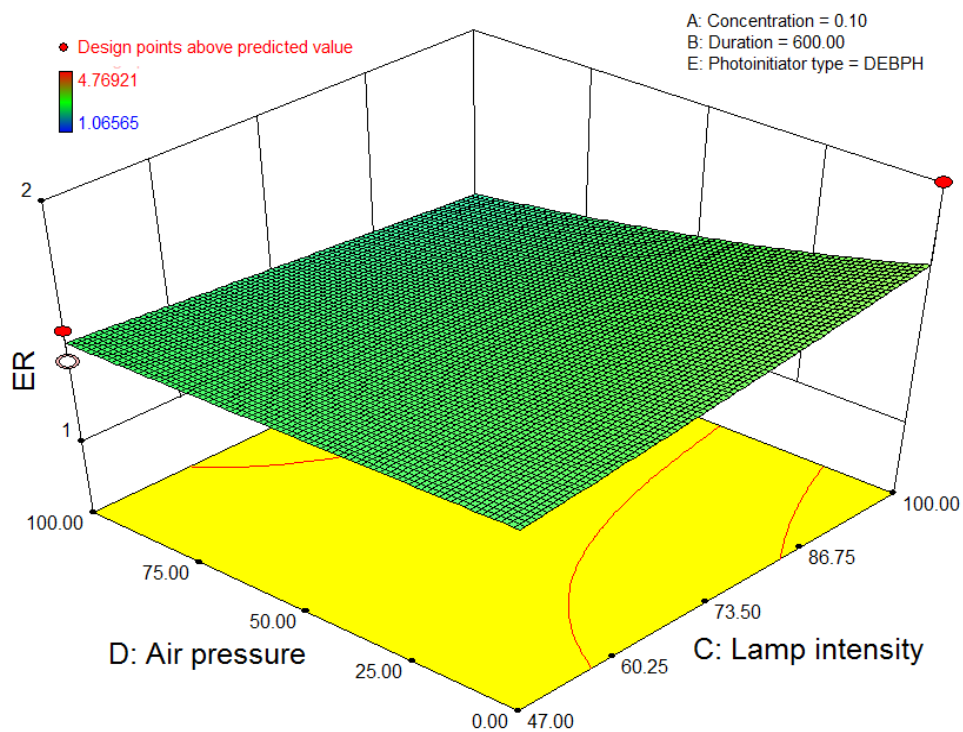
Figure 4-2: 3D response surface for  $\eta_0$  (a) and ER (b) when BPH is used

On the other hand, using DEBPH mostly results in degraded PP except when samples have the lowest concentration of DEBPH and are radiated for long durations (600 s). By decreasing the cooling air pressure and increasing lamp intensity,  $\eta_0$  and ER reach their highest values for this initiator (Figure 4-3). Although the above mentioned conditions result in the maximum of  $\eta_0$  and ER for DEBPH as photoinitiator, larger values for  $\eta_0$  and ER can be obtained using BPH at its optimum conditions (high concentration, long radiation duration, low lamp intensity and high cooling air pressure).

Run 29 (the red dot at the maximum of the  $\eta_0$  and ER graphs of Figure 4-3) was chosen among the runs prepared with DEBPH that shows indications of LCB. More detailed tests were thus conducted to confirm formation of LCB and/or CL using DEBPH at the above mentioned radiation conditions (see also Table 4-2).



a



b

Figure 4-3: 3D response surface for  $\eta_0$  (a) and ER (b) when DEBPH is used

### 4.3.1 OPTIMIZATION OF PROCESSING CONDITIONS FOR FORMATION OF LCBPP

The purpose of this section is to use the experimental results presented above in order to find optimal ranges of radiation variables for producing LCBPP. For this reason, certain specifications were set for the response variables of interest, such as  $\eta_0$ ,  $\lambda$ , ER and n. Table 4-5 shows these chosen specifications for determining the optimal conditions for LCB.

Table 4-5: Specifications chosen for each response variable to find optimal conditions

Response	Criteria
$n$	$<0.57$
$\eta_0$ (Pa.s)	$>7800$
$\lambda$ (s)	$>0.67$
ER	$>1.2$

The contour plots that correspond to these specifications were plotted with 95% confidence intervals. The optimal conditions for formation of LCBs (which satisfy the spec limits in Table 4-5) are indicated in bright yellow. The region in dark yellow represents 95% confidence intervals.

Figure 4-4 shows the optimal conditions when BPH was used as photoinitiator. It should be noted that these optimal conditions were found by setting the lamp intensity at 47 % and cooling air flow rate at its maximum.

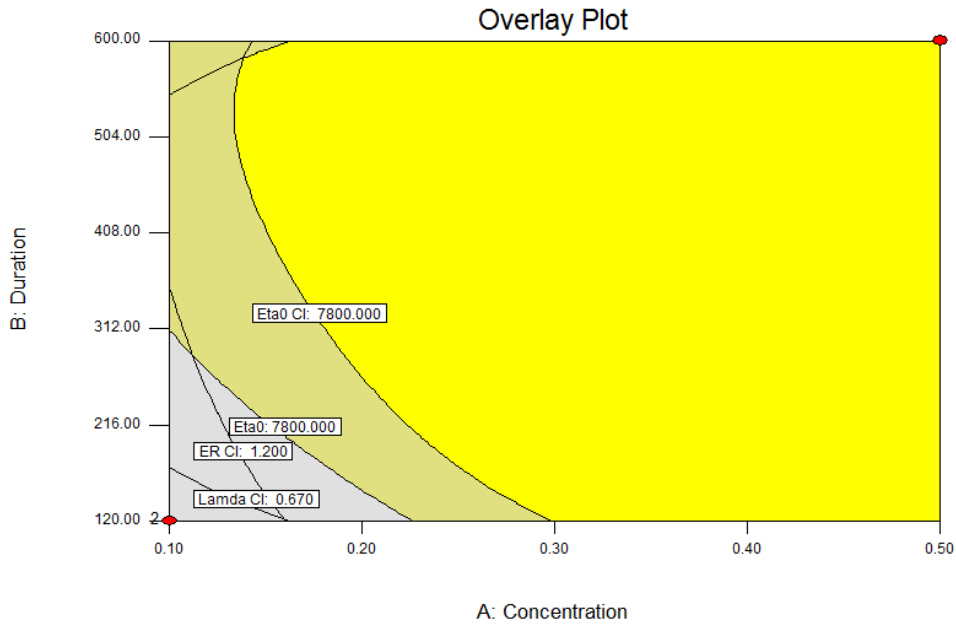


Figure 4-4: Processing window that maximizes degree of LCB using BPH

Figure 4-5 shows the conditions which satisfy the specs of Table 4-5 but when DEBPH was used as the photoinitiator. This region for DEBPH was found by setting the lamp intensity at its maximum (100%) when no cooling air was applied.

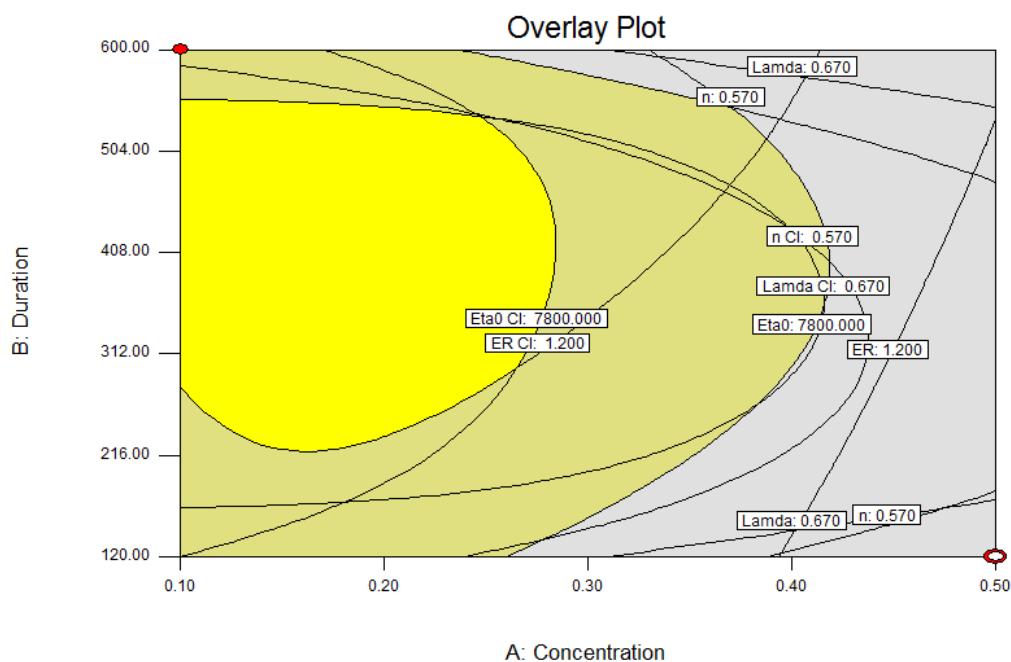


Figure 4-5: Processing window that maximizes degree of LCB using DEBPH

### 4.3.2 LVE GRAPHS OF SELECTED RUNS

In the previous section (section 4.3.1), LVE properties which were extracted from  $\eta^*$ ,  $G'$  and  $G''$  versus angular frequency ( $\omega$ ) graphs were analyzed to find conditions that result in the largest level of LCB. In this section, these graphs along with Cole-Cole plots and  $\tan \delta$  versus frequency information are analyzed more closely for selective runs. Other tests such as GPC, extensional rheometry and gel content determination were performed on the same representative runs to confirm formation of LCB or network or degradation. Among runs (see Table 4-2 to Table 4-4 for a summary of these runs along with brief commentary about the expectations from each run) that exhibited the potential for formation of branches or

network, runs 9, 13 and 29 were chosen. Run 29 was the only run, prepared via DEBPH, that showed indications of LCB. Runs 9 and 13 had the largest and second largest values of  $\eta_0$ ,  $\lambda$  and ER, respectively (see Table 4-3). Runs 10 and 11 were selected among the runs that showed a strong possibility for degradation, since the  $\eta_0$ ,  $\lambda$  and ER values of these runs were quite low (see Table 4-3). Figure 4-6 and Figure 4-7 show  $G'$  and  $\eta^*$  versus  $\omega$  for these runs in comparison to parent PP.

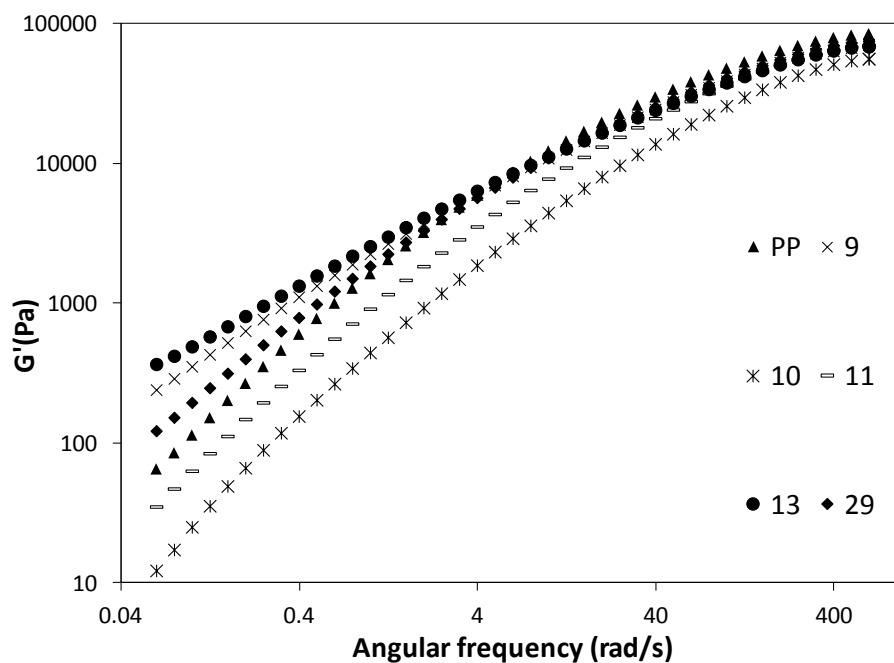


Figure 4-6: Storage modulus ( $G'$ ) versus angular frequency for runs 9, 10, 11, 13, 29 and parent PP

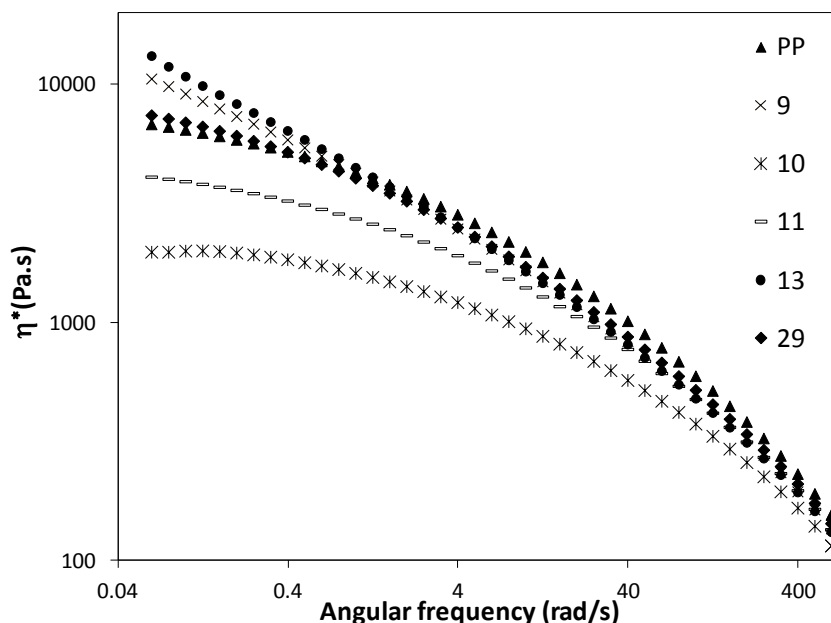


Figure 4-7: Complex viscosity ( $\eta^*$ ) versus angular frequency for runs 9, 10, 11, 13, 29 and parent PP

From Figure 4-6, it can be seen that runs 9, 13 and 29 have higher  $G'$  values in comparison to the parent PP. This is due to formation of structures in the polymer that are responsible for elasticity (LCB or CL). Figure 4-7 shows  $\eta^*$  versus  $\omega$  for these runs. Run 9, 13 and 29 show larger  $\eta^*$  values at low angular frequencies ( $\omega$ ). This is due to the presence of higher MW chains in their structure. Also, these curves are more shear sensitive (steeper slope of  $\eta^*$  versus  $\omega$ ) in comparison to parent PP and the ‘degraded’ runs (10 and 11). Both manifestations can be due to formation of LCB and/or broadening of MWD.

Figure 4-8 shows Cole-Cole plots. The ratio of  $G'$  versus  $G''$  is another indication for formation of LCB. Runs with broader MWD or runs with LCB in their chains deviate from linear PP (reference or parent PP) to higher  $G'$  values at low  $G''$  ranges (small frequencies). Run 9, 13 and 29 clearly show this deviation from parent PP (and the ‘degraded’ runs 10 and 11).

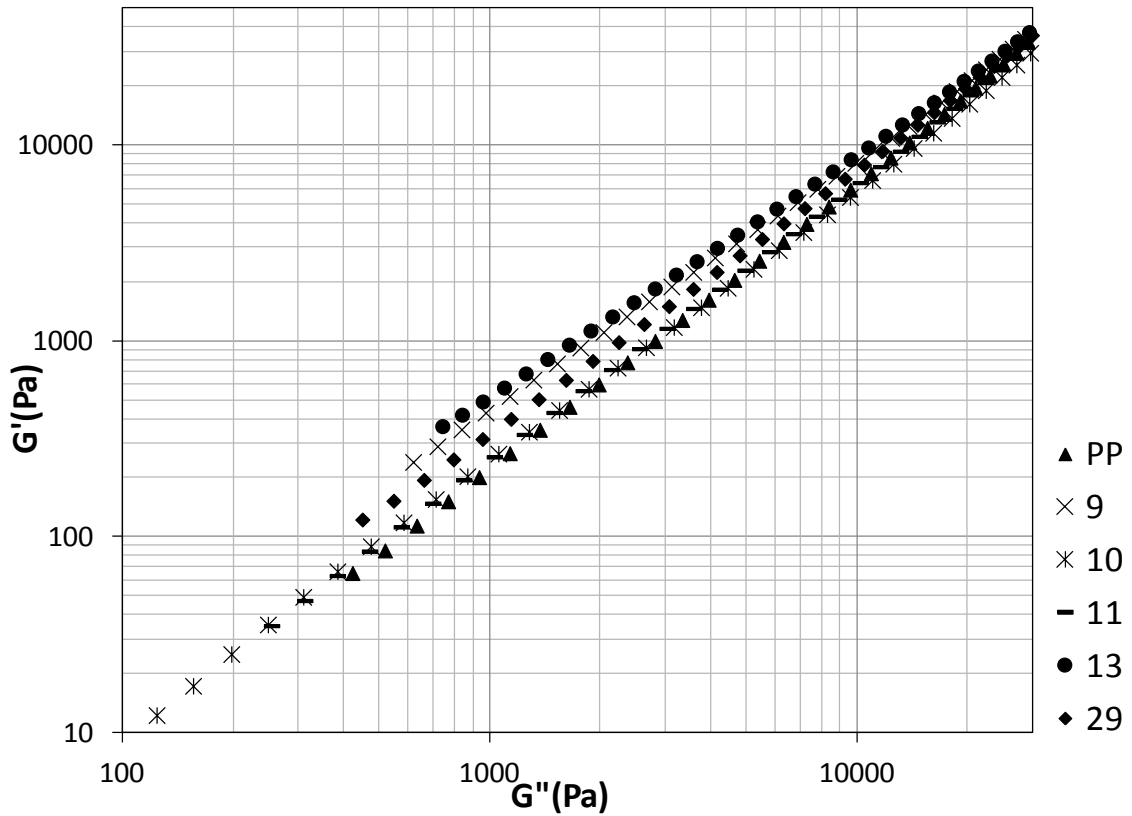


Figure 4-8: Cole-Cole plots for runs 9, 10, 11, 13, 29 and parent PP

For the final check, in this group of characterization tests, Figure 4-9 shows loss tangent ( $\tan \delta$ ) versus  $G^*$  for the same runs. Both Cole-Cole plots and  $\tan \delta$ - $G^*$  are affected by the PDI of the MWD rather than simply the MW.  $\tan \delta$ - $G^*$  plots are more sensitive to changes in MWD and LCB compared to Cole-Cole plots [32]. It can be seen that at low frequencies, runs 9, 13 and 29 that show signs of LCB have the lowest  $\tan(\delta)$ - $G^*$  curves compared to linear ‘degraded’ and parent PP. This again points to the direction towards the presence of long branches and/or broader MWD, as did Figure 4-8 earlier.

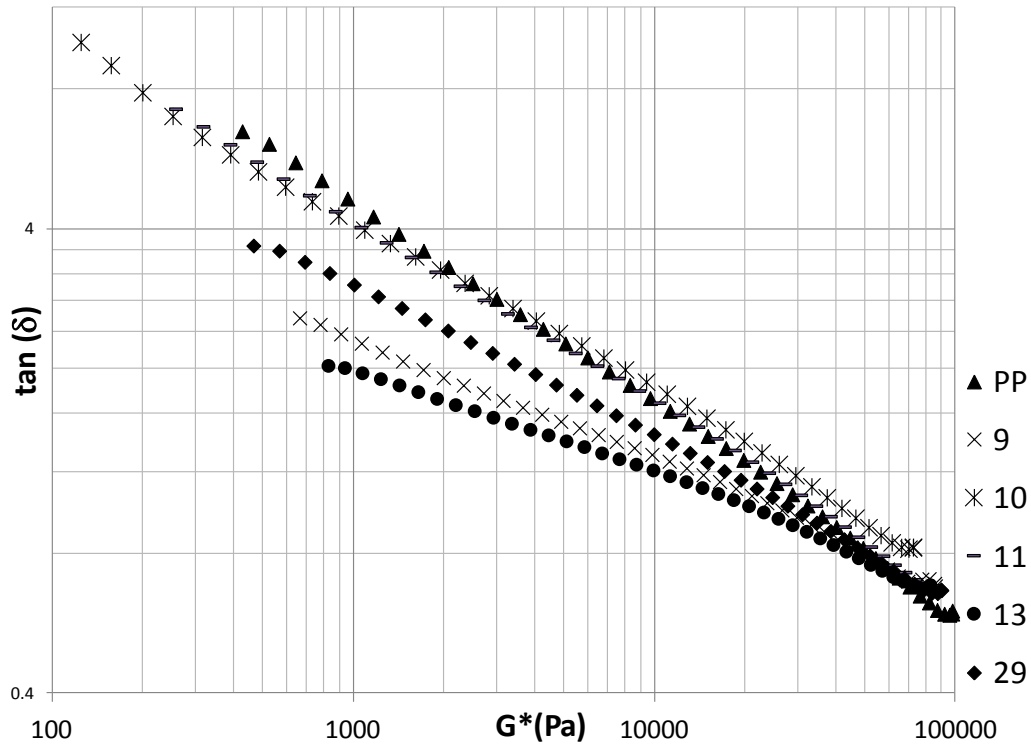
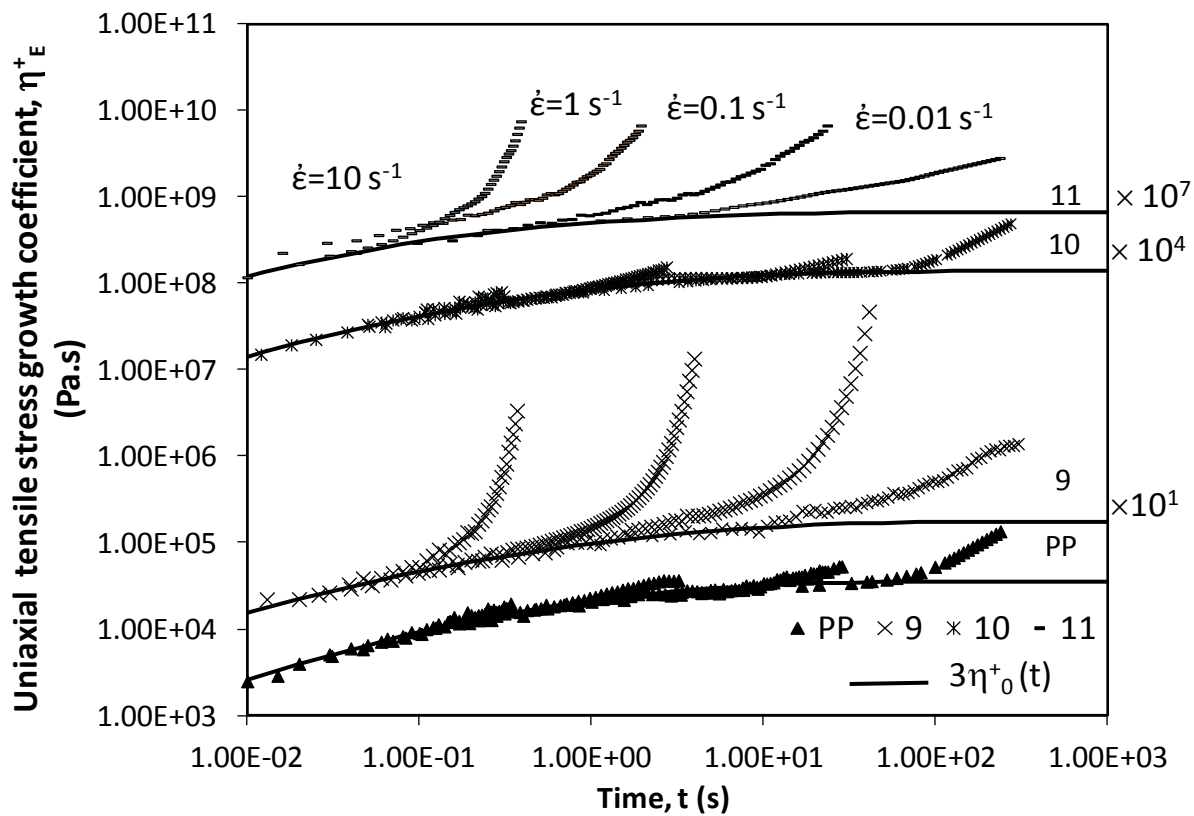


Figure 4-9:  $\tan(\delta)$  versus complex modulus ( $G^*$ ) for runs 9, 10, 11, 13, 29 and parent PP

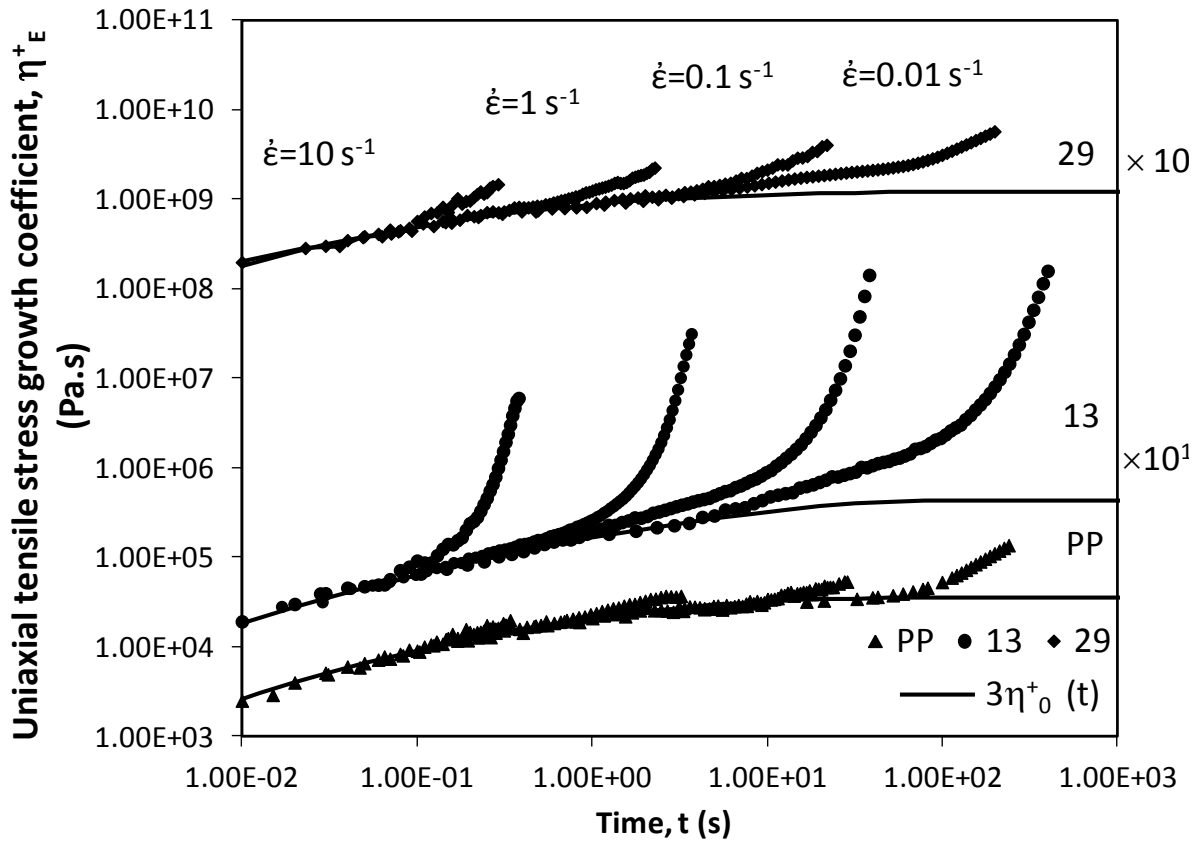
### 4.3.3 EXTENSIONAL RHEOMETRY

Extensional viscosity measurements were conducted to confirm the presence of LCB in the modified PP runs. The same experimental runs (9, 10, 11, 13, 29 and PP) were characterized using the Sentmanat extensional rheometer (SER). Each test was independently replicated three times. The values of the uniaxial tensile stress growth coefficient ( $\eta^+_{\text{E}}$ ) versus time for these runs are plotted in Figure 4-10 (a and b) at strain rates of 0.01, 0.1, 1 and 10  $\text{s}^{-1}$ , respectively. The continuous solid lines in Figure 4-10 (a and b) represent three times the shear stress growth coefficient from parallel plate rheometry (i.e.,  $3 \eta^+_0(t)$ ), in order to have a better visual comparison between the extensional viscosity data and Trouton's law. An increasing  $\eta^+_{\text{E}}$  above Trouton's law levels

indicates strain hardening and this behavior is expected from long chain branched polymers.



a



b

Figure 4-10: Uniaxial tensile stress growth coefficient ( $\eta^+_E$ ) vs. time for selected runs and parent PP at Hencky strain rates of 0.01, 0.1, 1, and  $10\text{ s}^{-1}$

Figure 4-10 indicates that the parent PP does not show significant strain hardening behavior.  $\eta^+_E$  clearly increased at all strain rates for runs 9 (Figure 4-10a) and 13 (Figure 4-10b) compared to parent PP. As expected, the ‘degraded’ runs (runs 10 and 11) do not show significant increases in  $\eta^+_E$  compared to the parent PP (Figure 4-10 a). Run 29, which has a larger  $\eta_0$  than parent PP (see Table 4-3), shows again rather insignificant strain hardening compared to runs 9 and 13. This might be due to formation (in run 29) of

isolated CL structures rather than LCB, since isolated CL does not lead to significant increase in extensional viscosity (see discussion about gel content which follows).

In order to compare the degree of strain hardening among the runs, the strain hardening coefficient (SHC) was determined (Equation 4-2) [15].

$$SHC = \frac{\eta_E^+(t, \dot{\epsilon})}{3\eta_0^+(t)} \quad \text{Equation 4-2}$$

In Equation 4-2,  $\eta_E^+(t, \dot{\epsilon})$  is the uniaxial tensile stress growth coefficient at the Hencky strain of 2.71.  $\eta_0^+(t)$  is the shear stress growth coefficient. Equation 4-2 describes the extent of deviation from Trouton's law, which is due to formation of LCB. Values of SHC acquired at different Hencky strain rates (0.01, 0.1, 1 and 10 s<sup>-1</sup>) are shown in Figure 4-11.

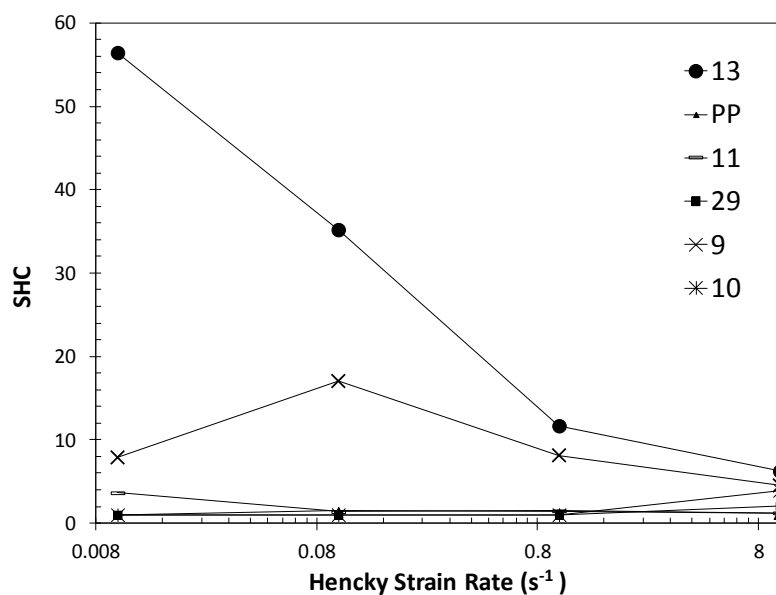


Figure 4-11: SHC versus Hencky strain rate for runs 9, 10, 11, 13, 29, and PP (lines are simply visual guides)

Figure 4-11 indicates that runs 9 and 13 show a much higher level of extensional viscosity at all strain rates compared to the other runs. This is in agreement with parallel plate rheometry data, thus confirming the presence of LCB or CL in these two runs. The parent

PP shows a slight increase in SHC which might be due to the presence of high molecular weight linear structures and the broad molecular weight distribution of the parent PP. Runs 10 and 11 fail to show considerable increases in SHC compared to parent PP.

#### 4.3.4 GEL CONTENT

Gel content levels of runs 9, 10, 11, 13, 29 and the parent PP were determined and the results are summarized in Figure 4-12. Each run was independently replicated and standard deviation values calculated and reported in Figure 4-12.

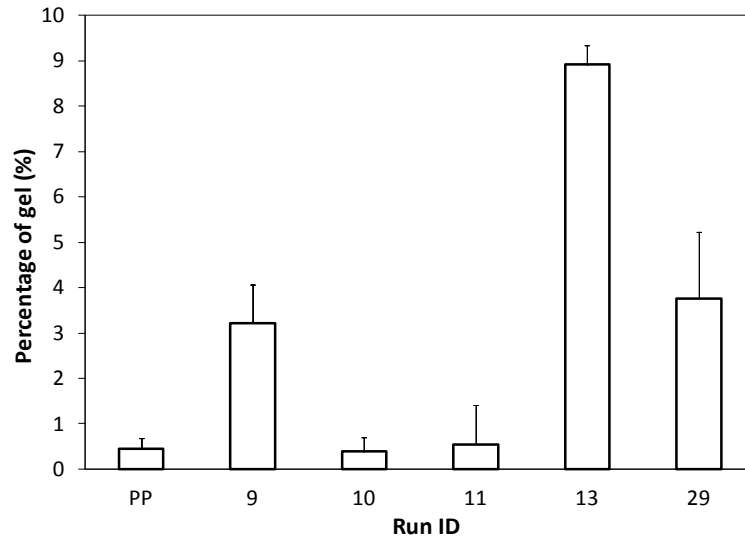


Figure 4-12: Gel fraction of runs 9, 10, 11, 13, 29 and parent PP

A gel fraction in Figure 4-12 below 1 % signifies zero gel content, for all practical purposes, as the calculation denotes typical noise related to the nature of the measurements. As expected, there was no gel in the parent PP. Similarly, runs 10 and 11, the ‘degraded’ runs, do not show any insoluble fraction either. Run 13 shows the highest percentage of gel. Thus, the strain hardening behavior observed from extensional rheometry for this run can be attributed to both formation of LCB and CL. Moreover, runs 9 and 29 show about the same percentage of gel. However, in extensional rheometry run 9 shows significantly

higher strain hardening behavior compared to run 29 (Figure 4-11). Thus, the higher SHC level of run 9 can be attributed to formation of LCB in addition to CL. LCB is not formed in run 29 and, therefore, the higher values of  $\eta_0$  and  $\lambda$  of run 29 can be due to the presence of 3.7 % gel. Formation of LCB in run 9 has also been confirmed by GPC test results (see further discussion in section 4.3.5).

### 4.3.5 GPC RESULTS

The results for number average MW ( $\bar{M}_n$ ), weight average MW ( $\bar{M}_w$ ), z-average MW ( $\bar{M}_z$ ) and polydispersity index (PDI) are summarized in Table 4-6.

Table 4-6: GPC analysis results

Run ID	$\bar{M}_n$ (kg/mol)	$\bar{M}_w$ (kg/mol)	$\bar{M}_z$ (kg/mol)	PDI
PP	46.3	272.9	828.5	5.9
9	48.95	311	1260.3	6.35
10	15.05	110.8	325.9	7.34
11	17.7	140.7	500.9	7.95
13	43.1	259.1	904.2	6.01
29	31.4	152.5	206.1	4.86

PDI values indicate that polydispersity of all runs increased compared to the parent PP, except for run 29. The MW of run 9 increased considerably compared to parent PP, which confirms formation of LCB in this run. Run 13, which also shows indication of LCB, has a larger z-average molecular weight ( $\bar{M}_z$ ) due to formation of longer chains as a result of LCB formation. The reason that the MW of run 13 is not as high as run 9 (despite larger strain hardening exhibited by run 13 in Figure 4-11) might be due to the larger gel fraction of this run. The gel from these runs was filtered out before entering the GPC columns and, consequently, was not taken into account in the MW determinations.

The full MWDs for these runs are plotted in Figure 4-13. Runs 9 and 13 have longer tails at high molecular weight ranges compared to parent PP; however, the ‘degraded’ runs (10 and 11) are shifted toward lower molecular weights.

The MWDs of runs 9, 10, 11 and 13 are in agreement with the rheological polydispersity indices (Table 4-3). All these runs have greater PI and lower ModSep than the parent PP, which is in agreement with the PDI values (Table 4-6). Moreover, the longer tail at high molecular weight ranges (Figure 4-13) for runs 9 and 13 reflects significantly large ER values for these runs.

A few comments are now in order for the behavior of run 29. Run 29 has greater  $\eta_0$ , PI and ER values than the parent PP; hence, higher MWs and a broader MWD were expected. However, GPC results showed that the MW for run 29 was lower than the parent PP, and in addition, the MWD was slightly narrower. Moreover, run 29 did not show significant strain hardening behavior, despite the presence of crosslinked material in its structure.

A possible explanation for such behavior is the presence of two domains in the polymer produced by run 29: degraded (low molecular weight), and isolated gel. Gel content experiments verified the presence of about 4 % gel in this sample. On the other hand, GPC data confirmed that the MW of run 29 had decreased. As mentioned before in the beginning of this section, since the isolated gel fraction in sample 29 was filtered out prior to injection into the GPC columns, the collected GPC chromatogram only reflected the degraded domains characteristics. Thus, GPC showed lower values for  $\bar{M}_w$  and  $\bar{M}_z$  compared to the other runs, including the parent PP.

Thus, the presence of isolated crosslinked domains in run 29 resulted in greater  $\eta_0$  and  $\lambda$  values compared to the parent PP (as illustrated by the parallel plate rheometry data). These isolated gel domains could act like a filler, and since they are dispersed in the sample, they can cause an increase in  $\eta^*$  and  $G'$  vs.  $\omega$ . However, these isolated gel domains do not cause significant changes in the strain hardening behavior, because the crosslinked regions and the linear chains are not interconnected.

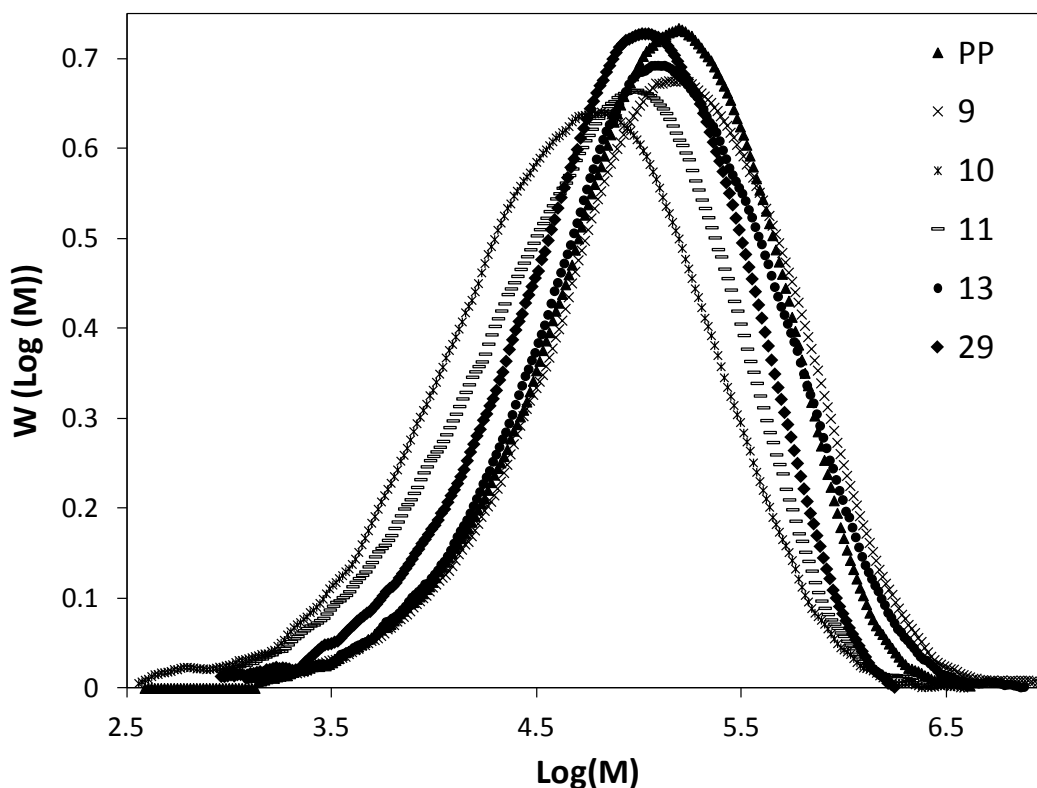


Figure 4-13: MWDs for runs 9, 10, 11, 13, 29 and parent PP

Log-log plots of intrinsic viscosity  $[\eta]$  vs. molecular weight for the different chromatograms are plotted in Figure 4-14 and Figure 4-15. Qualitative comparisons between the obtained curves can serve as an indicator of the molecular structure of the polymers. The Mark-Houwink relation stipulates that  $\log [\eta]$  versus  $\log M$  is linear for a linear polymer with known slope and intercept (Mark-Houwink constants). Presence of LCB in the polymer causes deviations from this linear relation by shifting the slope at higher molecular weights to lower values [41, 55]. In Figure 4-14, the parent PP shows linear behavior due to its linear structure and it is used as a reference for further comparisons between runs. Runs 10 and 11, the ‘degraded’ runs, do not show any change in slope towards lower intrinsic viscosities at high MW ranges. Run 29 shows a very slight deviation from parent PP around MW of 177 kg/mol. However, this deviation is not clear enough (it could simply be due to experimental noise), and formation of LCB cannot be

confirmed for this run (Figure 4-14). In order to see deviations from the parent PP more clearly for runs 9 and 13,  $\log [\eta]$  vs.  $\log M$  curves for runs 9 and 13 have been plotted separately in Figure 4-15. It can be seen that runs 9 and 13 show evidence of LCB by deviating from the linear PP at higher molecular weights. The slope of the  $\log [\eta]$ - $\log M$  curve is lower for these two runs compared to the parent linear PP (LPP), after a value of  $M$  around 180 kg/mol.

Furthermore, in Figure 4-15, run 13 deviates from parent PP over a broader range of MW ( $M$ ) values. This is in agreement with extensional rheology data, according to which run 13 exhibited significantly larger SHC levels compared to run 9 (see Figure 4-11).

Finally, using Equation 3-21 and Equation 3-22, the number of LCB per 1000 repeating units ( $N_{LCB}$ ) was also calculated for runs 9 and 13.  $N_{LCB}$  for run 9 is 0.035 in the MW range of 320-1,500 kg/mol, whereas for run 13,  $N_{LCB}$  is 0.042 in the range of 130-1,500 kg/mol. This confirms once more that run 13 has a greater amount of LCB.

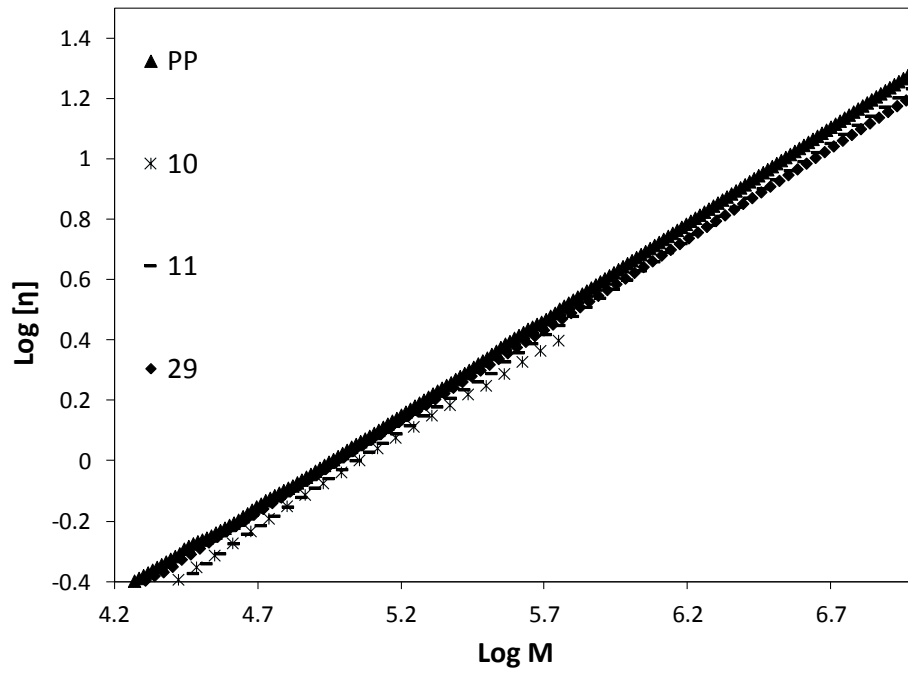


Figure 4-14: Comparison between Mark-Houwink plots for runs 10, 11, 29 and parent PP

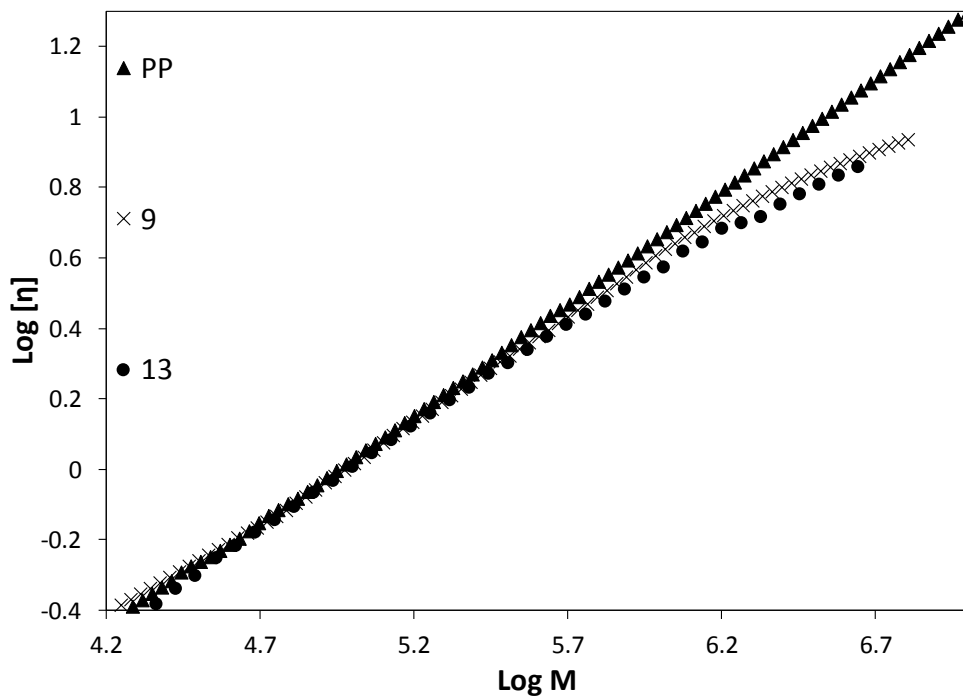


Figure 4-15: Mark-Houwink plots for runs 9, 13 and parent PP

### 4.3.6 DIFFERENTIAL SCANNING CALORIMETRY (DSC)

DSC tests were conducted on runs 9, 10, 11, 13, 29 and the parent PP. Heat flow versus temperature graphs are shown in Figure 4-16.

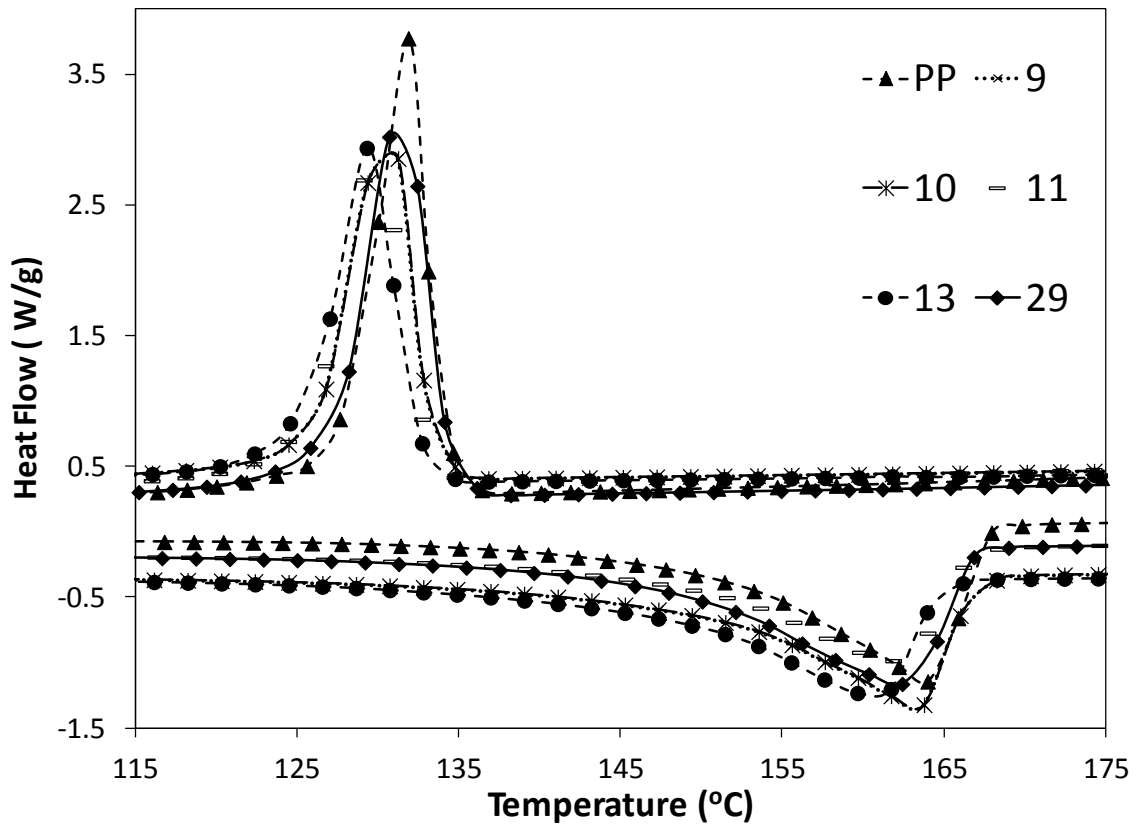


Figure 4-16: DSC graphs of runs 9, 10, 11, 13, 29 and the parent PP

Using these graphs, crystallization and melting points have been obtained by determining the maximum and the minimum of the exothermic and endothermic peaks, respectively. Percentage of crystallinity ( $X_c$ ) was also calculated using Equation 4-1. These data are summarized in Table 4-7.

Table 4-7: Melting, crystallization temperature, heat fusion of melting for runs 9, 10, 11, 13, 29 and the parent PP

Run ID	T <sub>m</sub> (°C)	T <sub>c</sub> (°C)	X <sub>c</sub> (%)
PP	164	131	44.4
9	162	130	45.5
10	162	130	37.8
11	163	131	39.3
13	163	129	44.5
29	163	131	45.7

Figure 4-16 and Table 4-7 show that the T<sub>m</sub> and T<sub>c</sub> values of the modified runs have not changed compared to the parent PP characteristics. T<sub>m</sub> was in the range of 162-164 °C and T<sub>c</sub> was in the range of 129-131 for the runs. Moreover, the crystallinity levels of all runs were in the range of 44-45 %, except for the runs that showed degradation (10 and 11). These ‘degraded’ runs exhibited lower crystallinity (38-39 %), as expected, due to the presence of shorter chains. There is also no significant changes in T<sub>c</sub> of the long chain branched runs compared to the parent PP.

#### 4.4 CONCLUDING REMARKS

The aim of this chapter was to develop a method for increasing the melt strength of PP with UV irradiation. Thirty two radiation trials were carried out at different photoinitiator concentrations, for different time periods, at different UV lamp intensities and cooling air pressures, for two different photoinitiators. LVE properties were measured and analyzed for all experimental trials. Processing conditions that can result in LCB and/or CL in the modified PP structure were identified for both photoinitiators (BPH and DEBPH). Out of these thirty two experimental runs, three representative samples that showed indications of LCB formation along with two degraded samples were selected to be discussed in more detail. Extensional viscosity, gel content, MW, MWD, intrinsic viscosity and thermal properties of these samples were measured. The results from detailed characterization tests

for all the selected runs are summarized in Table 4-8. From Table 4-8, it can be concluded that only when BPH was used as photoinitiator, formation of LCB and CL was confirmed. It was found that adding 0.5 wt-% of BPH to PP, for a radiation period of 600 s, with low lamp intensity and high cooling air pressure, significantly increased strain hardening behavior in PP.

Table 4-8: Summary of indicators for different runs, relative to parent PP

	9	10	11	13	29
LVE properties ( $\eta_0$ , $n$ , $\lambda$ and ER)	Yes*	No*	No	Yes	Yes
G' and $\eta^*$ vs. $\omega$	Yes	No	No	Yes	Yes
$\tan \delta$ -G* and Cole- Cole plots	Yes	No	No	Yes	Yes
Extensional rheometry	Yes	No	inconclusive	Yes	inconclusive
Gel content	Yes	No	No	Yes	Yes
Log $[\eta]$ -log M	Yes	No	No	Yes	No
Overall	LCB- CL	Linear- degraded	Linear- degraded	LCB- CL	CL

\*Yes/ (No): the test confirms formation of long chain branches in the run/ (no evidence for LCB)

## **5 CHAPTER 5: EFFECT OF RADIATION TIME AND SAMPLE THICKNESS ON PHOTOMODIFICATION REACTIONS**

In this chapter linear polypropylene (PP) was modified using UV radiation in the presence of 0.5 wt-% of benzophenone (BPH) photoinitiator to introduce long chain branching to the PP backbone. Irradiation was carried out in the solid state and the temperature level was kept below 60 °C. The effects of radiation duration and sample thickness on the extent of these branching modification reactions were investigated. Linear viscoelastic (LVE) properties, molecular weight (MW), molecular weight distribution (MWD), and gel content were determined and compared for runs having different sample thicknesses, irradiated for different times. Comparisons were also conducted with the parent PP and the PP mixed with photoinitiator. It was found that long chain branching (LCB) decreased by increasing the thickness of the samples. On the other hand, an increase in radiation duration resulted in enhanced LCB, but also led to larger gel content in the samples. Using LVE measurements, mechanism has been suggested to explain formation of long chain branches in PP in solid state reaction via photoinitiation.

### **5.1 INTRODUCTION**

Polypropylene (PP) is a commercial polymer with high stiffness and resistance to environmental stress cracking and solvents. PP applications can be expanded by increasing its melt strength. Increasing melt strength can be achieved by introducing long chain branching (LCB) to the PP backbone. In order to introduce long chain branches to PP backbone, first, a tertiary hydrogen should be abstracted from the PP backbone. Free radicals generated via peroxide initiator decomposition or high energy radiation, such as electron beam (EB) and gamma radiation, are often responsible for hydrogen abstraction. Combination of a tertiary radical center with another radical center results in formation of branches on the PP backbone. The main difficulty in this process is the tendency of PP

macroradicals to degrade via  $\beta$ -scission followed by termination via disproportionation [1]. This mechanism is shown schematically in Figure 5-1.

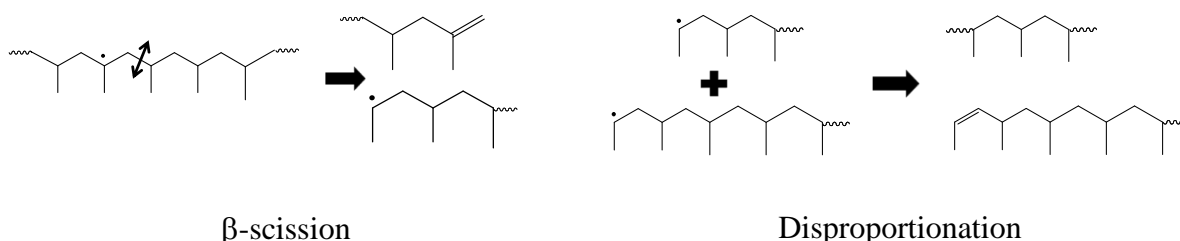


Figure 5-1: Schematic mechanism for PP degradation

Different methods have been used to control the  $\beta$ -scission reaction during PP modification. Using multi-functional monomers (along with peroxide initiators) or radiation (gamma or EB) in the solid state at low temperatures are some of the attempts to stabilize tertiary radical centers [6, 15, 18, 50, 56, 57].

Despite all these advances in modifying the melt strength of PP, the commonly employed techniques have several disadvantages. For example, peroxides have toxicity issues related to their use. Moreover, EB and gamma radiation are rather expensive sources of energy and utilizing them involves additional safety issues. Recently, UV radiation under controlled conditions was successfully used to introduce LCB to PP [51, 52, 58]. UV radiation is accessible and a rather inexpensive source of energy.

For modification with UV radiation, photoinitiators such as benzophenone (BPH) have been used. Photoinitiators are activated by UV radiation rather than thermal energy and are less toxic than peroxides. Controlling photoinitiation reactions is easier than peroxide thermal initiation, since temperature can be adjusted without activating the initiator in the former case.

BPH absorbs light in the wavelengths of 215, 254 and 330 nm and becomes excited [20, 59]. In the excited state, it can abstract a hydrogen atom from the PP backbone and form a macroradical. In Chapter 4, PP has been modified in the solid state using BPH as

photoinitiator. The effect of radiation conditions such as radiation time, UV lamp intensity and cooling rate, along with concentration (and type) of photoinitiator on PP modification were investigated. The operating conditions that maximize strain hardening in PP were identified.

One issue that arises during modification of polymers by UV radiation is related to the depth of radiation [60, 61]. It is known that penetration of UV light is limited and this can cause inhomogeneities in LCB (and crosslinking (CL)) of the samples. Chen and Rånby [60] investigated the effect of thickness of polyethylene (PE) samples by analyzing the variation in percent of gel formed and relating it to the thickness of the PE samples.

In this chapter, the effect of UV penetration depth was investigated by radiating solid PP discs with different thicknesses. Moreover, it is critical to investigate the effect of UV radiation duration along with radiation depth, since radiation time affects the overall extent of the modification process. In order to investigate the effects of these variables on the degree of modification, discs were prepared with specific thicknesses and radiated for different lengths of time.

## **5.2 MATERIALS AND METHODS**

### **5.2.1 MATERIALS**

PP homopolymer (Pro-fax PH 382M) from LyondellBasell with a melt flow rate (MFR) of 3.5g/10 min was used. Benzophenone (BPH) of 99% purity was purchased from Sigma Aldrich and used as received.

### **5.2.2 DESIGN OF EXPERIMENTS**

In order to study the effects of UV radiation duration and penetration depth (i.e., sample thickness), three-level factorial design experiments were conducted. Statistical analysis was carried out using Design Expert 8.0.7.1 software. This design is summarized in Table 5-1 (runs 1 to 9). Runs 10 and 11 of Table 5-1 were used as reference points. Run 10 used a

mixture of PP with 0.5 wt-% BPH but without any irradiation. Melt mixing for run 10 was achieved in a batch mixer. Run 11 used simply the parent PP. The experimental results from runs 10 and 11 were used for comparisons with runs 1-9.

Table 5-1: Design of experiments for 3-level factorial design

Run ID	BPH (wt-%)	Thickness-A (mm)	Time-B (min)
1	0.5	1	5
2	0.5	1	10
3	0.5	1	15
4	0.5	2	5
5	0.5	2	10
6	0.5	2	15
7	0.5	3	5
8	0.5	3	10
9	0.5	3	15
10	0.5	1	0
11	0	1	0

### 5.2.3 PREPARATION METHOD

PP pellets with 0.5 wt-% of photoinitiator were melt-mixed in a batch mixer at 190 °C and 100 rpm for 8 minutes. The samples were ground using a Wiley mill (model 1102, Arthur H. Thomas Co.). After grinding, the granules were compression-moulded into discs with 25 mm diameter and thickness of 1, 2, and 3 mm at 190 °C under an applied force of 4400 N for 10 to 15 minutes. The discs were irradiated using a Mercury UV lamp (Versa Cure) for varied amounts of time. Radiation was carried out at a distance of 30 cm from the UV light source. Samples were irradiated for 5, 10, and 15 minutes. During irradiation, pressurized air was used to cool down the area beneath the lamp and the temperature was kept constant at 55 °C.

### 5.2.4 CHARACTERIZATION

For these analyses the same procedures explained in section 4.2.3.1 of Chapter 4 were followed. From these tests, storage modulus ( $G'$ ), loss modulus ( $G''$ ), complex modulus

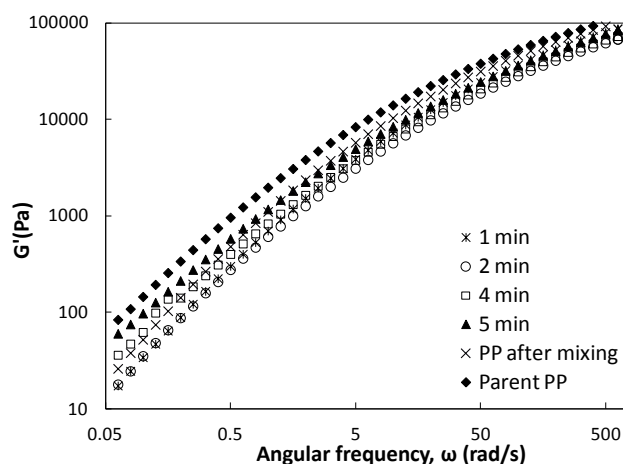
( $G^*$ ), loss tangent ( $\tan \delta$ ), and complex viscosity ( $\eta^*$ ) were obtained at different angular frequencies ( $\omega$ ).  $\eta^*$  vs.  $\omega$  graphs were used to find the shear thinning index ( $n$ ), zero shear viscosity ( $\eta_0$ ) and relaxation time ( $\lambda$ ) of each sample by fitting the Cross model (Equation 3-11 in section 3.1 of Chapter 3) utilizing MATLAB (7.11.0 R2010b).

Rheological polydispersity indices were determined using Equation 3-13, Equation 3-14 and Equation 3-15. NLREG, a nonlinear regression software [62], is the nonlinear regression software which was used to calculate the relaxation spectrum ( $H(\lambda)$ ).

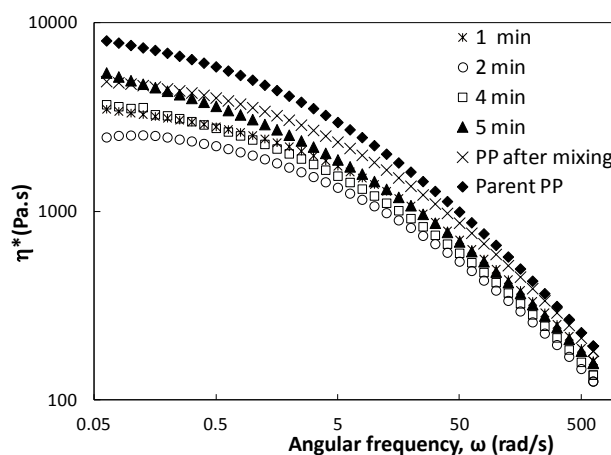
GPC and gel content measurements were conducted in the same way as described in section 4.2.3.3 and 4.2.3.2 of Chapter 4.

### 5.3 RESULTS AND DISCUSSION

In Chapter 4, conditions that maximize the LCB level in PP were found using LVE data. In addition, formation of LCB and CL under these conditions was confirmed by extensional rheometry, GPC, and gel content measurements. It was found that in order to maximize the amount of LCB, samples with 0.5 wt-% of BPH should be radiated for 10 min at a lamp intensity of  $0.67 \text{ W/m}^2$  in the UVA region at temperatures below  $60 \text{ }^\circ\text{C}$  (UVA refers to the wave length range of 320-390 nm where BPH absorbs light). In this chapter, the main objective is to investigate the effect of time and thickness on the degree of LCB. For this reason, first, preliminarily experiments were conducted to monitor the progress of photomodification with radiation time (from the onset of radiation until formation of branches and/or crosslinks). These results were used to suggest a mechanism for degradation and LCB formation for PP with UV radiation. Figure 5-2 shows  $G'$  (A) and  $\eta^*$  (B) of the runs radiated between 1 to 5 min compared to PP after melt mixing with BPH and the parent PP (runs 10 and 11 in Table 5-1). All the samples of Figure 5-2 have been prepared from the same polymer sheet (1 mm thickness), which was irradiated for different durations (from 1 min to 5 min).



**A**



**B**

Figure 5-2:  $G'$  (A) and  $\eta^*$  (B) vs.  $\omega$  for 1 mm thick samples which were radiated between 1 and 5 min

In Figure 5-2 A and B,  $G'$  and  $\eta^*$  of PP after mixing (with BPH) are lower than the parent PP due to thermal degradation during the processing in the batch mixer. It can also be seen that  $G'$  and  $\eta^*$  decrease after 1 minute of radiation and the decrease continues until 2 minutes from the onset of radiation. This is due to  $\beta$ -scission and degradation of the chains during the first 2 minutes from the beginning of the reaction (the mechanism is shown in Figure 5-1). For durations greater than 2 minutes, LVE properties ( $G'$  and  $\eta^*$ ) start to increase. This can be attributed to formation of LCB in the samples. LVE properties continue to increase even after 15 minutes from the onset of radiation. The effect of radiation time after formation of branches (after 5 minutes of radiation) is investigated further in the following subsections.

From the above observations, the following mechanism is suggested for formation of LCB in PP via UV radiation (see Figure 5-3).

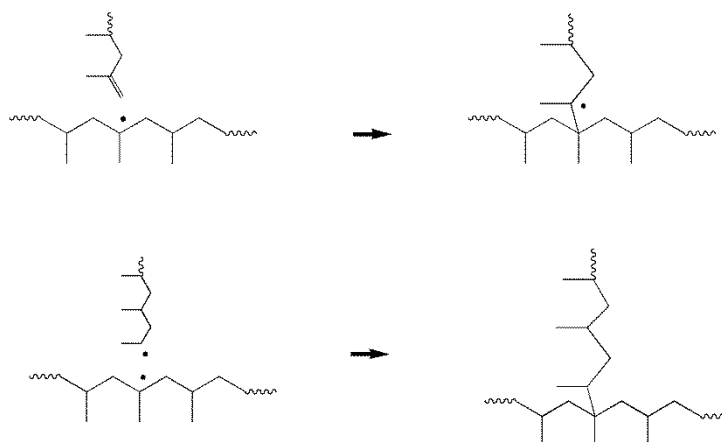


Figure 5-3: Schematic mechanism for formation of LCB in the PP backbone

According to Figure 5-3, in the first step, excited BPH molecules abstract hydrogens from the tertiary carbon atoms in the PP backbone and form macroradicals. These macroradicals are unstable and undergo  $\beta$ -scission (Figure 5-1). Due to  $\beta$ -scission reactions, PP chains with terminal double bonds are formed. When the concentration of these chains increases, the probability of reactions between PP macroradicals and chains with terminal double bonds also increases (Figure 5-3). Consequently, long chain branches will be formed.

During irradiation, degradation and LCB happen simultaneously, but as radiation proceeds, LCB will eventually overcome degradation. The validity of this mechanism is corroborated by the experimental observation that degradation is more prominent at the initial stages of radiation (observe the lower  $\eta^*$  and  $G'$  levels at the beginning of radiation, as per Figure 5-2). However, as irradiation proceeds, LCB prevails over degradation, which results in the subsequent increase in  $\eta^*$  and  $G'$  (see runs which were radiated for 4 and 5 minutes in Figure 5-2).

### **5.3.1 EFFECT OF RADIATION TIME AND SAMPLE THICKNESS ON LVE PROPERTIES**

LVE data are known to be sensitive tools for comparison between degrees of LCB (and MWD) of different samples [11, 63].

In this section, the effects of thickness and time on LVE properties are analyzed and empirical models developed for each LVE response variable. Subsequently, factor interaction graphs are discussed.

Figure 5-4 A and B show  $G'$  and  $\eta^*$  for runs 3, 6 and 9, which have the same exposure time to UV (15 min) but different thicknesses (1, 2 and 3 mm, respectively). A lower sample thickness results in larger  $G'$  and  $\eta^*$  at low frequencies. This trend is also observed for runs that were radiated for 5 minutes (runs 1, 4 and 7) and 10 minutes (runs 2, 5 and 8). This is due to the limited depth of radiation for thicker samples. Chen and Rånby [60] found that 1 mm is the critical depth of UV penetration in PE films. Therefore, above this critical thickness, inhomogeneities are expected in crosslinking through the depth of the samples. Since  $\eta^*$  and  $G'$  decrease with increasing the thickness of the samples, one can conclude that the critical thickness is either lower than or at 1 mm for discs at the experimental lamp intensity.

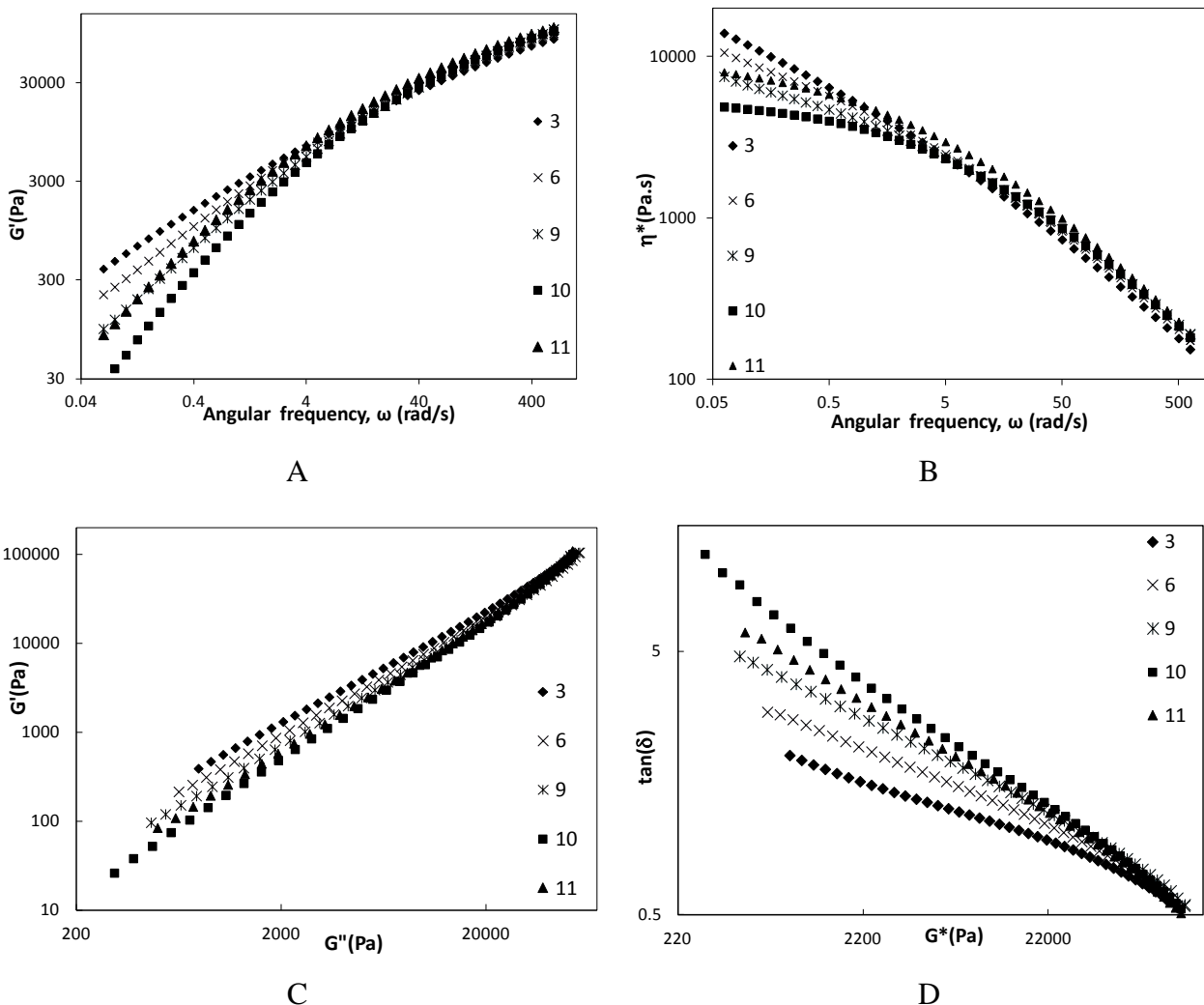


Figure 5-4: Comparison between LVE properties of the runs with different thickness after 15 min radiation A)  $G'$ - $\omega$ , B)  $\eta^*$ - $\omega$ , C) Cole-Cole plots and D)  $\tan(\delta)$ - $G^*$

Cole-Cole and  $\tan(\delta)$ - $G^*$  plots for the same runs are shown in Figure 5-4 C and D. These two plots are sensitive to the MWD rather than a single MW average, and, in fact,  $\tan(\delta)$ - $G^*$  is even more sensitive to MWD than Cole-Cole plots [32]. In Cole-Cole plots, long chain branched polymers deviate from the linear reference (greater  $G'$  values at low  $G''$  ranges). Despite the thermal degradation of run 10 (PP after melt mixing without UV treatment), no significant deviation was observed in the Cole-Cole plots and  $\tan \delta$ - $G^*$  from run 11 (parent PP), which suggests that thermal degradation does not affect significantly

the MWD at the processing conditions used. The increase in  $G'$  vs.  $G''$  (Figure 5-4 C) and decrease in  $\tan(\delta)$  vs.  $G^*$  (Figure 5-4 D) with a decrease in the sample thickness are mainly due to broadening of the MWD and the larger number of long chain branches in the thinner samples.

Figure 5-5 compares  $G'$ ,  $\eta^*$ , Cole-Cole plots and  $\tan(\delta)$ - $G^*$  plots for the runs with the same thickness (1 mm) but radiated for different amounts of time (5, 10 and 15 min). An increase in radiation time above 5 minutes increases elasticity ( $G'$ ) (Figure 5-5 A) and complex viscosity ( $\eta^*$ ) (Figure 5-5 B), and broadens the MWD (Figure 5-5C and D). This is due to formation of a larger number of branches as the reaction proceeds over time. The same trend was observed for runs with 2 mm (runs 4, 5 and 6) and 3 mm (runs 7, 8, and 9) thickness that were radiated for varied durations.

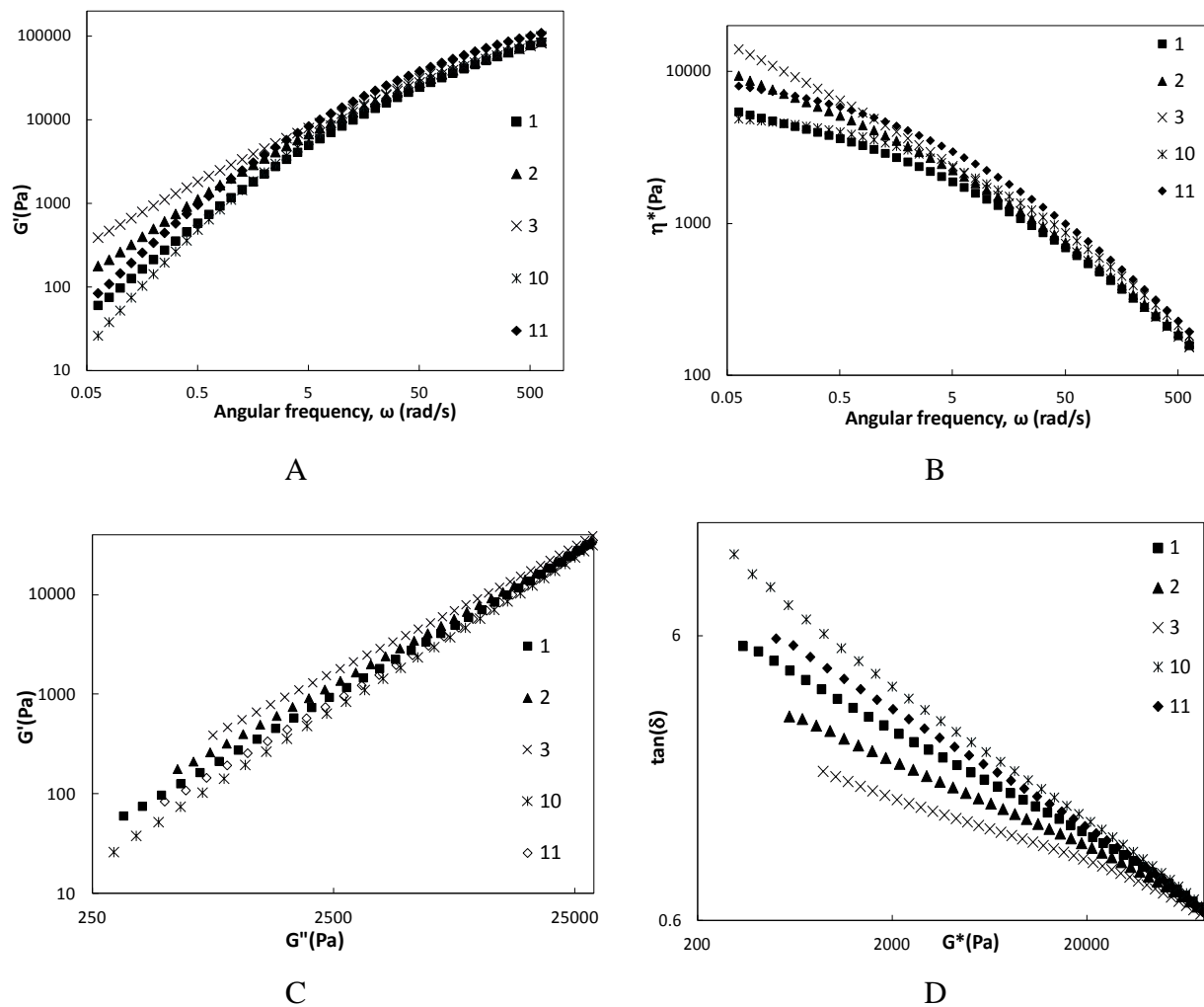


Figure 5-5: Comparison between LVE properties of the runs with 1 mm thickness with different radiation times A)  $G'$ - $\omega$ , B)  $\eta^*$ - $\omega$ , C) Cole-Cole plots and D)  $\tan(\delta)$ - $G^*$

The effects of radiation time and depth on the relaxation spectrum, which is an indication of rheological polydispersity, are shown in Figure 5-6 and Figure 5-7. Figure 5-6 A compares the relaxation spectra of the 1 mm thick samples, which were radiated for 5, 10 and 15 minutes, respectively. Broadening in the relaxation spectrum occurs after 10 minutes from the onset of radiation. Increasing the radiation time leads to formation of a bimodal relaxation spectrum, as can be observed for run 3, which was irradiated for 15 minutes (Figure 5-6 A). This shows formation of chains with very long relaxation times, due to long chain branching and crosslinking, along with chains with short relaxation times

(formation of crosslinks in this run has been confirmed independently and will be discussed in more detail in Section 5.3.3). Since the UV radiation depth is limited, long chain branched and crosslinked chains with high molecular weight tend to form on the surface of the radiated discs but the molecular properties in the middle of the sample remain unchanged. Consequently, a bimodal relaxation spectrum will most likely result due to differences in relaxation times (and molecular properties) between the sample surface and sample core.

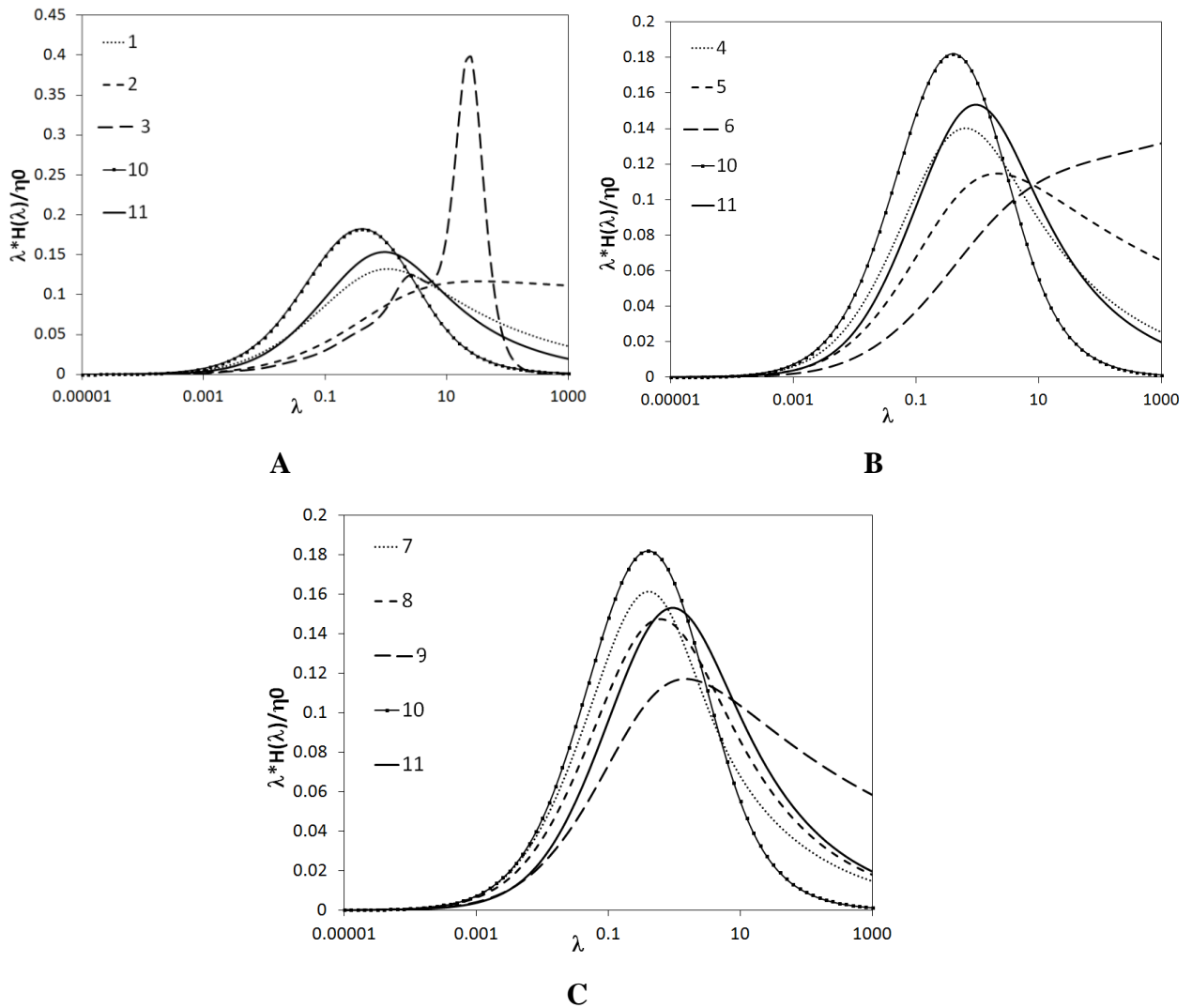


Figure 5-6: Comparison between relaxation spectra of the runs with the same thickness A) 1 min, B) 2 mm C) 3 mm

A broadening in the relaxation spectrum is also evidenced for runs 4, 5, 6 (Figure 5-6 B) and 7, 8, 9 (Figure 5-6 C), which again confirms the above mentioned trends (broadening of the relaxation spectrum with radiation time). Broadening of the relaxation spectrum is less pronounced for thicker samples, because the ratio of the surface region to the core region of these (thick) samples is lower. Surface region refers to the outer face of the sample, up to the depth that UV can penetrate, while core region refers to the middle (and lower) part of the sample which UV cannot penetrate.

Scrutinizing now the relaxation spectra of the runs that have the same radiation time reveals that thicker samples have a narrower relaxation spectrum. In order to compare the effect of thickness on the relaxation spectrum of the runs with the same radiation time, runs 1, 4 and 7 (Figure 5-7 A) are plotted along with runs 2, 5, 8 (Figure 5-7 B) and runs 3, 6, 9 (Figure 5-7 C). When the radiation time is constant, thinner samples have a broader relaxation spectrum. The relaxation spectrum not only becomes broader by decreasing sample thickness, but also shifts to longer times ( $\lambda$ ). This is because the number of high MW chains with a high relaxation time is greater in thinner samples.

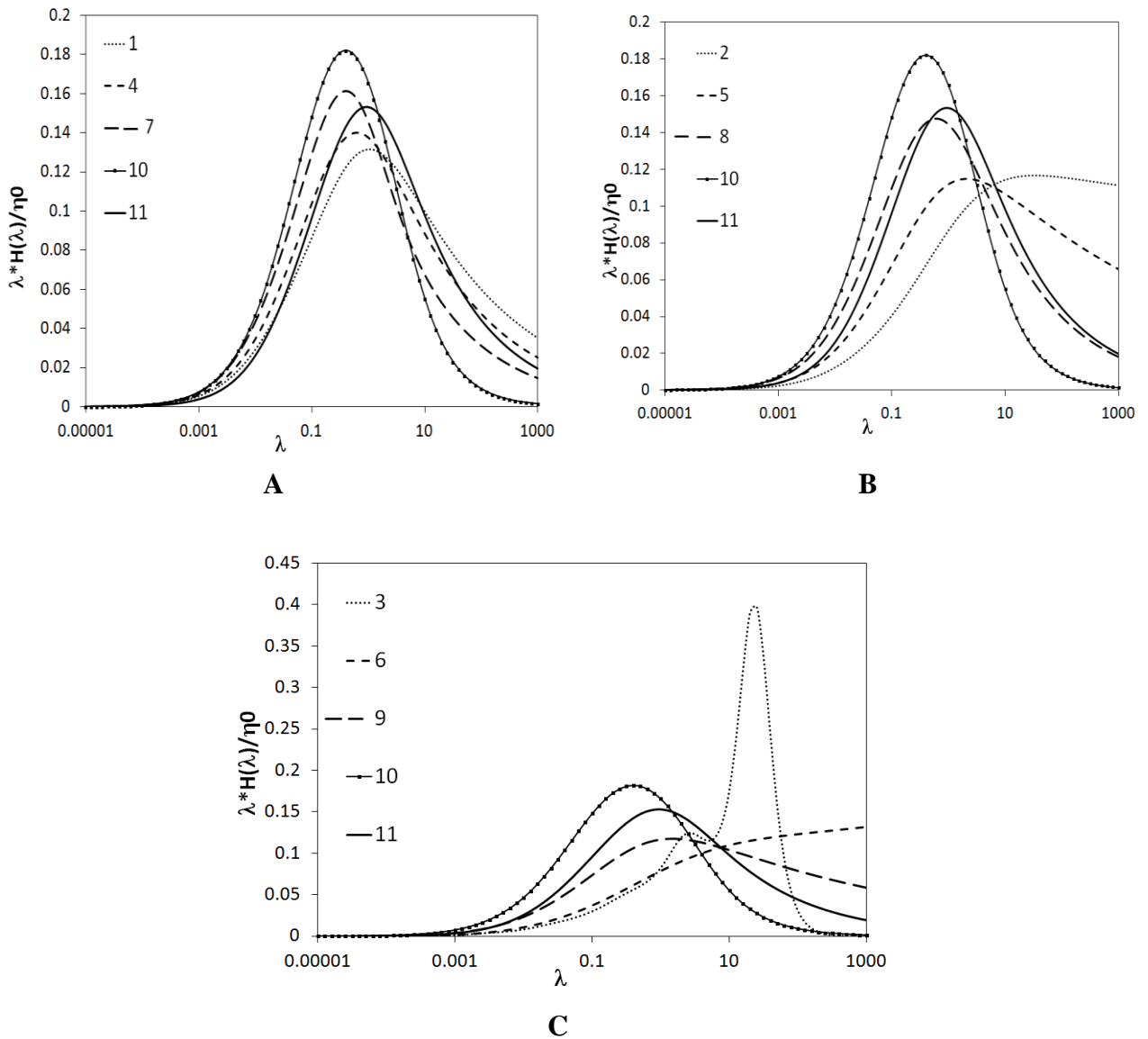


Figure 5-7: Comparison between relaxation spectra of the runs with the same radiation time A) 5 min, B) 10 min C) 15 min

Linear viscoelastic constants ( $\eta_0$ ,  $\lambda$  and  $n$ ) along with rheological polydispersity indices (PI, ModSep and ER) can be found using Equation 3-13, Equation 3-14 and Equation 3-15, respectively.

Runs with larger ER values indicate a broader distribution of the high molecular weight chains. PI and ModSep are polydispersity indicators for the shorter chains. An increase in

PI and a decrease in ModSep indicate broadening of the MWD [32]. It is expected that LCBPP have a larger ER due to the presence of high molecular weight chains and broader MWD. An increase in PI and decrease in ModSep are also expected due to broadening of the MWD during UV modification. Moreover, formation of LCB results in a larger  $\eta_0$  and  $\lambda$ , and a lower shear thinning index (n).

$\eta_0$ ,  $\lambda$ , n and polydispersity indices of the runs are summarized in Table 5-2. It can be seen that all radiated runs (1 to 9) have larger  $\eta_0$ ,  $\lambda$  and ER, and lower n values compared to run 10, which is PP after melt mixing with BPH.

Table 5-2: Linear viscoelastic properties of the runs

Run #	Thickness (mm)	time (min)	$\eta_0$ (Pa.s)	$\lambda$ (s)	n	PI	ModSep	ER
1	1	5	6,620	1.5	0.50	4.22	3.37	1.46
2	1	10	16,700	12.3	0.47	4.78	2.94	1.95
3	1	15	39,900	71.1	0.48	7.46	2.31	3.27
4	2	5	6,730	0.96	0.51	3.56	3.69	1.23
5	2	10	9,400	2.53	0.48	3.72	3.44	1.42
6	2	15	17,400	10.9	0.47	4.30	3.04	2.12
7	3	5	6,130	0.46	0.55	3.08	4.01	1.03
8	3	10	6,980	0.82	0.52	3.26	3.81	1.28
9	3	15	9,980	2.37	0.49	3.52	3.53	1.39
10	1	0	5,290	0.30	0.60	3.43	3.94	0.82
11	1	0	9,325	0.79	0.57	3.63	3.64	1.27

Comparison between runs 1, 2 and 3 shows that longer exposure time to UV results in larger  $\eta_0$ ,  $\lambda$  and lower n values, as expected from the  $\eta^*$  vs.  $\omega$  graphs (Table 5-2 and Figure 5-5). This trend is also observed for the 2 mm (runs 4, 5 and 6) and 3 mm (runs 7, 8, and 9) samples. On the other hand, an increase in the thickness of the samples limits UV light penetration and subsequently results in lower  $\eta_0$ ,  $\lambda$  and higher n at the same exposure times (compare runs 1, 4 and 7, or 2, 5 and 8, or 3, 6 and 9). This is because all these LVE constants are indicators of an average property within the sample. Therefore, due to the limited UV penetration in the samples, formation of LCB or CL is not uniform in thicker samples.

The data points presented in Table 5-2 were analyzed next with the Design-Expert software. Empirical models were fit for each response. These models and their regression coefficients ( $R^2$  and adjusted  $R^2$ ) are cited in Table 5-3.

Table 5-3: Empirical models for LVE properties

Empirical model	$R^2$	Adj. $R^2$	Equation #
$1/\sqrt{\eta_0}=0.02-0.000642*A-0.000941*B+0.000226*AB$	0.97	0.95	Equation 5-1
$\ln(\lambda)=-1.31-0.11*A+0.49*B-0.11*AB$	0.98	0.97	Equation 5-2
$n=0.50071+0.017833*A+0.0041*B$	0.75	0.68	Equation 5-3
$PI=2.09+0.3*A+0.43*B-0.14*AB$	0.86	0.80	Equation 5-4
$ModSep=3.76+0.17*A-0.13*B+0.03*AB$	0.98	0.97	Equation 5-5
$ER^{-1.39}=0.58+0.19*A-0.04*B$	0.91	0.88	Equation 5-6

In Table 5-3, variables A and B are sample thickness and radiation time, respectively, and AB denotes the factor interaction between thickness and time. In all of these models, the time-thickness interaction (AB) is significant except for ER and n. AB interaction plots for  $\eta_0$ ,  $\lambda$ , PI and ModSep are shown in Figure 5-8, Figure 5-9, Figure 5-10 and Figure 5-11, respectively. In these figures, the full and dashed lines show the statistical fit (based on the equations of Table 5-3) at 5 and 15 minutes of radiation, respectively, while the square, triangle and cross symbols represent the actual data points corresponding to the 1, 2 and 3 mm samples, respectively. For all these responses, the effect of thickness is not as pronounced at low radiation times. However, at longer radiation times, an increase in thickness results in a decrease in  $\eta_0$ ,  $\lambda$  and PI. At high radiation times, ModSep shows the opposite trend and correlates directly with the time-thickness interaction (i.e., an increase in thickness results also in an increase in ModSep). This is expected as ModSep has an inverse relation with MWD (unlike PI and ER). In the same way, the effect of time is more significant when the thickness of the samples is low. The increase in  $\eta_0$ ,  $\lambda$ , PI and decrease in ModSep of the runs is less pronounced for thicker samples.

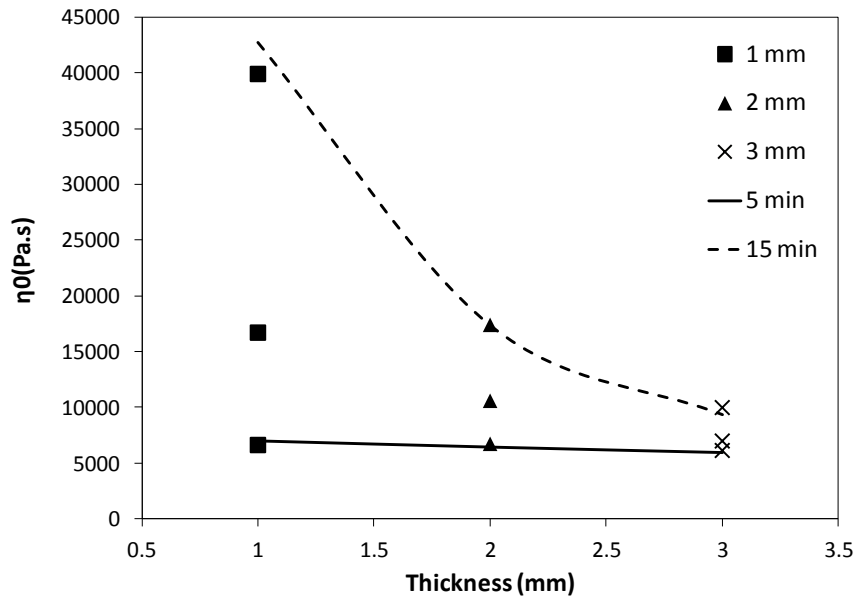


Figure 5-8: Effect of the time-thickness interaction on zero shear viscosity ( $\eta_0$ )

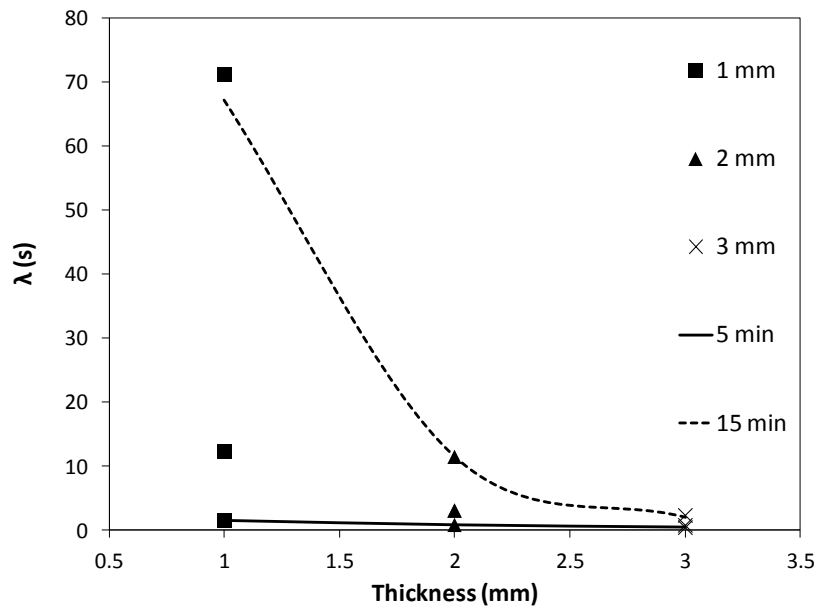


Figure 5-9: Effect of the time-thickness interaction on relaxation time ( $\lambda$ )

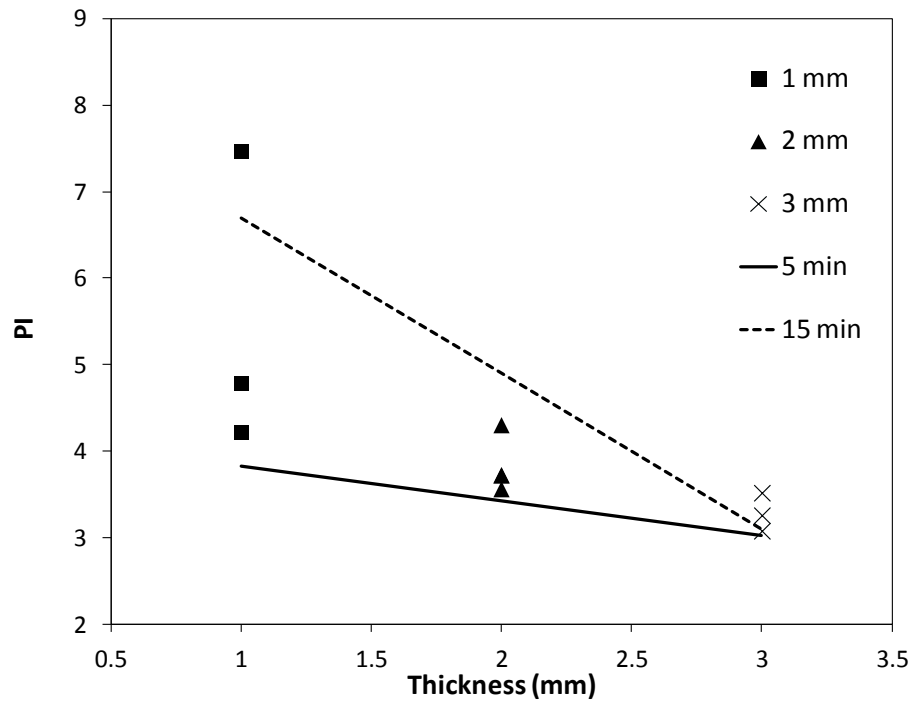


Figure 5-10: Effect of the time-thickness interaction on rheological polydispersity index (PI)

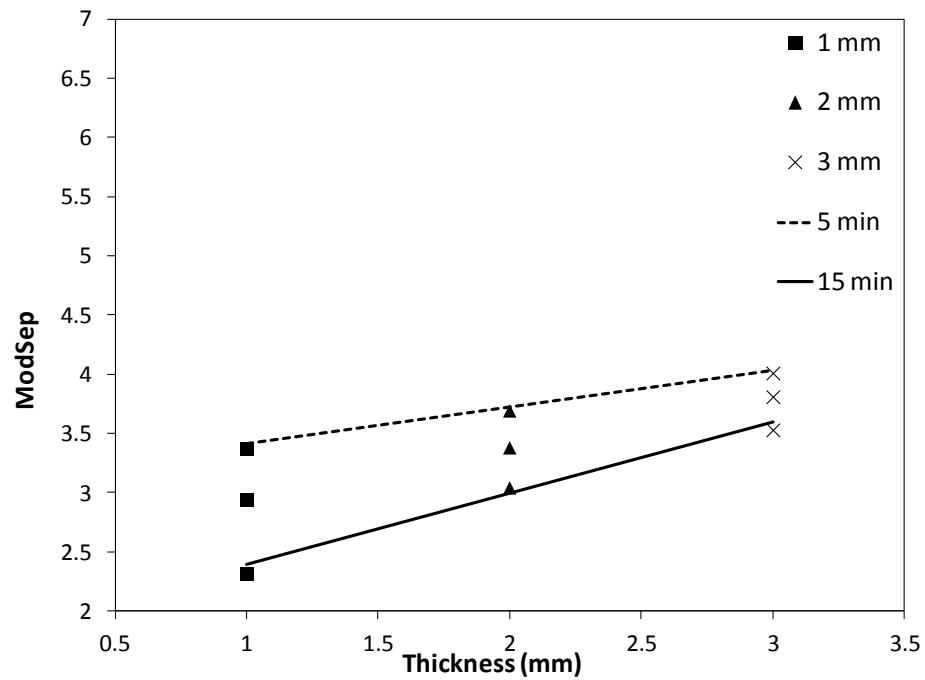


Figure 5-11: Effect of the time-thickness interaction on ModSep

### 5.3.2 EFFECT ON MOLECULAR WEIGHT AND MOLECULAR WEIGHT DISTRIBUTION

In this section, the effects of sample thickness and radiation time on MW, MWD and intrinsic viscosity  $[\eta]$  of the samples are investigated.

Number average ( $\bar{M}_n$ ), weight average ( $\bar{M}_w$ ), z average ( $\bar{M}_z$ ) and polydispersity index (PDI) values from all runs are summarized in Table 5-4.

In Table 5-4, when the thickness is low, the effect of radiation time is more significant. Comparing the 1 mm thick samples (runs 1, 2, and 3), it can be inferred that longer radiation times result in larger average molecular weights (in principle) and PDI; however, these changes are less pronounced when the thickness increases (2 mm and 3 mm runs). The molecular weight trends will be revisited shortly.

Having the weight average MW ( $\bar{M}_w$ ) values from GPC,  $\eta_0$  can be calculated using Equation 3-12. Comparing the calculated  $\eta_0$  (Equation 3-11) and  $\eta_0$  from the LVE measurements (Cross model), one can make inferences [6] about the type of the long chain branches (see also the section 3.1.1 under Chapter 3). Figure 5-12 shows these calculated  $\eta_0$  and measured  $\eta_0$  values (from LVE) versus  $\bar{M}_w$  for all experimental runs.

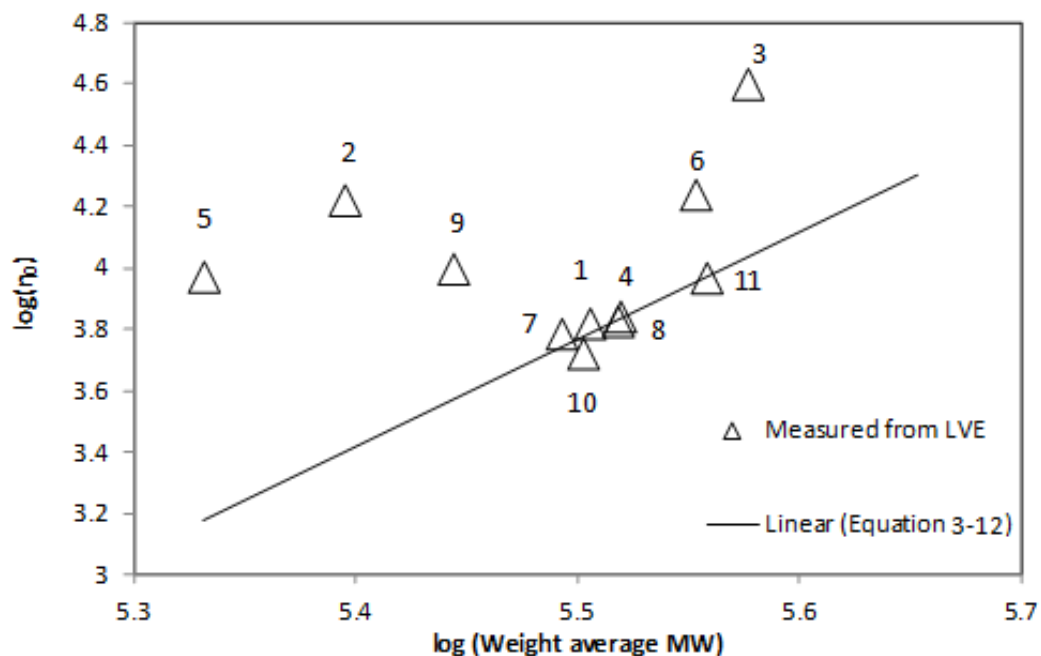


Figure 5-12: Comparison between calculated (linear reference) and measured  $\eta_0$

Runs 2, 3, 5, 6 and 9 are above the linear reference (Figure 2-1), which indicates that the long chain branches in these runs are possibly star-shaped. In the 1 mm thick samples (runs 1, 2 and 3), radiation for 5 minutes does not cause a significant deviation above the linear reference, whereas after 10 minutes of radiation  $\bar{M}_w$  decreases (Table 5-4), but  $\eta_0$  increases (Table 5-2). If one increases the radiation time to 15 minutes, this results in an increase in both molecular weight and  $\eta_0$ . Samples with thickness of 2 mm (runs 4, 5 and 6) also exhibit a similar trend. The suggested reason for this trend is degradation, which happens at the onset of radiation and then in parallel to the LCB reactions. Degradation results in a decrease in molecular weight; however, a subsequent formation and increase in the amount of long chain branches can compensate for the effect of initial degradation. Radiation for 5 min does not cause significant changes in the molecular weight of the samples (runs 1 and 4). After 10 min, and despite formation of long chain branches ( $\eta_0$  is above the linear reference), the effect of degradation on the molecular weight is still more dominant than that of LCB (runs 2 and 5). In other words, the population of long chain branches is not high enough to compensate for initial degradation effects on  $\bar{M}_w$ . An increase in  $\bar{M}_w$  is

observed after 15 minutes from the onset of radiation, when the amounts of long chain branched (and crosslinked) molecules are large. This subsequently results in an increase in  $\bar{M}_w$  and deviation of  $\eta_0$  above the linear reference.

Table 5-4: Molecular weight averages and PDI of the radiated runs along with melt mixed and parent PP

Sample ID	Thickness (mm)	Radiation time (min)	$\bar{M}_n$ (kg/mol)	$\bar{M}_w$ (kg/mol)	$\bar{M}_z$ (kg/mol)	PDI
1	1	5	69.2	320.2	908.9	4.6
2	1	10	43.1	259.1	904.2	6.0
3	1	15	36.5	377.1	1,331.8	10.3
4	2	5	71.8	329.6	650.2	4.6
5	2	10	53.0	214.5	502.9	4.0
6	2	15	67.5	357.3	919.3	5.3
7	3	5	77.7	310.9	676.7	4.0
8	3	10	76.3	330.4	582.4	4.3
9	3	15	66.8	277.9	700.8	4.2
10	1	0	75.0	317.9	591.2	4.2
11	1	0	78.4	361.4	714.8	4.6

For the 3 mm thick samples, the decrease in  $\bar{M}_w$  (Table 5-4) and increase in  $\eta_0$  (Table 5-2) were only evident after 15 minutes from the onset of radiation. This is because the molecular weight of the thick samples is not as affected due to UV penetration limitations, and therefore the average molecular properties of the samples can remain unchanged even after long radiation times.

In order to compare the MWDs of the runs with 1 mm thickness at different radiation durations, the MWDs are summarized in Figure 5-13 A. Figure 5-13 B contrasts the MWDs of the runs with different thickness that were exposed to UV for 15 min. In Figure 5-13 (A and B), the parent PP (run 11) is not shown as its MWD overlaps with run 10, which is PP after melt mixing with 0.5 wt-% BPH.

In Figure 5-13 A, the MWD of run 1 is slightly shifted towards lower MWDs (relative to that of the reference of run 10). This shift towards lower MWDs is more significant in run 2, which is radiated for longer durations. Moreover, the MWD of run 2 has become

significantly broader compared to run 1 and run 10 (the reference run). Radiation for 15 min (run 3) not only results in a broader MWD (compared to runs 1, 2 and 10) but also shifts the MWD tail to larger molecular weights. This is in agreement with the mechanism of Figure 5-3, which suggests degradation and LCB happening simultaneously. Hence, an increase in molecular weight (MW) happens after long radiation time when the population of long chain branches are large enough to compensate for degradation effects on both the MW and MWD.

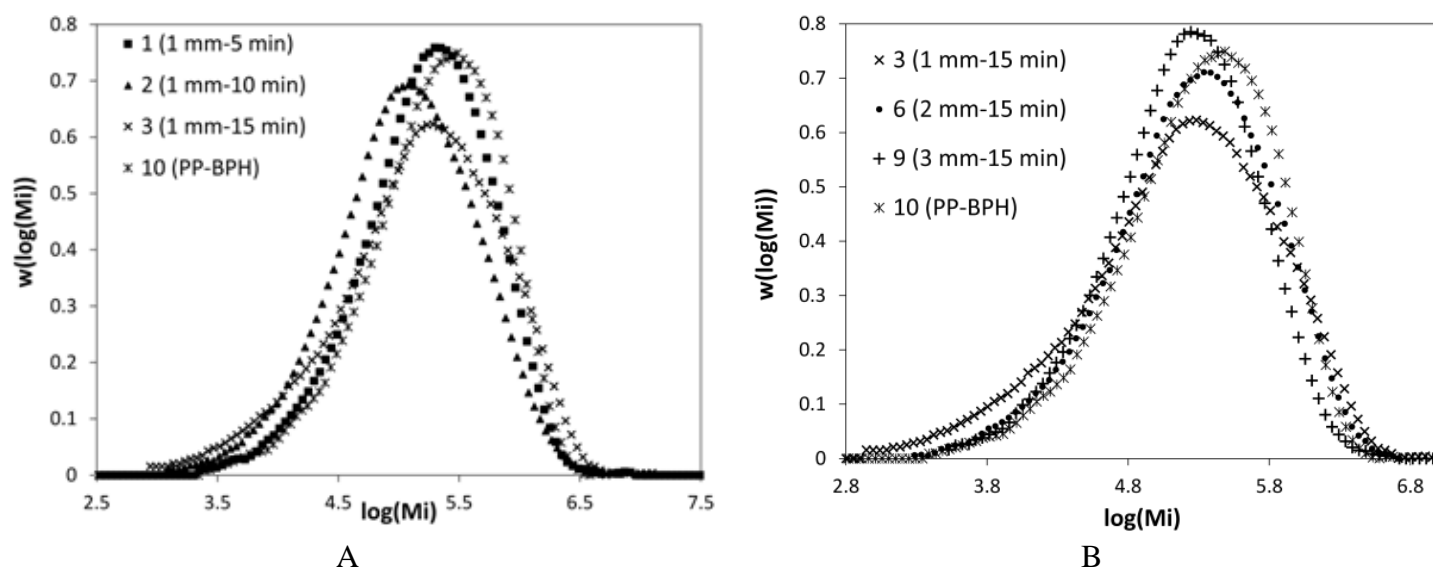
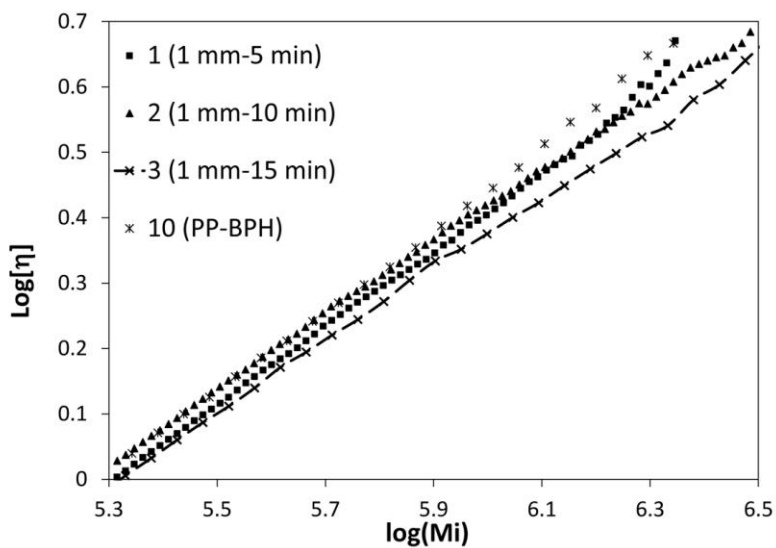


Figure 5-13: MWDs of the runs A) with 1 mm thickness at different exposure times to UV B) with different thickness after 15 min radiation

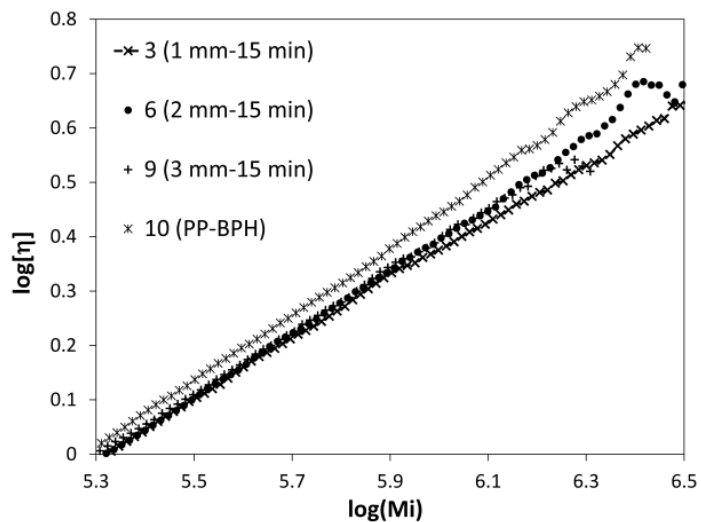
Figure 5-13 B shows the effect of sample thickness on the MWD of the runs that are radiated for 15 min. Comparison between runs 3, 6 and 9 shows an increase in the population of long chains with a decrease in samples thickness. Consequently, this shifts the distribution towards higher molecular weights (larger tail in runs 3 and 6 compared to the parent PP). This is because UV can penetrate thoroughly into the whole depth of the samples, in thinner samples, and hence formation of high molecular weight chains due to LCB is more effective. For run 9, the distribution becomes narrower and shifts towards lower MWs compared to the reference run (run 10). This is again due to limitations in UV

penetration into the depth of the samples, which results in formation of fewer long chain branches in the sample.

The intrinsic viscosity ( $[\eta]$ ) of the samples was also measured via GPC and compared for different runs. Qualitative comparisons between the obtained curves can serve as an indicator of the molecular structure of the polymers. It is known that formation of LCB in the polymer results in a lower intrinsic viscosity due to the smaller radius of gyration of long chain branched chains. Thus,  $\log [\eta]$  versus  $\log (M_i)$  is linear for a linear polymer with known slope and intercept (Mark-Houwink constants).  $M_i$  here represents molecular weight values. However, presence of LCB in the polymer causes deviations from this linear relation by shifting the slope at higher molecular weights to lower values. As changes in the slope of  $\log [\eta]$ - $\log (M_i)$  are more significant for thin samples and long radiation times, plots are shown for different radiation times for samples of thickness of 1 mm (Figure 5-14A), and subsequently at 15 min radiation time for different thicknesses (Figure 5-14 B). This way is analogous to the results of Figure 5-13 (with curve 10 (solid line) representing the reference run). In Figure 5-14 A, runs 2 and 3 show a change in their slope to lower intrinsic viscosities. This change is more pronounced in the slope of run 3 at MW values of about 790 kg/mol ( $\log (M_i)$  values of about 5.89). Figure 5-14 B shows the intrinsic viscosity of the runs with different thicknesses but with the same radiation time (15 min of radiation). As the thickness of the samples decreases, the deviation from the linear reference becomes clearer (and hence, the presence of LCB).



A



B

Figure 5-14: Intrinsic viscosity  $[\eta]$  vs.  $\log(Mi)$  A) with 1 mm thickness at different exposure times to UV B) with different thickness after 15 min radiation

### 5.3.3 EFFECT ON GEL CONTENT

In order to investigate the presence of gel (due to crosslinking) in each run, extraction experiments were carried out. The results from these measurements are summarized in Figure 5-15. The parent PP (run 11) and PP after melt mixing with BPH (run 10) are not shown in Figure 5-15 since there was no gel found in these samples.

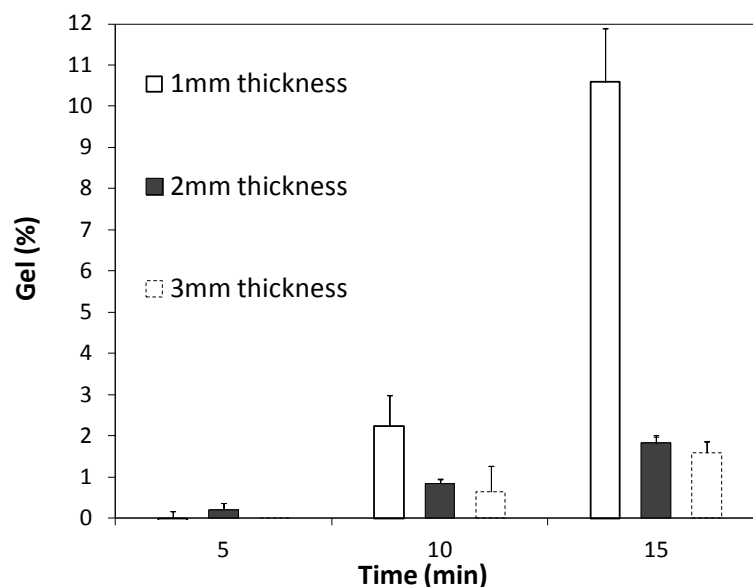


Figure 5-15: Gel content of the runs with different thickness at different radiation times

Figure 5-15 shows that after 5 min radiation almost no gel was detected in the runs and only after 10 min from the onset of radiation significant formation of gel was detected. Increases in radiation time cause larger percentage of CL in the samples with the same thickness. Moreover, decrease in the thickness increases the percentage of gel in the runs. An increase in gel content upon increasing radiation time is more significant at low thicknesses. This is the same trend that was observed in rheological properties earlier.

Formation of gel in the samples might be due to addition of more branches to the chains that are already long chain branched, which may result in formation of network structures. Figure 5-16 explains this mechanism. These reactions are probable since long chain branched chains have more repeating units and they are statistically more favored to undergo hydrogen abstraction again.

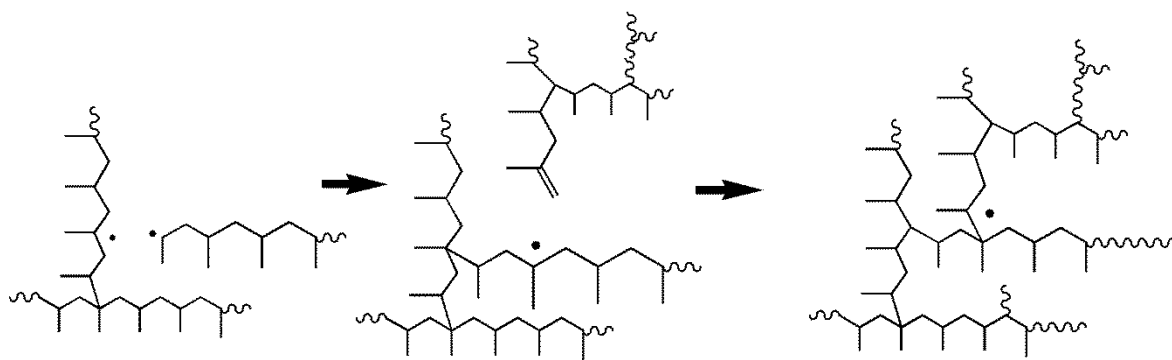


Figure 5-16: Schematic of mechanism that leads to crosslinking of long chain branched polymers

The amount of gel content of the runs was analyzed statistically and the empirical model is shown in Table 5-5. As expected, the AB two-factor interaction is significant (A=thickness, B=time).

Table 5-5: Empirical model for gel content in the radiated runs

Statistical model	R2	Adj. R2	Equation #
$\sqrt{Gel} = -3.10 + 0.55 * A + 0.37 * B - 0.10 * AB$	0.89	0.83	Equation 5-7

Figure 5-17 shows the effect of the AB interaction on the percent gel in the samples. As expected from the previous effects on LVE and molecular weight properties, an increase in thickness at constant radiation time results in lower gel content in the samples. This effect is more pronounced after 15 min of radiation.

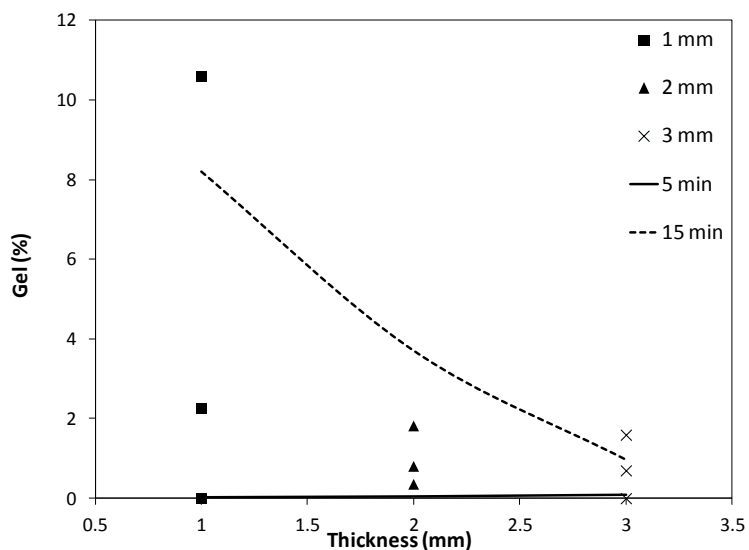


Figure 5-17: Effect of the time-thickness interaction on gel content

## 5.4 CONCLUDING REMARKS

PP has been modified using 0.5 wt-% BPH as photoinitiator and UV radiation to introduce LCB to its structure and increase its melt strength. The effects of radiation time and thickness of samples were investigated simultaneously using three-level factorial experiments. Both factors and their interaction were found to significantly affect the rheological properties, such as  $\eta_0$ ,  $\lambda$ , PI, and ModSep, the molecular properties (MW and MWD), and, finally, gel content. ER and the shear thinning index depended on radiation time and thickness, but seemed independent of the interaction.

Both an increase in radiation time and a decrease in thickness of the samples result in a broader relaxation spectrum and larger  $\eta_0$ ,  $\lambda$  and ER, and more shear thinning behaviour (smaller  $n$ ). On the other hand, at the same radiation time, thicker samples have lower  $\eta_0$ ,  $\lambda$  and ER, and larger  $n$ . Moreover, thick samples are less sensitive to changes in radiation times. Broadening of the relaxation spectrum with increasing radiation time was observed after longer radiation times for thicker samples (2 and 3 mm) compared to 1 mm samples.

The MW and MWD data show that an increase in radiation time and a decrease in sample thickness result in an increase in MW and broadening of MWD. The same trends were observed for the gel content of the samples. Thinner samples which were irradiated for longer durations showed greater gel content than thick samples which were radiated for shorter durations. Lower gel content and lower MW of the thick samples were attributed to limitations in UV penetration depth, which causes inhomogeneities in the formation of LCB throughout the sample.

## **6 CHAPTER 6: COMBINATION OF COAGENT EFFECT AND PHOTOMODIFICATION**

In this chapter trimethylolpropane triacrylate (TMPTA) as coagent was utilized along with benzophenone (BPH) to modify polypropylene (PP) by generating long chain branches in the PP molecular structure with the related benefits. The effects of TMPTA concentration, BPH concentration, and irradiation duration on viscoelastic properties and gel content were studied. Using statistical tools, the processing conditions that result in the greatest amount of long chain branching (LCB) with minimum amount of gel content were identified. It was found that when the radiation duration was above 45 s, increasing BPH content at low coagent concentration resulted in a great improvement in viscoelastic properties, while the gel content remained relatively low. Gel permeation chromatography (GPC) was used to confirm formation of branches and determine the branching content, whereas FTIR spectroscopy confirmed the contribution of TMPTA in the formation of long chain braches.

### **6.1 INTRODUCTION**

The extensional viscosity of a polymer melt is an important property for processes such as film blowing, blow molding, extrusion coating, thermoforming, foaming and fiber spinning [18, 64, 65]. In these processes, the polymer chains experience significant extensional deformation. The polymer melt strength (polymer resistance to extensional deformation) is an important property for these processes.

The increase of the extensional viscosity of a polymer melt when stretched is called strain hardening [35, 66]. Strain hardening results in greater melt strength in the polymer and prevents sagging, shape deformation and necking during melt processing [67]. Strain hardening in polymer melts can be due to broad molecular weight distribution (MWD), high molecular weight (MW), presence of long chain branches or blending with high melt strength polymers [10, 65]. Among all these methods, long chain branching (LCB) is the most effective way to improve strain hardening and consequently enhance the melt strength

of the polymer. Presence of small amounts of LCB can lead to a significant increase in melt strength, thus inducing strain hardening in the polymer melt [67].

Polypropylene (PP) is a commercial polymer with low melt strength and extensional viscosity. LCB has been introduced to PP to increase its melt strength and broaden its processing window in applications that demand high extensional viscosity (for example, foaming, thermoforming, extrusion coating and blow moulding) [30, 45]. In order to modify the melt strength of PP via introduction of LCB, the first step is controlled generation of PP macroradicals. There are several methods to generate PP macroradicals: 1) using chemical initiators such as peroxides, which are activated by heat [1, 10], 2) using high energy radiation such as gamma or electron beam [8, 15, 18], and 3) using UV radiation to activate photoinitiators [50, 51]. In methods that involve the use of chemical initiators or photoinitiators, the activated initiator can abstract a tertiary hydrogen atom from the PP backbone and form a macroradical [50]. The second step in this kind of modifications is to control the  $\beta$ -scission reaction (Figure 6-1 a) and prevent excessive decrease in the MW of the polymer.

Hence, different techniques have been used to control chain degradation by stabilizing the radical center (e.g., reducing processing temperature or using coagents) [6, 10]. Coagents are reactive multifunctional monomers that react with the radical center and prevent  $\beta$ -scission so the radical center can react with another PP macroradical and form branches [6, 7, 50, 68]. Different coagents have been used along with different initiators to find efficient systems for this purpose. It was found that coagents such as furfuryl sulphide (FS), trimethylolpropane triacrylate (TMPTA) and triallyl phosphate (TAP) were suitable for branching, while the efficiency of coagents like divinylbenzene (DVB) were relatively low [69].

Parent et al. [6] compared the effect of acrylic coagents, such as trimethylolpropane triacrylate (TMPTA), and allylic coagents, such as triallyl trimesate (TAM) and TAP, on the modification of PP rheology and formation of long chain branches. It was found that TMPTA (trifunctional acrylic monomer) had faster kinetics compared to the other coagents and a more pronounced effect on improving shear and extensional rheology. Isolated gel

regions were formed due to addition of TMPTA. It was also found that TMPTA was the only coagent among the three studied that showed hyper-branching even at low percentages [6].

In this chapter, benzophenone (BPH) is used as photoinitiator with UV irradiation, being responsible for formation of radical centers in PP, and TMPTA is used to control  $\beta$ -scission reactions. Figure 6-1 illustrates reactions that lead to the formation of radical centers in PP chains.

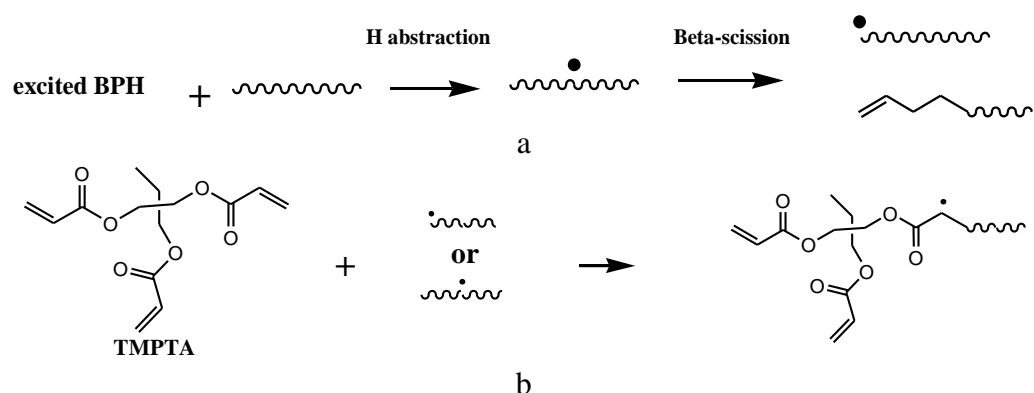


Figure 6-1: Schematic mechanism of a) photoinitiation and  $\beta$ -scission, b) TMPTA reactions with macroradicals

Photoinitiators, which are activated via UV irradiation, abstract tertiary hydrogens from PP backbones and form macroradicals (Figure 6-1 a). Depending on the radiation conditions or photoinitiator content, the molecular properties of the modified PP are either dominated by degradation or macroradical combination (resulting in LCB). Process variables such as photoinitiator concentration, UV lamp intensity, irradiation time, and temperature, were recently studied in detail and found to affect the final properties of the modified PP in the absence of coagent [52, 58]. The modified PP in this case could be either degraded or imparted with long chain branches, so maintaining a balance becomes the controlling factor. It was found that the highest amount of LCB in PP can be achieved by using 0.5 wt-% BPH and radiation for 10 min (or longer) at temperatures below 60 °C. Maintaining low temperature was necessary to prevent degradation due to  $\beta$ -scission reactions. Thus, in the absence of coagents, a large degree of LCB was only attained when radiation time was

greater than 5 minutes [70]. Since this irradiation time might arguably be long for certain processing applications, it was decided to combine UV irradiation with a multifunctional coagent, such as TMPTA, with a fast reaction rate. TMPTA protects the macroradicals from  $\beta$ -scission and promotes formation of LCB (Figure 6-1 b). However, utilizing multifunctional coagents can also increase the gel content of the modified runs by adding a large number of double bonds, which encourage formation of crosslinked networks in the polymer structure (Figure 6-1 b exhibits such possible reactions).

Therefore, in this chapter, the effects of coagent concentration in combination with BPH concentration and irradiation time are investigated. A central composite design (CCD) is used to study the effects of these variables on the formation of long chain branches, identifying the most significant variables and their interactions. Viscoelastic properties and gel content of the runs were measured and used to find optimal conditions yielding the largest LCB content while keeping gel content relatively low. Viscoelastic properties were employed since they are very sensitive to the molecular structure of the polymers and greatly affected by LCB and crosslinking (CL). Gel content measurements can help distinguish runs with LCB from runs with large amounts of CL.

## **6.2 EXPERIMENTAL**

### **6.2.1 MATERIALS**

Polypropylene homopolymer (PP2255E1) from ExxonMobil with melt flow rate (MFR) of 3.5g/10 min (230 °C, 2.16 kg) was used as the parent PP. Benzophenone (BPH), 99 % purity, was purchased from Sigma-Aldrich and used as photoinitiator. Trimethylolpropane triacrylate (TMPTA) was purchased from Sigma-Aldrich and used as coagent. Irganox 1010, Ciba Specialty Chemicals, was used as antioxidant to prevent PP thermal degradation.

## 6.2.2 DESIGN OF EXPERIMENTS

In order to study the effect of coagent and photoinitiator concentration along with radiation time on the modification of PP, and determine the conditions which result in the optimum rheological behavior, a central composite design (CCD) was used (see Table 6-1). The aim is to locate the processing window which yields the largest amount of LCB, while the percentage of gel remains low. This window was found by statistically analyzing viscoelastic responses along with gel content. The analysis was carried out using Design Expert software (version 8.0.7.1). Table 6-1 shows the different levels of the actual and coded variables (factors). The coded levels (the last three columns) are used in the models of Table 6-3. A, B and C indicate the coded levels for coagent concentration, BPH concentration and radiation time, respectively.

Table 6-1: Design of experiments (CCD design)

Run ID	Coagent (wt-%)	BPH (wt-%)	Time (s)	A	B	C
1	0.25	0.1	10	-1	-1	-1
2	0.75	0.1	10	+1	-1	-1
3	0.25	0.5	10	-1	+1	-1
4	0.75	0.5	10	+1	+1	-1
5	0.25	0.1	60	-1	-1	+1
6	0.75	0.1	60	+1	-1	+1
7	0.25	0.5	60	-1	+1	+1
8	0.75	0.5	60	+1	+1	+1
9	0.20	0.3	35	-1.215	0	0
10	0.80	0.3	35	+1.215	0	0
11	0.5	0.06	35	0	-1.215	0
12	0.5	0.54	35	0	+1.215	0
13	0.5	0.3	4.6	0	0	-1.215
14	0.5	0.3	65.4	0	0	+1.215
15	0.5	0.3	35	0	0	0
PP	0	0	0	-	-	-

### 6.2.3 PREPARATION METHOD

Certain quantities of BPH and TMPTA (based on the conditions in Table 6-1) along with 0.1 wt-% Irganox 1010 were dissolved in 30 ml of acetone. This solution was hand-mixed with PP granules and heated at 60 °C for 12 hr until all acetone evaporated.

PP pellets coated with photoinitiator (BPH), Irganox, and coagent (TMPTA) were melt-mixed in a batch mixer at 190 °C and 100 rpm for 8 minutes. The samples were subsequently ground using a Wiley mill (model 1102, Arthur H. Thomas Co.). After grinding, granules were compression-moulded into discs with 25 mm diameter and 1 mm thickness at 190 °C under an applied force of 4,400 N for five minutes. The discs were subsequently irradiated using a mercury UV lamp (Versa Cure).

Prior to irradiation of the samples, the lamp was turned on for two minutes so that a steady level of radiation intensity was achieved. During irradiation, pressurized air was used to cool down the area beneath the lamp (temperature was maintained around 38 °C).

### 6.2.4 CHARACTERIZATION

For rheological measurements (parallel plate rheometry), the same steps explained in section 4.2.3.1 of Chapter 4 were followed. From parallel plate measurements, storage modulus ( $G'$ ), loss modulus ( $G''$ ), complex modulus ( $G^*$ ), loss tangent ( $\tan \delta$ ), and complex viscosity ( $\eta^*$ ) were obtained at different angular frequencies ( $\omega$ ). Using Equation 3-11 in section 3.1 of Chapter 3,  $\eta^*$  vs.  $\omega$  graphs were used to find the shear thinning index ( $n$ ), zero shear viscosity ( $\eta_0$ ) and relaxation time ( $\lambda$ ) of each sample by fitting the Cross model (Equation 3-11) using MATLAB.

For the runs with high gel content, shear creep tests were conducted and creep compliance ( $J(t)$ ) vs. time data were used to evaluate the zero shear viscosity ( $\eta_0$ ). The creep tests were conducted at 190 °C and 30 Pa for 3 hours to evaluate zero shear viscosity ( $\eta_0$ ). A stress sweep was performed first to verify the linear viscoelastic region and it was found that 30 Pa was well within the linear viscoelastic region. NLREG, a nonlinear regression

software, was used to calculate zero shear viscosity from creep compliance (J(t)) vs. time data.

ER (rheological polydispersity index corresponds to high MW chains distribution) was determined using Equation 3-15.

Having G' and G'' at different frequencies, the relaxation spectrum (H( $\lambda$ )) can be calculated using Equation 3-9 and Equation 3-10 in section 3.1 of Chapter 3. NLREG is the nonlinear regression software which is used to calculate the relaxation spectrum (H( $\lambda$ )) [62]. A broader relaxation spectrum is expected from LCBPP. Dispersion and skewness of the relaxation distribution were compared using RSI (relaxation spectrum index) and RSS (relaxation spectrum skewness) (Equation 6-1 and Equation 6-2, respectively).

$$RSI = \frac{\mu_{II}}{\mu_I}; \mu_I = \frac{\sum_{i=1}^n \lambda_i H(\lambda_i)}{\sum_{i=1}^n H(\lambda_i)}; \mu_{II} = \frac{\sum_{i=1}^n H(\lambda_i)}{\sum_{i=1}^n \frac{H(\lambda_i)}{\lambda_i}} \quad \text{Equation 6-1}$$

$$RSS = \frac{1/n \sum_{i=1}^n (H(\lambda_i) - \bar{H}(\lambda))^3}{(1/n \sum_{i=1}^n ((H(\lambda_i) - \bar{H}(\lambda))^2)^{3/2}} \quad \text{Equation 6-2}$$

RSI is the ratio of the second moment ( $\mu_{II}$ ) to the first moment ( $\mu_I$ ) of the distribution and RSS is derived from the ratio of the third to the second mean centered moments [71]. RSI was used to compare linear and long chain branched PP samples [6]. In this chapter, we suggest the RSS measure for an even more detailed comparison between the relaxation spectra of different runs.

#### 6.2.4.1 GEL PERMEATION CHROMATOGRAPHY (GPC)

1 g of the ground polymer was placed in pouches (sample holder). The pouches were made from stainless steel 120 mesh sheets. The pouches were sealed and immersed in 100 ml of xylene at its boiling temperature. Dissolution process was continued for 4 hours and then the stainless steel pouches were taken out of the solution. 20 ml acetone was used as non-solvent to precipitate the dissolved polymer from the solution. The precipitated polymer was filtered and dried in an oven at 60 °C for 6 hr. This procedure leads to the elimination

of gel (insoluble fraction) from the samples to be subsequently analyzed via GPC. Hence, only the sol fraction of each sample was analyzed via GPC.

For the rest of GPC measurements and analysis the same procedure as section 4.2.3.3 in Chapter 4 were followed. Equation 3-20 and Equation 3-21 were used to calculate long chain branching distribution in the samples.

Gel content measurements were conducted and the same steps explained in section 4.3.4 of Chapter 4 were followed.

#### **6.2.4.2 FTIR SPECTROSCOPY**

FTIR spectra of the runs was obtained using an ABB Fourier-transform infrared spectrometer in two ranges of wavelength ( $1500\text{-}2000\text{ cm}^{-1}$  and  $1070\text{-}2000\text{ cm}^{-1}$ ), with  $2\text{ cm}^{-1}$  resolution. For the FTIR tests, 0.1 mm thick films were made by compression moulding at  $190\text{ }^{\circ}\text{C}$ .

### **6.3 RESULTS AND DISCUSSION**

#### **6.3.1 INFORMATION FROM THE VISCOELASTIC MEASUREMENTS**

Table 6-2 shows values for the shear thinning index ( $n$ ), zero shear viscosity ( $\eta_0$ ), relaxation time ( $\lambda$ ) and ER for all experimental runs along with the parent PP (its other columns will be discussed shortly). All modified runs have lower  $n$ , larger  $\eta_0$ ,  $\lambda$  and ER compared to the parent PP, which indicates formation of LCB and/or CL in all runs. As mentioned earlier, the zero shear viscosity of the runs with high gel content (runs 6, 8 and 10) was determined by conducting creep tests. Thus,  $n$  and  $\lambda$  were not calculated for these three runs, since the Cross model fit was not used for these runs. The reason is that these runs are found to exhibit power law behaviour due to the presence of significant amounts of crosslinked structures. Thus, the Cross model predications are not reliable for these three runs. The gel content in these runs will be discussed in more detail in the next section.

Moreover, increasing coagent concentration (compare runs 1-2 or 3-4 or 5-6 or 7-8 or 9-10) or increasing photoinitiator concentration (compare runs 1-3 or 2-4 or 5-7 or 6-8 or 11-13) or increasing radiation time (compare runs 1-5 or 2-6 or 3-7 or 4-8 or 13-15) result in an increase in  $\eta_0$ ,  $\lambda$  and ER and a decrease in n. Although n is not calculated for runs 6, 8 and 10, they show more shear thinning behavior compared to runs with lower TMPTA or BPH concentration, or runs radiated for shorter times. The plateau region has almost disappeared for these runs, which is a reflection of very long relaxation time. The reason for substantially greater  $\eta_0$ ,  $\lambda$  and enhanced shear thinning behavior in these runs might be the formation of interconnected crosslinked structures (the dominant structures formed in these runs). These CL structures are more favored at higher levels of coagent (the mechanism of formation of these structures at high TMPTA concentration will be revisited shortly).

Table 6-2: Viscoelastic properties, rheological polydispersity (ER), RSI and RSS measurements, gel content and FTIR measurements for the experimental runs

Run ID	n	$\eta_0$ (kPa.s)	$\lambda$ (s)	ER	RSI	RSS	Gel content (%)	C=O/-CH3
1	0.57	12.7	1.3	0.25	7,581	0.88	1.2	0.028
2	0.57	12.8	1.3	0.26	221	1.54	6.2	0.043
3	0.53	18.4	3.3	0.45	2,658	1.24	5.9	0.053
4	0.53	18.9	3.1	0.48	368	1.88	13.3	0.144
5	0.50	42.1	22.1	1.05	9,532	1.21	7.5	0.063
6	-	179.9	-	2.02	9640	6.10	36.1	0.071
7	0.49	93.0	138.2	1.55	399	1.80	5.6	0.072
8	-	231.3	-	2.97	3,689	1.57	26.4	0.134
9	0.50	52.6	40.0	1.17	7,800	1.09	6.1	0.078
10	-	114.5	-	1.42	763	1.70	23.8	0.167
11	0.56	17.0	2.0	0.38	271	1.59	10.7	0.048
12	0.50	195.1	421.4	2.28	2,935	1.38	12.5	0.111
13	0.59	10.5	0.7	0.17	72	1.89	4.2	0.136
14	0.50	157.8	286.0	2.09	21,739	1.14	16.00	0.119
15	0.50	124.2	157.9	2.02	4,660	1.39	12.6	0.099
PP	0.61	8.8	0.6	0.13	128	1.53	0	-

In order to find the effect of significant variables and interactions on each of these responses ( $\eta_0$ ,  $\lambda$ ,  $n$  and ER), Design Expert software was used. Empirical models were fit to each response. These models and their regression coefficients ( $R^2$  and adjusted  $R^2$ ) are listed in Table 6-3. These models, cited in Table 6-3, were constructed based on coded variables (shown in Table 6-1).

Table 6-3: Empirical models fitted on viscoelastic properties and gel content

Empirical model	$R^2$	Adj. $R^2$	Equation #
$\text{Log}(\eta_0)=4.71+0.13*A+0.19*B+0.45*C+0.11*AC$	0.83	0.77	Equation 6-3
$\text{Log}_{10}(\lambda)=+1.32+0.5*B+0.91*C$	0.78	0.73	Equation 6-4
$(n)^{-3}=7.14+0.02*A+0.6*B+1.18*C+0.65*A^2-0.58*C^2$	0.92	0.85	Equation 6-5
$ER=1.25+0.25*A+0.37*B+0.78*C+0.28*AC$	0.85	0.80	Equation 6-6
$(\text{Gel content})^{0.5}=3.31+1.06* A+0.15* B+0.82*C$ $+0.43*AC-0.47 *BC$	0.97	0.95	Equation 6-7

As exhibited in Table 6-3,  $\eta_0$ ,  $n$  and ER are significantly affected by coagent (A) and BPH concentration (B), and radiation time (C). It was also found that  $\lambda$  is only significantly affected by BPH concentration and radiation time. The only significant factor interaction was the one between coagent concentration and radiation time. The factor interaction graphs for  $\eta_0$  and ER are shown in Figure 6-2 and Figure 6-3, respectively. The dashed and solid lines show the fitted empirical model at high and low levels of radiation time, respectively, and the dots indicate the experimental results (Table 6-2). The interaction plots are shown at the high level of BPH concentration, but the trends are the same at the low level of BPH as well.

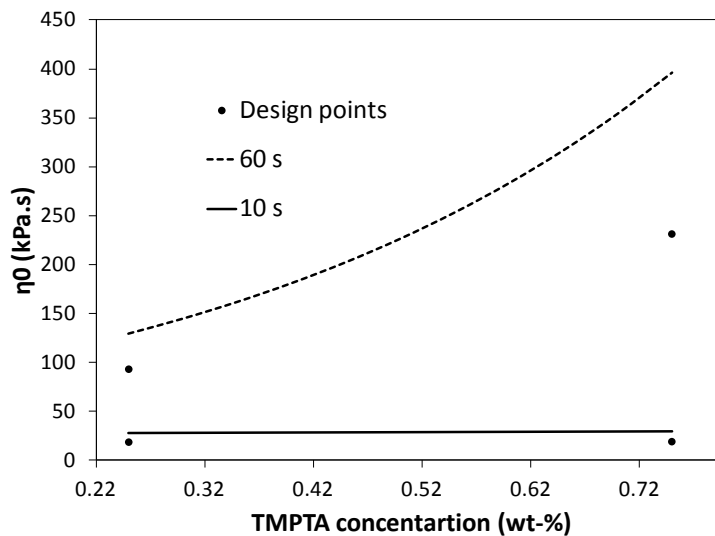


Figure 6-2: Effect of coagent concentration-irradiation time interaction on  $\eta_0$

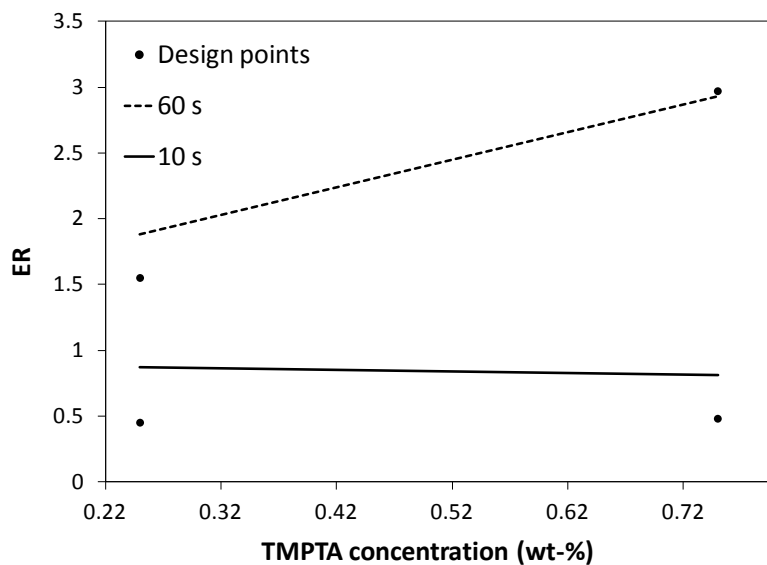


Figure 6-3: Effect of coagent concentration-irradiation time interaction on ER

Interaction graphs for  $\eta_0$  and ER (Figure 6-2 and Figure 6-3) indicate that increasing the coagent concentration at low radiation time does not affect  $\eta_0$  and ER significantly, but at long radiation time, increasing coagent concentration results in a greater  $\eta_0$  and ER. It is worth noting that an increase in  $\eta_0$  and ER means formation of a greater amount of long chain branches and/or crosslinks (greater MW and broader MWD);

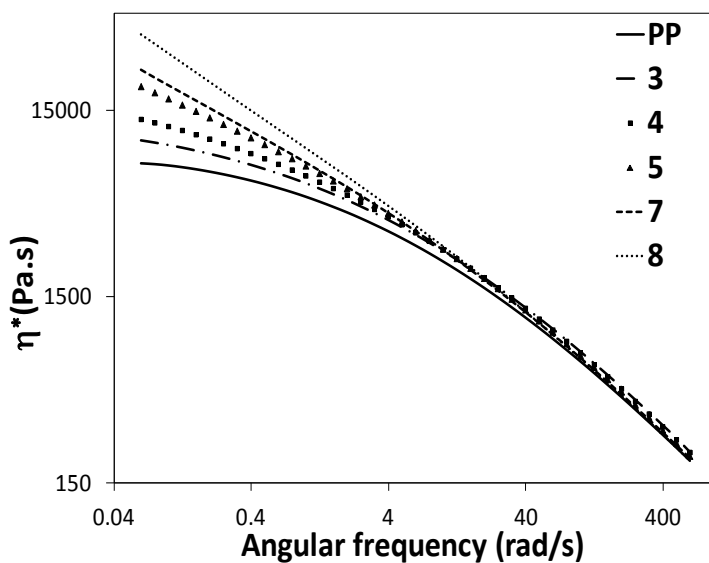
### 6.3.2 INFORMATION FROM THE RELAXATION SPECTRUM

Equation 3-9 and Equation 3-10 were used to calculate the relaxation spectra from  $G'-\omega$  and  $G''-\omega$  data, utilizing the NLREG software. Since a qualitative comparison between different spectra might be inaccurate, dispersity (RSI) and skewness (RSS) measures of the relaxation spectra were calculated using Equation 6-1 and Equation 6-2, respectively. Table 6-2 summarizes RSI and RSS values of the modified runs along with those of the parent PP. In general, either the relaxation spectrum of the modified runs becomes broader and/or it is skewed towards longer relaxation times after the modification. Broadening of the relaxation spectrum indicates formation of new chains due to long chain branching reactions. Formation of long chain branches (or crosslinks) in PP can also shift the distribution towards long relaxation times by forming more entangled structures.

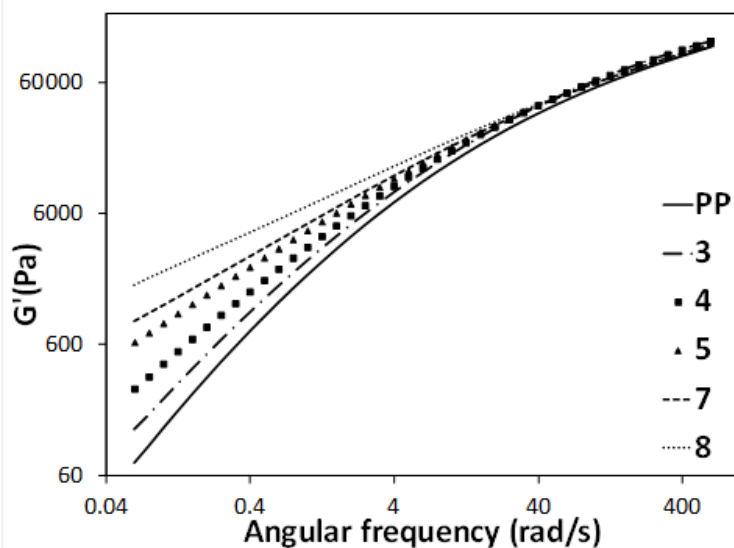
In general, increasing radiation time results in an increase in RSS values. The reason is that more macroradical combination reactions can happen at longer radiation time and more long chain branches and/or crosslinks can form. Furthermore, increasing coagent or BPH concentration causes larger RSS and lower RSI values. This is again due to formation of more long chain branched molecules (or crosslinked structures), which overpower the relaxation spectrum and skew the distribution towards high relaxation times. The only exception (run 8) shows a decrease in RSS and a dramatic increase in RSI, as coagent concentration increases, relative to run 7. The reason might be due to the high level of BPH and TMPTA in run 8, which increases the probability of hydrogen abstraction from a broader range of polymer molecules in the molecular weight distribution. Consequently, macromolecules with different molecular weights will have long chain branches. The relaxation spectrum of run 8 will be revisited shortly, in more detail.

Now, in order to make some more specific comments, let's scrutinize the effect of coagent, photoinitiator and radiation time on the rheological properties in more detail.  $\eta^*-\omega$ ,  $G'-\omega$ ,  $\tan(\delta)-G^*$  and  $G'-G''$  plots of runs 3, 4, 5, 7, 8 and the parent PP are shown in Figure 6-4 a, b, c and d. Runs 3 and 4 have the same BPH content and radiation time, runs (5-7) have the same TMPTA content and radiation time, and runs (3-7) and (4-8) have the same BPH and

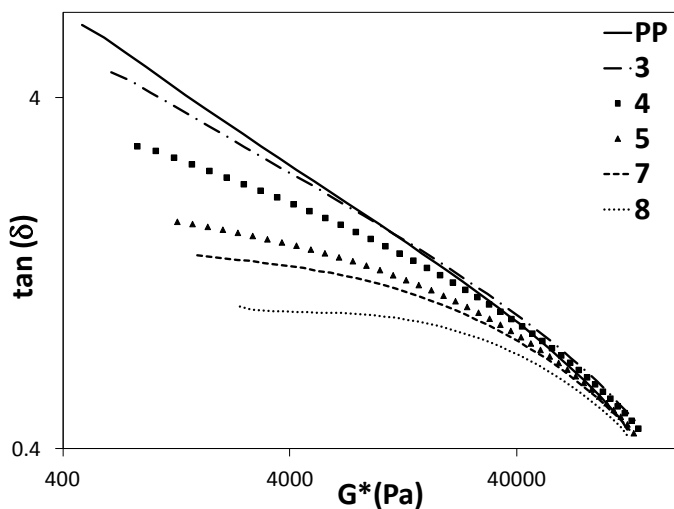
TMPTA content. Comparisons among all the other runs of Table 6-2 result in the same trends and consistency of observations. For example, in order to investigate the effect of TMPTA concentration at constant BPH concentration and radiation time, any of these pairs of runs (1-2, 3-4, 5-6, 7-8 and 9-10) can be compared and the trends will be the same. Thus, only runs 3 and 4 were compared among these pairs for the sake of brevity.



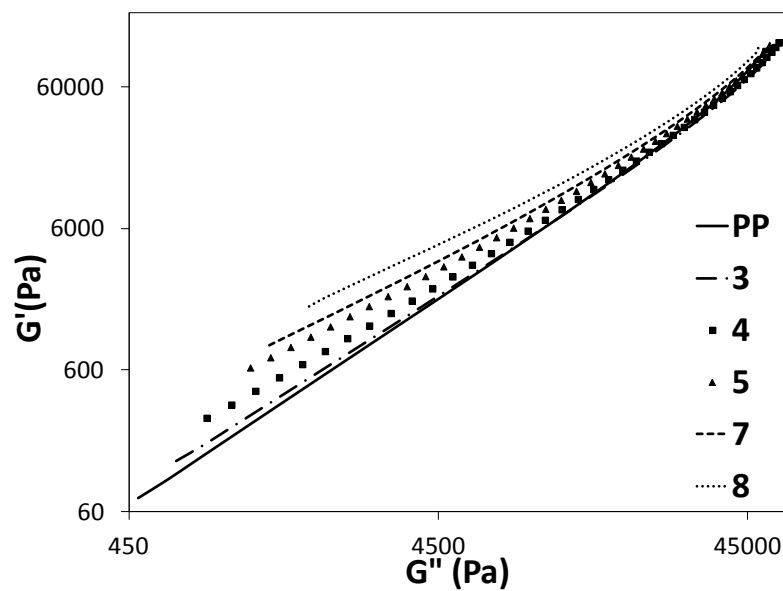
a



b



c



d

Figure 6-4: Comparison between viscoelastic properties of runs 3, 4, 5, 7, 8 and PP a)  $\eta^*$ - $\omega$ , b)  $G'$ - $\omega$ , c)  $\tan(\delta)$ - $G^*$  d) Cole-Cole plot ( $G'$ - $G''$ )

Figure 6-4a shows that increasing TMPTA concentration (runs 3-4), or increasing BPH concentration (runs 5-7), or increasing radiation time (runs (4-8) and runs (3-7)) result in a greater  $\eta^*$  at low frequencies and more shear thinning behavior in the samples.

Comparisons between runs (3-4) and runs (7-8) show that an increase in coagent concentration results in formation of more elastic structures (Figure 6-4b). Increasing BPH concentration (compare runs (5-7)) and radiation time also leads to greater elastic modulus (compare runs (3-7) or (4-8)). Moreover, the slope of  $G' - \omega$  for all modified runs is lower than that of the parent PP, which is an indication of formation of long chain branches [30]. Deviation of the modified runs from the parent PP in  $\tan(\delta) - G^*$  and Cole-Cole plots (Figure 6-4c and d) is an indication of broadening in the MWD [32]. Figure 6-4c and Figure 6-4d suggest that the MWD has become broader by increasing TMPTA concentration (runs (3-4) and (7-8)), or by increasing BPH concentration (runs 5-7) or by irradiating samples for longer time (runs (4-8) or runs (3-7)). A broader MWD reflects greater LCB content in the samples.

The relaxation spectra of the same selected runs are compared in Figure 6-5. Looking at the spectra shows that the RSI and RSS values (Table 6-2) correctly indicate the dispersity and skewness of the runs. The differences between the relaxation spectra of runs 5 and 7 show that a low amount of coagent in run 5 results in degradation and broadening of the molecular weight distribution. Broadening is towards the low relaxation time range, which corresponds to low molecular weights.

Increasing TMPTA concentration from run 3 to 4 results in a decrease in the broadness of the distribution due to stabilized radical centers that were formed via photoinitiation using TMPTA. This is followed by radical combination and formation of larger chains. However, as mentioned earlier, the only exception to this trend is run 8. The relaxation spectrum of run 8 is broader than run 7 despite the larger TMPTA concentration (possible reasons for this deviation from the general trend have been mentioned earlier in this subsection).

Moreover, as the radiation time increases (runs (3, 7) or (4, 8)), more combination reactions occur, which increases the molecular weight and relaxation time of the polymer chains and causes skewness towards high relaxation time ranges. Formation of crosslinked structures, which is promoted by increasing radiation time (going from run 4 to 8), is also responsible for shifting the spectrum towards longer relaxation times.

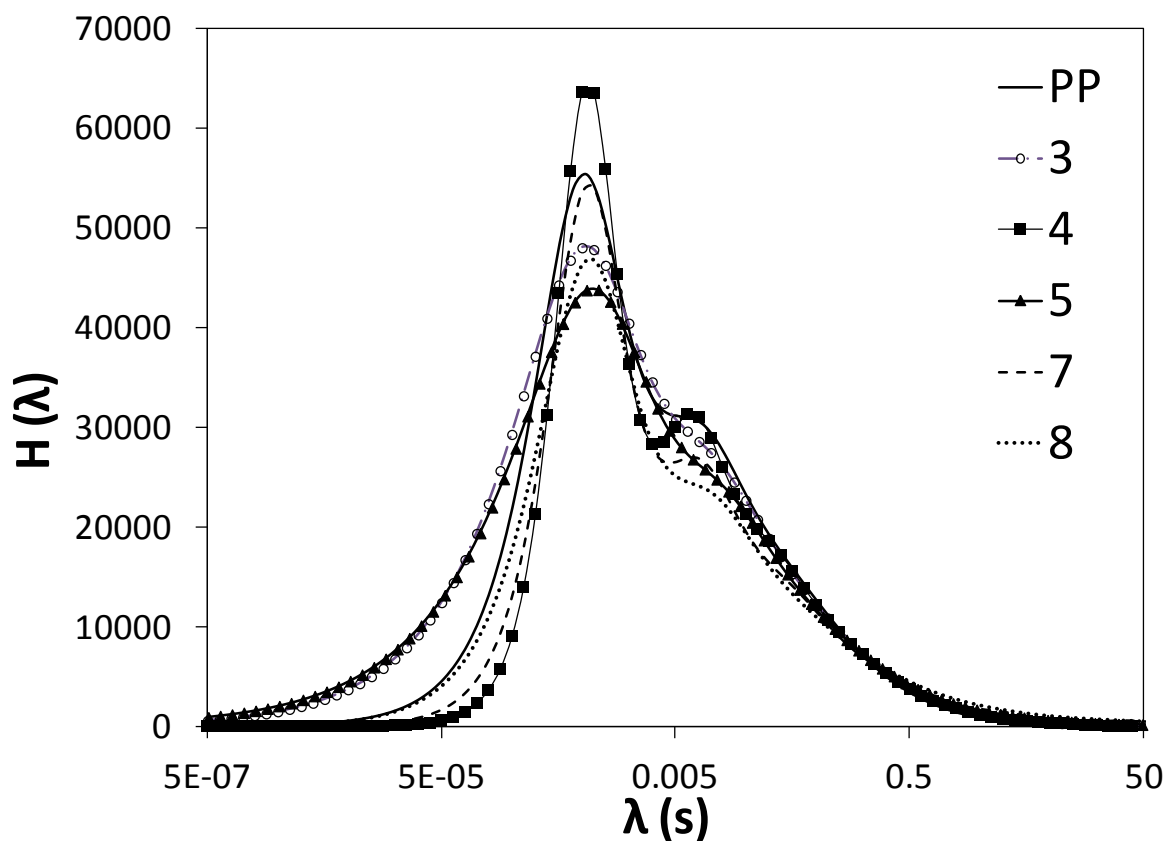


Figure 6-5: Comparison between relaxation spectrum of runs 3, 4, 5, 7, 8 and PP

### 6.3.3 INFORMATION FROM THE MOLECULAR WEIGHT DISTRIBUTION

GPC tests have been conducted on the same selected runs to study the effect of TMPTA, BPH concentration and radiation time on the molecular weight (MW), molecular weight distribution (MWD) and intrinsic viscosity  $[\eta]$  of the runs.

Figure 6-6 shows the molecular weight distributions of the runs. Modification reactions result in a broader tail at high molecular weight ranges ( $> 1,259$  kg/mol) for all runs due to formation of long chain branches. MWD graphs are in agreement with the relaxation spectra of the runs shown in Figure 6-5. In Figure 6-5, runs 4 and 7 have the most distinct shoulder at high relaxation time, which reflects the broad tail at the high molecular weight range for these runs (Figure 6-6). Also the broad relaxation spectrum of run 5 is in

agreement with its broad molecular weight distribution (this run has the broadest MWD and relaxation spectrum among all selected runs). From the MWDs, molecular weight averages ( $\bar{M}_n$ ,  $\bar{M}_w$  and  $\bar{M}_z$ ) and polydispersity index (PDI) were calculated (Table 6-4).

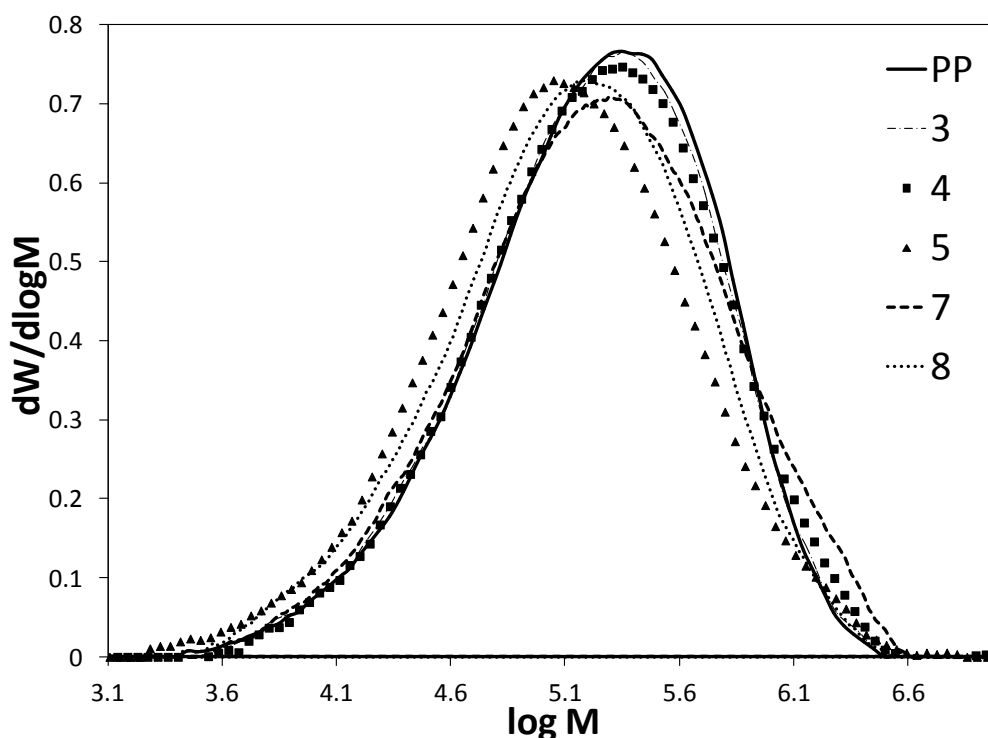


Figure 6-6: MWD of selected runs along with the parent PP

Table 6-4 shows the molecular weight averages and PDI of these runs. As expected, all runs have greater z average molecular weight ( $\bar{M}_z$ ), than the parent PP. Moreover, all runs have broader molecular weight distributions (reflected by a larger PDI) than the parent PP. This indicates broadening in the distribution and a shift towards high molecular weight ranges, which both reflect formation of long chain branches. Although  $\eta_0$  of run 8 is significantly larger than that of all other selected runs, its  $\bar{M}_w$  seems "smaller" than the parent PP. The reason is that only the soluble fraction of the runs has been used for the GPC measurements (gel has been removed; see procedure explained in section 2). Comparing runs 3 and 4 shows that increasing coagent concentration results in an increase

in MW and slight increase in PDI. As explained earlier, this is because coagent stabilizes the radical centers formed via photoinitiation and prevents them from degradation. The same trend cannot be observed for runs 7 and 8, due to the removal of gel from the samples. It is speculated that most long chain branched structures in run 8 were excluded while removing the insoluble fraction. High concentration of coagent and long radiation duration in the runs gives enough time and multifunctional sites for crosslinking reactions, so most long chain branched molecules were connected and formed insoluble gel structures. The same reason causes lower average molecular weight values for run 8 compared to run 4, which has a lower radiation time. On the other hand, MW averages ( $\bar{M}_w$  and  $\bar{M}_z$ ) of run 7 are larger than run 3 due to a larger radiation time; the MWD has also become broader (larger PDI). The reason is due to the low concentration of TMPTA in these runs (which prevents high gel content), so most long chain branched molecules are soluble. As expected, increasing BPH concentration (compare runs 5 and 7) also results in higher molecular weight.

Table 6-4: Molecular weight averages and PDI of selected runs along with the parent PP

Sample ID	Coagent content (wt-%)	BPH content (wt-%)	Radiation time (s)	$\bar{M}_n$ (kg/mol)	$\bar{M}_w$ (kg/mol)	$\bar{M}_z$ (kg/mol)	PDI
3	0.25	0.5	10	76.8	297.5	691.9	3.9
4	0.75	0.5	10	78.8	313.2	752.4	4.0
5	0.25	0.1	60	49.8	252.7	879.4	5.1
7	0.25	0.5	60	74.5	336.3	742.1	4.5
8	0.75	0.5	60	59.1	264.5	711.1	4.5
PP	-	-	-	75.3	277.8	263.6	3.7

Having the weight average MW ( $\bar{M}_w$ ) values from GPC,  $\eta_0$  can be calculated using Equation 3-12. Comparing the calculated  $\eta_0$  (Equation 3-12) and  $\eta_0$  from the viscoelastic measurements (Cross model), one can make inferences about the type of the long chain branches (see GPC subsection in section 2) [15, 72]. Figure 6-7 shows these calculated  $\eta_0$  (Equation 3-12) and measured  $\eta_0$  (fitting the Cross model to rheometry data) values versus  $\bar{M}_w$  for all selected experimental runs.

Parent PP viscosity lies on the linear reference (Equation 3-12) due to its linear structure. Runs 3 and 4, which were radiated for 10 s, show only a slight deviation from the linear prediction. On the other hand, runs radiated for 60 s (runs 5, 7 and 8) show large deviations from Equation 3-12 due to formation of more branches in the molecules. Since deviations from Equation 3-12 are towards larger  $\eta_0$  values, it is suggested that long chain branches are mostly star-shaped. The measured zero shear viscosity of run 8 is significantly above the linear reference. This can be explained by considering the high gel content of run 8, which was removed by filtering from the GPC samples. Hence, structures which were responsible for its large  $\eta_0$  in the rheological measurements were removed from the GPC tests.

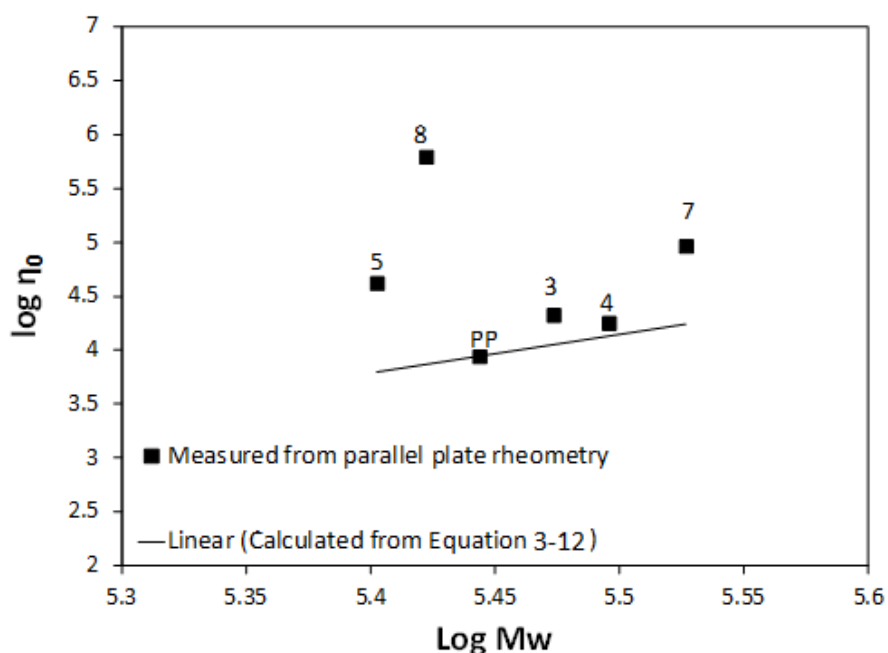


Figure 6-7: Comparison between calculated (linear reference) and measured  $\eta_0$  from parallel plate rheometry

As mentioned earlier in section 2 (GPC subsection), using intrinsic viscosity one can also look at the frequency of formation of long chain branches in the polymer chains. Figure 6-8 shows intrinsic viscosity ( $[\eta]$ ) and the weight average number of branches per chains (Bw).

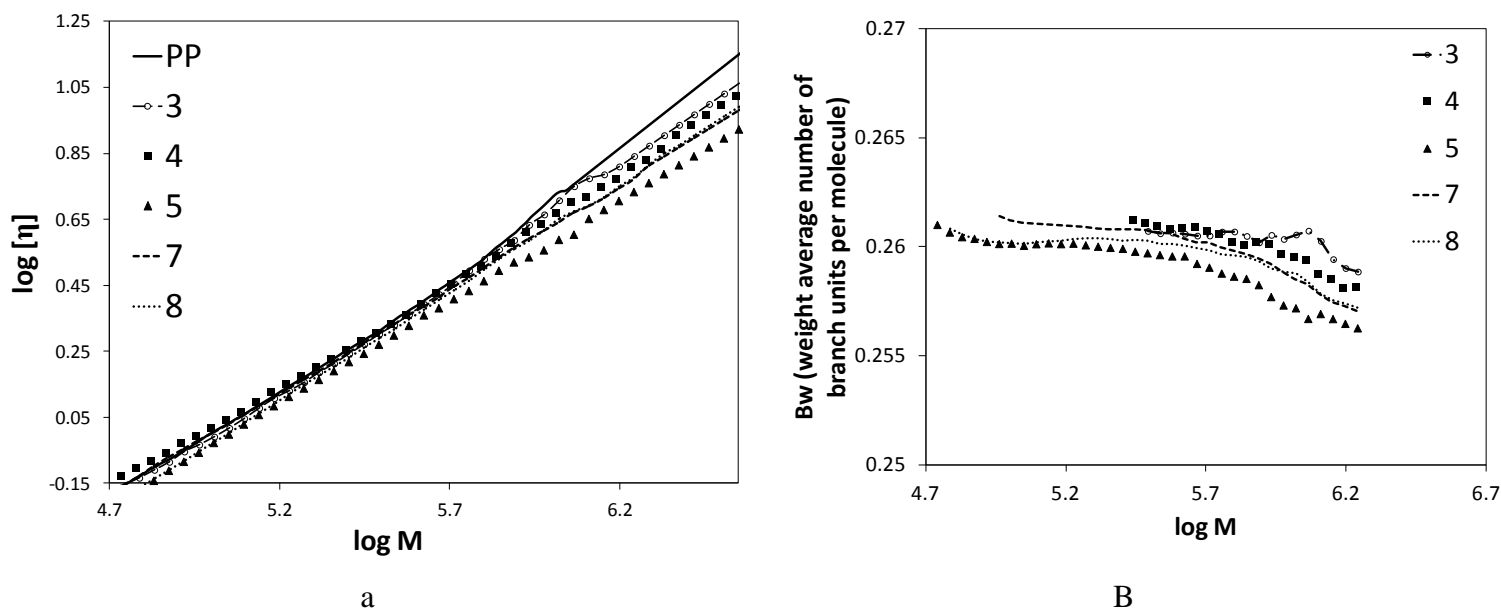


Figure 6-8: a) Intrinsic viscosity and b) weight average of number branches per polymer chains

Qualitative comparisons between the  $\log [\eta]$ - $\log M$  curves of the parent PP and the modified runs indicate negative deviations of the modified runs from the parent PP. This is expected, since, at the same molecular weight, long chain branched PP has lower  $[\eta]$  than the linear counterpart.

Significant deviations from the intrinsic viscosity of the parent PP (linear polymer) to lower values happen at the high molecular weight ranges (1,585 kg/mol). Figure 6-8b shows weight average number of branches ( $B_w$ ), calculated using Equation 3-20 and Equation 3-21. It is shown that the number of branching points is almost the same for different runs. The slight decrease in  $B_w$  at high molecular weight ranges is due to the lower concentration of high MW chains in the polymer solution during GPC measurements (see Figure 6-6). Increasing the radiation time (compare runs (3,7) and (4,8)) results in broadening of the molecular weight range over which long chain branches appear in the molecules.

### 6.3.3.1 INFORMATION FROM THE GEL CONTENT MEASUREMENTS

The gel content of the samples shows the fraction of the samples which is highly crosslinked, and consequently, insoluble in solvents. Isolated crosslinked domains can decrease PP melt drawability by acting as stress concentration points, hence high gel content is not preferred in the samples. However, formation of gel might be inevitable due to the presence of a multifunctional coagent. Table 6-2 shows gel content of the modified samples and the parent PP.

In order to confirm that formation of gel is due to reactions between PP macroradicals rather than TMPTA homopolymerization, experiments were conducted in which 0.8 wt-% TMPTA (the highest coagent content in the runs) and 0.1-0.5 wt-% BPH were dissolved in toluene and irradiated for 66 s (the longest irradiation time in Table 6-1). The radiated solution was filtered to separate the insoluble fraction; however, no amount of insoluble fraction was detected. Consequently, it may be assumed that the insoluble fraction in the modified runs is due to formation of crosslinked networks in the PP structure rather than TMPTA homopolymerization. More evidence will be given later in subsection 6.4.

Comparisons between the gel content of different runs (Table 6-2) show that increasing the coagent concentration, or BPH concentration, or radiation time, leads to formation of higher gel content in the samples. Table 6-3 shows that gel content is significantly affected by all three main factors and the two-factor interactions between coagent concentration-radiation time and BPH concentration-radiation time.

Figure 6-9 shows the effect of coagent concentration-irradiation time interaction on the gel content when BPH concentration is 0.5 wt-% (the trend is the same at the low level of BPH). Increasing the coagent concentration results in greater gel content and this effect is more significant at high radiation time. This trend is in agreement with the same two-factor interaction effect on  $\eta_0$  and ER, as observed earlier.

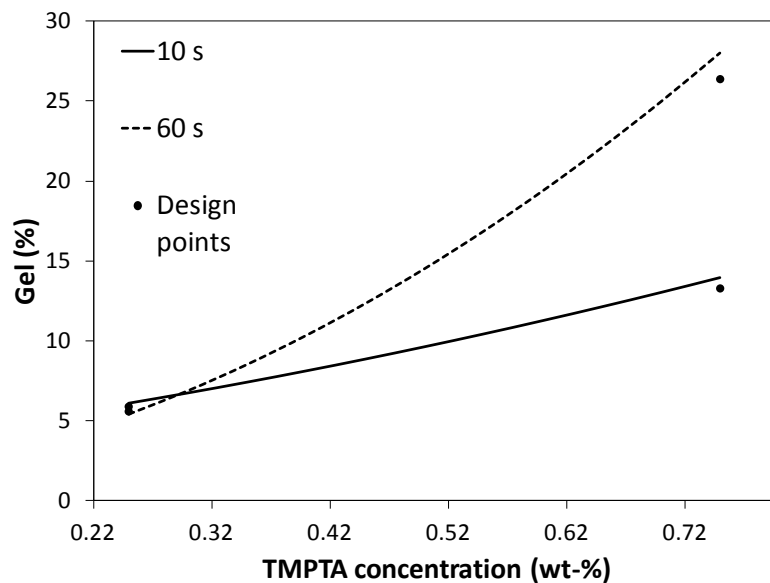


Figure 6-9: The effect of coagent concentration-irradiation time interaction on gel content

Figure 6-10 shows the possible reaction scheme when TMPTA concentration is high. These reactions lead to insertion of more TMPTA in the PP chains. It should be noted that unreacted double bonds in TMPTA can react with another macroradical. Hence, presence of a greater number of multifunctional double bonds in the PP chains encourage formation of long chain branched and crosslinked structures.

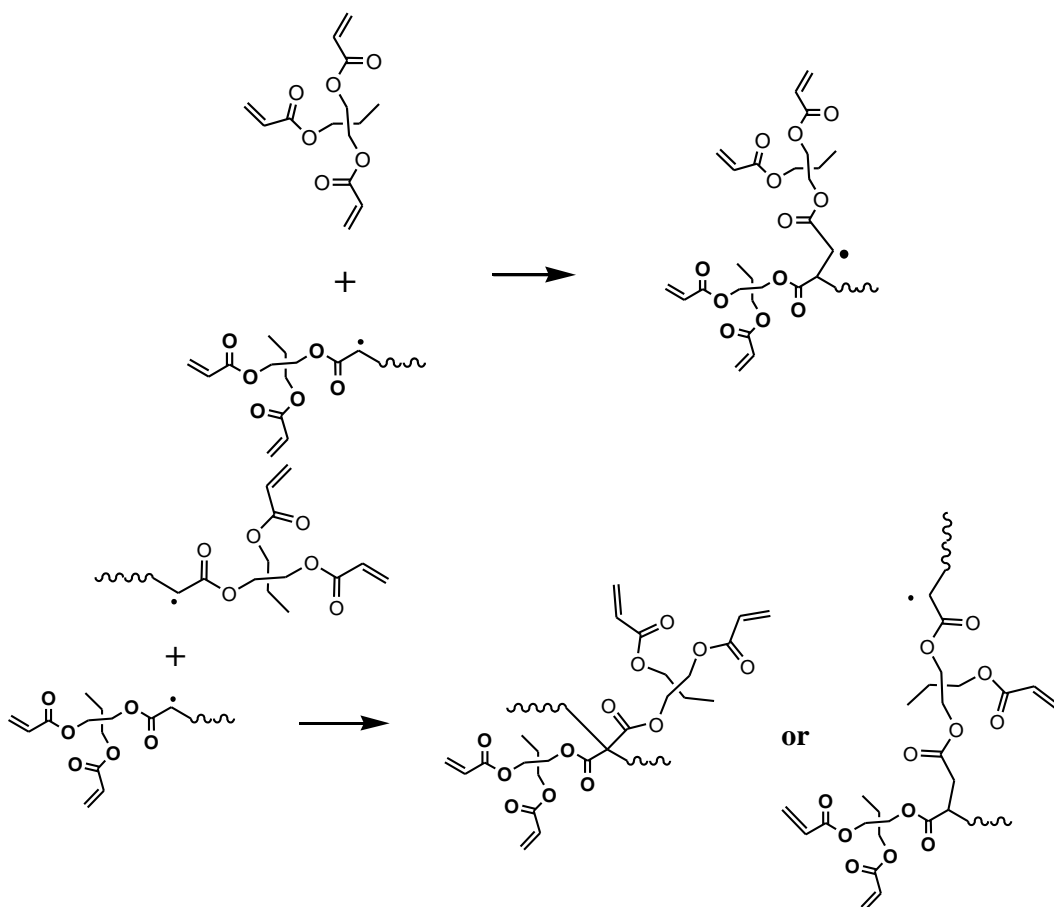


Figure 6-10: Schematic mechanism of possible reactions at high concentration of TMPTA

The other significant interaction is BPH concentration-radiation time. The effect of this interaction on gel content is shown in Figure 6-11 at the low level of TMPTA concentration (the trend is the same at the high coagent concentration). In Figure 6-11, the effect of increasing BPH concentration on gel content is different at high and low radiation duration. At low radiation duration, increasing BPH concentration results in formation of more gel; however, at high radiation time, increasing BPH concentration leads to lower gel content in the samples.

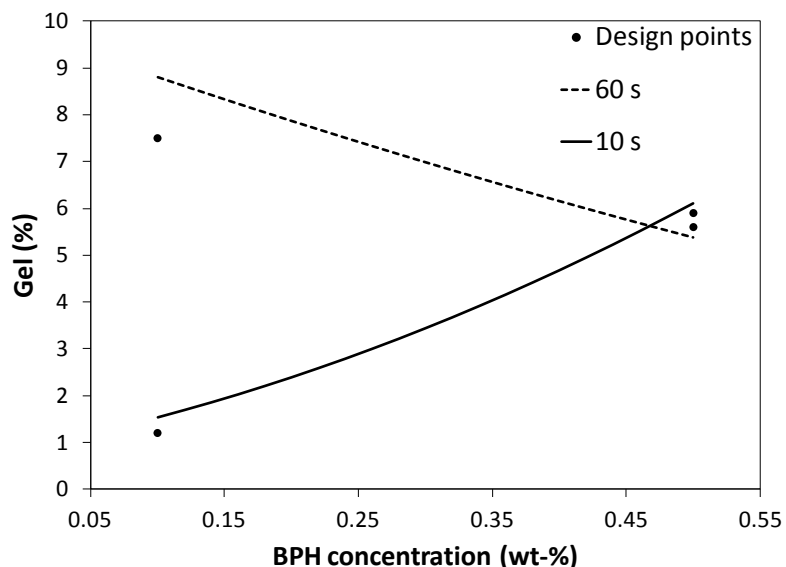


Figure 6-11: The effect of BPH concentration-irradiation time interaction on gel content

This interesting interaction effect of obtaining less gel at high radiation times can be explained by the competition between degradation and chain combination. When BPH concentration increases, more radicals can form; consequently, the number of PP macroradicals that go through degradation ( $\beta$ -scission) increases (especially when concentration of TMPTA is low). Also, the number of PP macroradicals which do not have TMPTA in their structure increases. Thus, the probability of reaction between a PP macroradical (which is protected by TMPTA) and products of  $\beta$ -scission (PP with a double bond at the chain end or PP secondary macroradicals), or PP tertiary macroradicals (PP macroradicals prior to  $\beta$ -scission), increases (see Figure 6-9). These reactions encourage formation of long chain branches rather than crosslinked networks. Hence, although  $\eta_0$  and ER of the runs (conducted at high BPH concentration and irradiated for 60 s) have been significantly increased, the gel content is relatively low (i.e., see run 7 of Table 6-2). At low radiation time, the concentration of radicals is not large enough due to insufficient progress in the extent of reactions. Thus, the probability of reactions depicted in Figure 6-12 is lower.

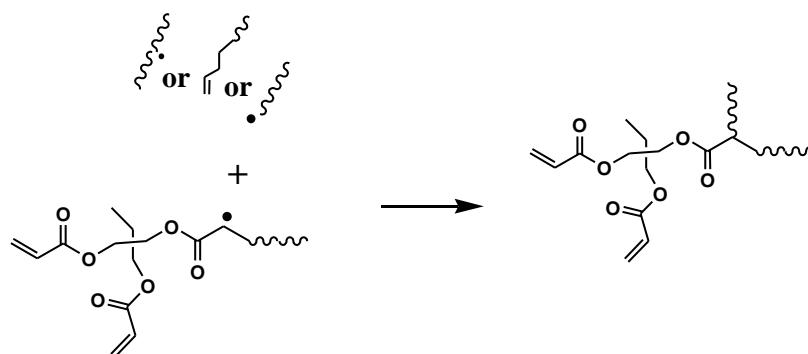


Figure 6-12: Effect of increasing BPH concentration on formation of LCB in PP in presence of TMPTA

After all this analysis on  $\eta_0$ ,  $\lambda$ ,  $n$  and ER, and gel content, operational contour plots can be constructed. A certain specification can now be set for each response in order to locate the (optimal) processing window which results in formation of a high amount of long chain branches with minimum gel content. Table 6-5 shows such specifications that lead to optimized processing conditions.

Table 6-5: Response variables and specs to find optimized processing condition region

Response	Specifications
$n$	$< 0.49$
$\eta_0$ (Pa.s)	$> 50,000$
$\lambda$ (s)	$> 50$
ER	$> 1.3$
Gel content (%)	$< 7$

The contour plots corresponding to these processing specs are shown in Figure 6-13, and the optimal processing window, which satisfies these limits for the response variables (specs of Table 6-5) is shown in yellow ("trapezoidal" upper left region on the plot).

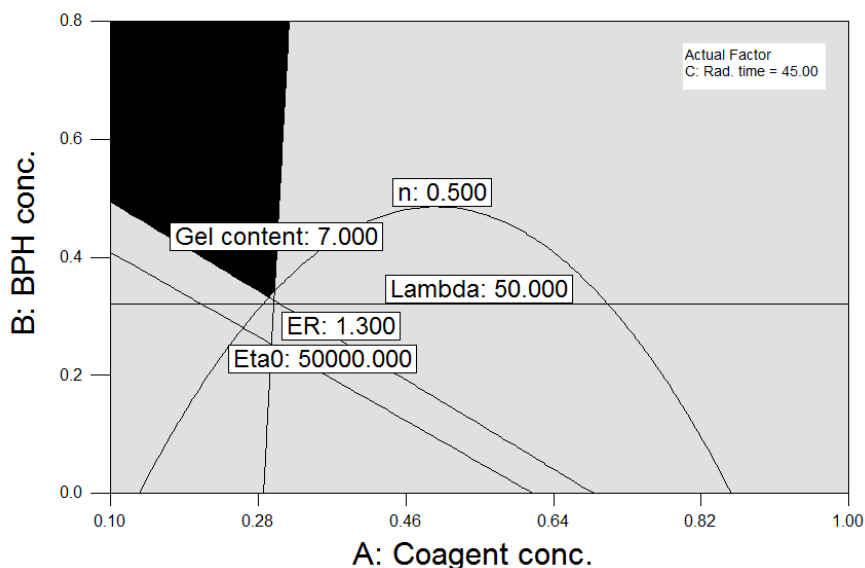


Figure 6-13: Conditions that yield high degree of LCB without significant gel content

## 6.4 INFORMATION FROM FTIR SPECTROSCOPY

TMPTA can homopolymerize and form polymer and oligomer chains. These homopolymers do not contribute to the formation of long chain branches in PP, as alluded to as earlier in subsection 6.3.3.1. The aim of this subsection is to give further details with respect to assessing the contribution of TMPTA in the formation of long chain branches.

For this reason, peaks attributed to TMPTA double bonds ( $1668\text{ cm}^{-1}$ ) and carbonyl groups ( $1730\text{ cm}^{-1}$ ) were studied [73]. All samples were first washed using refluxed xylene for 12 hours. By washing samples using xylene below its boiling temperature, unreacted TMPTA monomers and homopolymerized TMPTA oligomers are removed. In order to confirm that the unreacted TMPTA has indeed been removed from the samples after washing with xylene, the FTIR spectra of PP mixed with 0.75 wt-% TMPTA and 0.5 wt-% BPH (the same mixture used to prepare runs 4 and 8), before and after this procedure, were compared (Figure 6-14a). Note that this mixture was not irradiated so all TMPTA should dissolve in xylene. Both C=C and C=O peaks, which indicate the presence of TMPTA,

were eliminated after washing the samples with xylene. Thus, unbound TMPTA can be eliminated by simply washing samples with refluxed xylene.

Figure 6-14b shows the FTIR spectrum of run 8 before and after washing the sample with xylene. It is shown that the C=C peak in TMPTA is eliminated after washing the sample with xylene, since it reflects the presence of unreacted TMPTA monomers. However, the presence of C=O peak in run 8, after washing the sample, indicates that TMPTA remains in the sample if it is bound to the PP backbone. Thus, insertion of TMPTA in PP chains can be confirmed. The insertion of TMPTA in the PP backbone can be via any of the suggested mechanisms in Figure 6-1, Figure 6-10 or Figure 6-12.

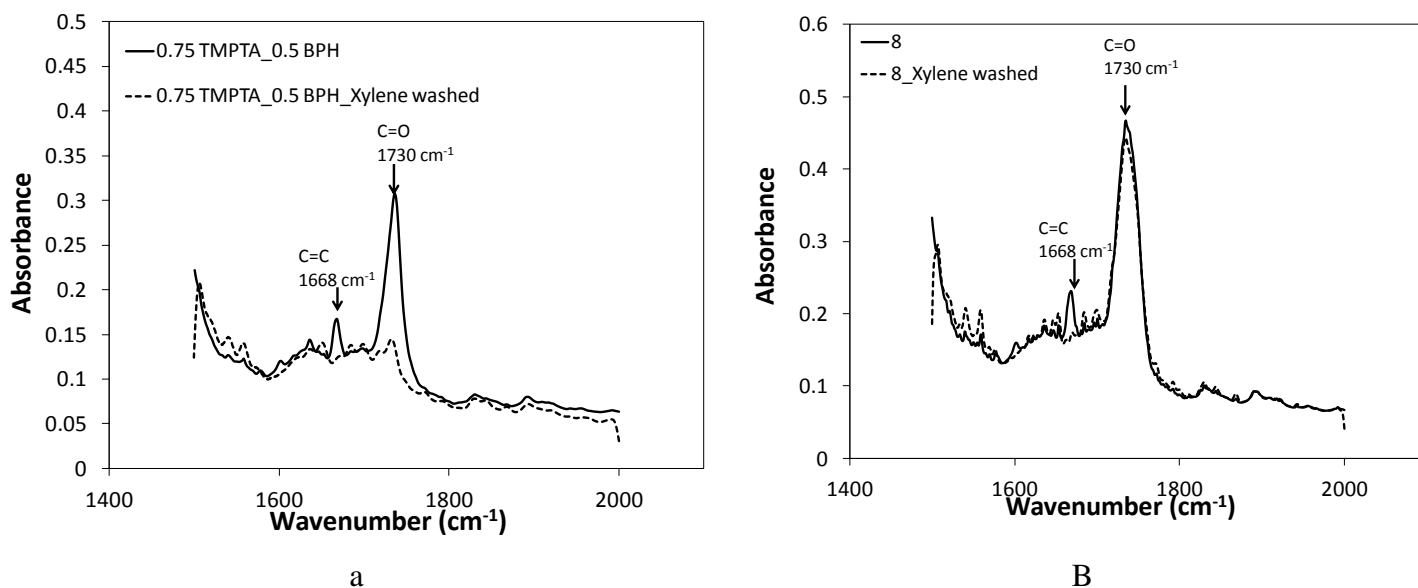


Figure 6-14: FTIR spectra of a) PP/0.75 wt-% TMPTA/0.5 wt-% BPH before and after washing with xylene  
b) run 8 before and after washing with xylene

In order to quantify the amount of bound TMPTA in the modified runs (runs of Table 6-1), the C=O peak height was considered after washing with xylene. This peak is normalized to the PP internal standard (-CH<sub>3</sub> wagging peak at 1168 cm<sup>-1</sup>) and the ratios are presented in the last column of Table 6-2.

As expected, increasing TMPTA or BPH concentration results in an increase in the amount of TMPTA in the chains. Moreover, longer radiation time also leads to more TMPTA in the

PP chains. Thus, formation of a larger number of long chain branches in the runs with increased TMPTA or BPH concentration or longer radiation time is due to insertion of more TMPTA in the PP chains.

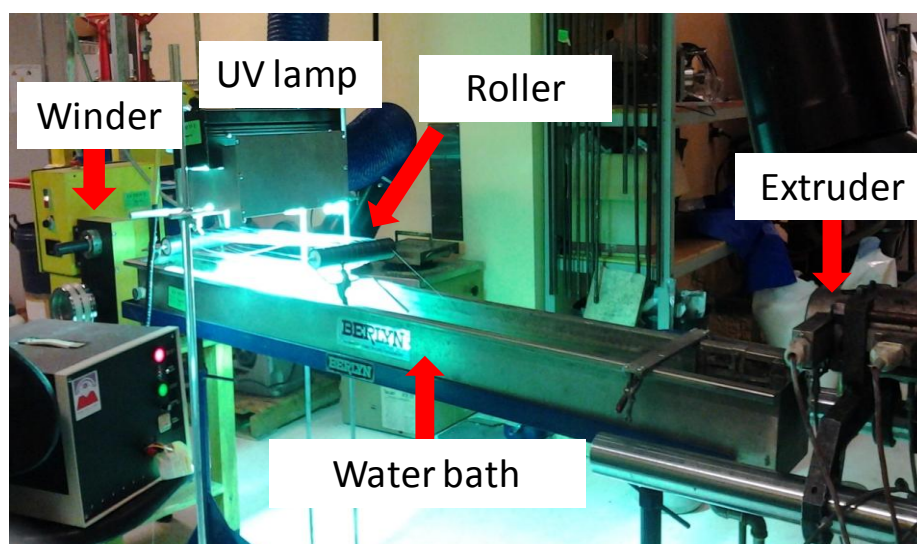
## **6.5 CONCLUDING REMARKS**

Modification of PP via photoinitiation was carried out in the presence of TMPTA as a coagent. It was found that increasing coagent content, or photoinitiator (BPH) content or radiation time led to more shear thinning behavior and an increase in  $\eta_0$ ,  $\lambda$  and ER due to formation of LCB and/or CL. It was confirmed via FTIR tests that increasing coagent content, BPH content, or radiation time led to insertion of more TMPTA monomer into the PP chains, which resulted in formation of more long chain branches.

Gel content levels of the modified runs were measured. Generally, increasing TMPTA concentration or photoinitiator concentration, or radiation time, resulted in an increase in gel content of the samples. However, increasing the photoinitiator concentration, at long radiation time, resulted in lower gel content in the runs. An optimal processing window was thus identified that allowed for formation of long chain branches (desirable) rather than gelled networks (undesirable).

## 7 CHAPTER 7: CONTINUOUS PHOTOMODIFICATION OF PP

A twin screw extruder was used for continuous modification of polypropylene (PP) via UV radiation. Long chain branches were incorporated in the PP backbone to modify its rheological properties. Benzophenone (BPH) as photoinitiator and trimethylolpropane triacrylate (TMPTA) as coagent were utilized during PP photomodification. Radiation was carried out after mixing in the extruder on solid stretched strands with approximately 0.3 mm thickness. The effects of photoinitiator concentration, radiation time and coagent presence were studied via a two-level full factorial design of experiments. It was shown that photomodification of PP can be done continuously. Formation of long chain branches (LCBs) in the experimental runs was confirmed via rheological measurements. Gel content of the samples was also measured. It was found that long chain branches can be formed in PP, both with and without TMPTA, at certain processing conditions. The amount of gel in the samples prepared with TMPTA was higher; however, the gel content could be controlled by manipulating BPH concentration and radiation time.



## 7.1 INTRODUCTION

Extruders have long been used as continuous reactors for polypropylene (PP) chemical modification [74-77]. This process is known as reactive extrusion (REX) and it has been employed to produce controlled rheology PP (CRPP) [1, 78]. In order to produce CRPP via REX, PP and peroxides are fed into the extruder, and initiation reactions followed by  $\beta$ -scission of the PP chains take place during melting and mixing in the extruder. These reactions are responsible for degradation of PP. As soon as temperature reaches the peroxide decomposition temperature, the peroxide abstracts hydrogens from the PP backbones and macroradicals are thus formed. Since PP tertiary radicals are unstable, the chain will break ( $\beta$ -scission) and polymer with lower molecular weight (MW) and narrower molecular weight distribution (MWD) will be formed [1].

Utilizing thermo-chemical initiators, such as peroxides, in REX has its own disadvantages, such as limited controllability. Peroxides reach their decomposition temperature prior to effective mixing with PP, thus causing an excessive and non-homogenous degradation in PP. In order to overcome this issue, photoinitiators were used along with UV irradiation to efficiently degrade PP. In this way, the reaction initiation step and subsequent formation of macroradicals become independent of the processing temperature and the reaction only starts when UV irradiates the PP/photoinitiator mixture. He et al. [20] used this technique to modify PP rheology during extrusion. Photomodification was conducted in the last two zones of the extruder by opening the barrel and exposing the mixture to UV irradiation.

Photoinitiators were not only used to produce CRPP, but also to modify the melt strength of PP or other polyolefins by incorporating long chain branches (LCBs) to their structure [5, 79-81]. Increasing PP melt strength is possible by introducing LCBs to the PP structure. Producing long chain branched PP (LCBPP) is more challenging than CRPP, since  $\beta$ -scission reactions should be controlled by stabilizing PP radical centers. This is not trivial, since  $\beta$ -scission reactions are dominant at temperatures above 60 °C [10]. The typical temperature for PP processing is well above 60 °C ( $T_{\text{process}} > 160$  °C-PP melting point); thus, excessive degradation is inevitable. In order to overcome this issue, and make sure that the

modification was indeed feasible, the radiation was first carried out in the batch mode and solid state [58]. Processing conditions that essentially "preserve" macroradicals were determined by manipulating the processing variables. The processing variables, such as photoinitiator concentration, duration of irradiation, UV lamp intensity, process temperature, and photoinitiator type, were optimized to encourage radical combinations rather than  $\beta$ -scission. The effect of different combinations of these variables on rheological properties, molecular weight characteristics and branching level were studied in solid state. It was found that when UV lamp intensity was low, BPH concentration was more than 0.3 wt-% (in the total mixture), and radiation was carried out for more than 5 minutes at temperatures below 60 °C, the melt strength of PP was increased significantly. It was found that LCB and degradation happen in parallel, and during the first minute of the modification process, degradation was the dominant reaction. As the radiation duration increased, more branches were formed (chain combination reactions dominant) [70].

When lower radiation time was needed, trimethylolpropane triacrylate (TMPTA) was added to PP/photoinitiator mixture as a coagent to increase the rate of LCB. TMPTA is a trifunctional acrylic monomer, which reacts with the radical centers and prevents them from  $\beta$ -scission. However, addition of coagent encourages formation of excessive gel in the samples [50], which might not be desirable for certain applications. Hence, processing variables were manipulated to find conditions which result in minimum gel content in the samples, while the number of long chain branches was still high. It was found that when the concentration of BPH was high (above 0.5 wt-%) and the TMPTA concentration low (below 0.2 wt-%), branching content was sufficiently large, while gel content could be controlled below 5 %. All these modifications (producing LCBPP via UV radiation) were successfully conducted after mixing PP with the photoinitiator in the batch mode in solid state [58, 70].

However, since LCBPP has numerous commercial applications, there is a need to find a method to continuously modify PP and scale up the system. He et al. [49] irradiated a PP/photoinitiator (BPH)/ pentaerythritol triacrylate (PETA) mixture during melt mixing in the extruder by removing the barrel (REX). They found that the modified PP had better

foamability due to greater melt strength compared to the parent PP. PETA was used as a crosslinking agent along with BPH to generate long chain branched PP. However, possible drawbacks of UV radiation in the extruder include limited UV penetration depth into the thick plastic melt and excessive degradation due to high processing temperature. As mentioned before, the latter issue makes formation of long chain branches possible only if coagents (like PETA) are used to "block"  $\beta$ -scission reactions.

In this chapter, the target is to introduce a continuous processing method for modification of PP via UV-irradiation. Modification was conducted in the solid state, and a twin screw extruder was used to continuously supply polypropylene for the modification. Although continuous photomodification of PP is inspired from REX, UV modification was carried out after the strand exits the die and solidifies. Formation of long chain branches (LCBs) in PP was assessed with and without coagent's aid as a radical stabilizer. Trimethylolpropane triacrylate (TMPTA), a trifunctional acrylic coagent was used to "block" chain scission. The extruded solid strands were stretched to increase UV radiation penetration depth by decreasing strand thickness. Also, it is speculated that chain orientation, which happens due to external extensional forces, decreases degradation. Rheological measurements were used to evaluate the effect of BPH concentration, radiation time and coagent presence on viscoelastic properties and gel content. The (optimal) combination of these variables that results in long chain branching (LCB) rather than degradation or crosslinking (CL) was found.

## **7.2 MATERIALS AND METHODS**

### **7.2.1 MATERIALS**

Polypropylene homopolymer (PP2255E1) from ExxonMobil with melt flow rate (MFR) of 3.5g/10 min (230 °C, 2.16 kg) was used as the parent PP. Benzophenone (BPH), 99 % purity, was purchased from Sigma-Aldrich and used as photoinitiator. Trimethylolpropane triacrylate (TMPTA) was purchased from Sigma-Aldrich and used as coagent.

Irganox 1010, Ciba Specialty Chemicals, was used as antioxidant to prevent PP thermal degradation.

### **7.2.2 DESIGN OF EXPERIMENTS**

In order to study the effect of photoinitiator concentration, radiation time and coagent presence on the continuous modification of PP, a two-level full factorial design was used (see Table 7-1). Runs 1 to 8 represent the  $2^3$  factorial design and run 9 is the center point, which was independently replicated (run 10). Runs 11 and 12 were conducted in addition to the  $2^3$  factorial design (and its center points) in order to generate more information about the process. Finally, run 13 is PP mixed with 1 wt-% BPH, which has only been passed through the extruder with no UV radiation. The properties of this run are shown for the sake of comparison. Viscoelastic properties along with the gel content of the runs were measured and statistically analyzed via Design Expert 8.0.7.1 software. Runs 9 and 10 were used to obtain an error estimate for further assessments of the significance of mathematical model terms. These models are discussed later in section 7.3 (Table 7-3).

Table 7-1 shows the different levels of the actual and coded variables (factors). The coded levels (the last three columns) are used in the models of section 7.3.1.1.

Table 7-1: Experiments for 2<sup>3</sup> full factorial design

Run #	BPH-A (wt-%)	Time-B (s)	Coagent-C (wt-%)	A (wt-%)	B (s)	C (s)
1	0.5	16	0	-1	-1	-1
2	1	16	0	1	-1	-1
3	0.5	36	0	-1	1	-1
4	1	36	0	1	1	-1
5	0.5	16	0.25	-1	-1	1
6	1	16	0.25	1	-1	1
7	0.5	36	0.25	-1	1	1
8	1	36	0.25	1	1	1
9	0.75	26	0.13	0	0	0
10	0.75	26	0.13	0	0	0
11	0.75	26	0	0	0	-1
12	0.75	26	0.25	0	0	1
13	1	0	0	-	-	-
Parent PP	-	-	-	-	-	-

### 7.2.3 PREPARATION METHOD

In order to improve mixing of photoinitiator and PP in the twin screw extruder, a PP/BPH master batch was prepared prior to extrusion. PP with 7 wt-% BPH were melt-mixed in a batch mixer at 190 °C and 80 rpm for 8 minutes. The same processing conditions were used for preparing the TMPTA and polypropylene master batch (2 wt-% TMPTA). The mixtures were subsequently ground using a Wiley mill (Model 1102, Arthur H. Thomas Co.). After grinding, the master batches were diluted with PP to prepare the recipes of the runs in Table 7-1. The final mixing was carried out in a Leistritz LSM 30.34 co-rotating twin-screw extruder (L/D=28) with 8 heating zones (including the die). The temperature set points for these eight zones along with the screw configuration are shown in Figure 7-1.

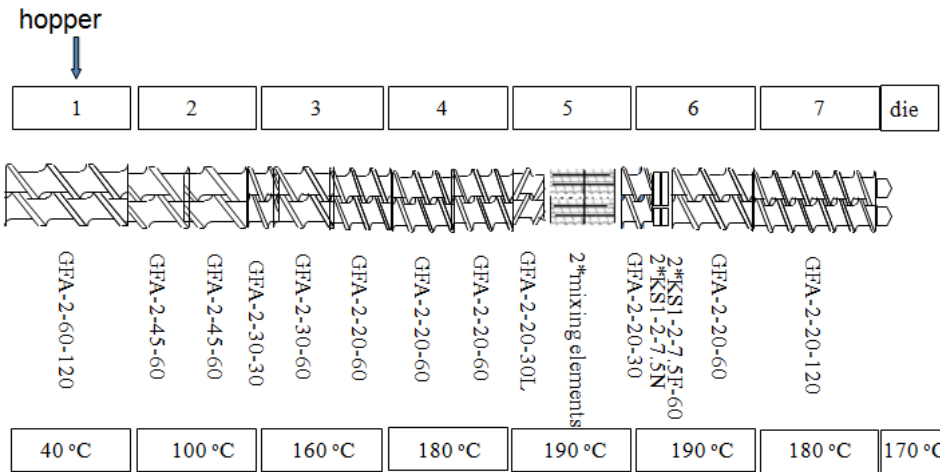


Figure 7-1: Twin screw extruder screw combination and temperature of the zones

The feeding rate was maintained around 20-25 g/min and the screw speed was 20 rpm. The die diameter was 1.5 mm and the melted strand was cooled down in a water bath subsequent to its exit from the die. The solidified strand was stretched via two freely rotating rollers (see the schematic of the operation in Figure 7-2). Irradiation was carried out at this step via a UV a Developer Kit from UV Process Supply Inc. (Versa Cure). The mercury lamp power was 3.0 kW. The irradiated strand was collected using a winder (35 rpm). The strands reach the diameter of approximately 0.3 mm after stretching between the rollers due to extensional forces applied by the winder. UV-modified PP was compression-moulded into discs with 25 mm diameter and 1 mm thickness at 190 °C under an applied force of 4,400 N for five minutes. The discs were used for further rheological characterization tests.

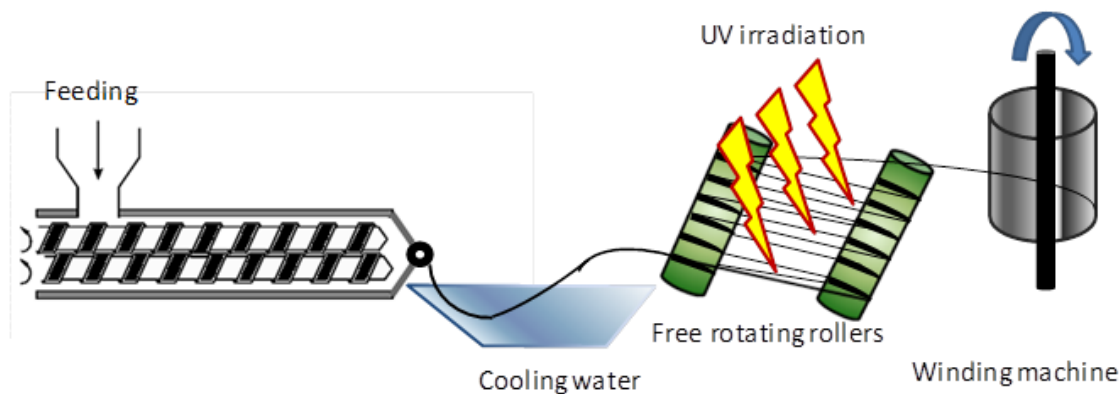


Figure 7-2: The experimental setup for continuous modification of polypropylene via UV radiation

## 7.2.4 PARALLEL PLATE RHEOMETRY

For the analysis herein the same procedures explained in section 4.2.3.1 of Chapter 4 were followed. From these tests, storage modulus ( $G'$ ), loss modulus ( $G''$ ), complex modulus ( $G^*$ ), loss tangent ( $\tan \delta$ ), and complex viscosity ( $\eta^*$ ) were obtained at different angular frequencies ( $\omega$ ).  $\eta^*$  vs.  $\omega$  graphs were used to find the shear thinning index ( $n$ ), zero shear viscosity ( $\eta_0$ ) and relaxation time ( $\lambda$ ) of each sample by fitting the Cross model (Equation 3-11 in section 3.1 of Chapter 3) utilizing MATLAB (7.11.0 R2010b).

Rheological polydispersity indices were determined using Equation 3-13, Equation 3-14 and Equation 3-15. PI, ModSep and ER were calculated for all of the runs and the results are presented and discussed in detail in section 7.3.

## 7.2.5 GEL PERMEATION CHROMATOGRAPHY (GPC)

In order to eliminate the gel content prior to GPC the same steps as section 6.2.4.1 in Chapter 6 were followed. The GPC test was also conducted using the same equipment as described in section 4.2.3.3 of Chapter 4.

## **7.2.6 DETERMINATION OF GEL CONTENT**

The gel content of samples was found by solvent extraction. The method followed is described in ASTM D2765-11, as explained in section 4.2.3.2 of Chapter 4.

## **7.3 RESULTS AND DISCUSSION**

### **7.3.1 RHEOLOGICAL PROPERTIES**

Zero shear viscosity ( $\eta_0$ ), relaxation time ( $\lambda$ ), shear thinning index ( $n$ ), and rheological polydispersity indices (PI, ModSep and ER) of the runs were calculated using Equation 3-13, Equation 3-14 and Equation 3-15. Table 7-2 summarizes these values for all experimental runs along with the parent PP. The last column in Table 7-2 (gel content) will be discussed later in section 7.3.2.

Run 13 is PP mixed with 1 wt-% BPH, which has only been passed through the extruder with no radiation. Comparing the viscoelastic properties of this run with the parent PP (last row) shows that the processing step in the twin screw extruder followed by extension of the solid strand does not significantly affect the viscoelastic properties of the polymer.

Table 7-2: Viscoelastic properties ( $\eta_0$ ,  $\lambda$  and  $n$ ), rheological polydispersity indices (PI, ModSep and ER) and gel content of the experimental runs

Run #	$\eta_0$ (kPa.s)	$\lambda$ (s)	$n$	PI	ModSep	ER	Gel content (%)
1	5.5	0.8	0.52	4.0	3.5	0.18	0
2	7.3	1.2	0.51	3.7	3.5	0.20	0
3	6.5	2.7	0.50	6.9	2.9	0.27	0
4	$1.8 \cdot 10^2$	$1.21 \cdot 10^4$	0.43	8.5	1.8	0.69	6.3
5	8.2	0.6	0.57	3.3	3.9	0.15	0
6	$8.1 \cdot 10$	$8.49 \cdot 10^2$	0.45	11.0	1.9	0.73	2.6
7	$9.8 \cdot 10^2$	$1.07 \cdot 10^5$	0.50	16.1	1.2	0.94	16.4
8	$1.1 \cdot 10^3$	$1.11 \cdot 10^5$	0.47	11.2	1.3	1.22	12
9	$2.2 \cdot 10$	44.2	0.46	7.4	2.3	0.42	0
10	$1.8 \cdot 10$	29.4	0.46	7.0	2.3	0.45	1.4
11	4.7	1.4	0.50	5.9	3.1	0.22	0
12	6.4	7.8	0.45	8.4	2.6	0.37	1.4
13	9.3	0.6	0.60	3.5	3.7	0.14	0
Parent PP	$1.1 \cdot 10$	0.6	0.60	3.3	3.8	0.16	0

Data presented in Table 7-2 show that when the BPH concentration increases,  $\eta_0$ ,  $\lambda$  and ER increase and  $n$  decreases (compare runs 1 vs 2, 3 vs 4, 5 vs 6 and 7 vs 8). As mentioned in section 7.2, these changes in  $\eta_0$ ,  $\lambda$ ,  $n$  and ER reflect formation of LCBs. The reason is higher possibility of hydrogen abstraction from PP chains due to the presence of a larger amount of photoinitiator. Thus, more chain combination reactions will happen, which leads to a larger number of LCBs.

In addition, as the radiation time increases, an increase in  $\eta_0$ ,  $\lambda$ , ER and a decrease in  $n$  happen, which again reflect formation of a larger number of LCBs (compare runs 1 vs 3, 2 vs 4, 5 vs 7 and 6 vs 8). When radiation time increases, chances for macroradical combination increase, which again leads to formation of more LCBs [70].

Addition of coagent stabilizes PP radical centers and prevents them from degradation. Thus, runs with coagent show larger  $\eta_0$ ,  $\lambda$ , ER and more shear thinning behaviour (decrease in  $n$ ) compared to the runs prepared with no coagent.

Unlike ER, changes in PI and ModSep do not directly indicate formation of branches and can be due to changes in the breadth of the MWD, which might have happened during UV modification. However, analysis of these indices is important in order to identify the effect of modification on the MWD of the polymer. In general, increase in BPH concentration, radiation time, or addition of coagent lead to broadening of the MWD, and consequently, an increase in PI and a decrease in ModSep will result. The main factors and factor interactions which affect PI and ModSep significantly will be discussed shortly in section 7.3.1.1, along with other response variables ( $\eta_0$ ,  $\lambda$ ,  $n$  and ER). It is worth emphasizing that since ER is only affected by the distribution of the high molecular weight chains, it can reflect formation of branches directly.

The above mentioned trends are in agreement with our earlier results for batch modification of PP [58, 82], as described in Chapters 4 and 6. However, in previous offline/batch experiments (irradiation of sheets with 1 mm thickness- Chapter 5), no significant change in the properties of the polymer samples was obtained after a few seconds (16-36 s) of radiation. It was found that at least 5 min of radiation time was needed to reach significant LCB levels in these runs. The reason for the significant increase in  $\eta_0$ ,  $\lambda$  and ER after low radiation times (see runs 4 and 6 of Table 7-2) is the low thickness of the radiated strands. It was found in Chapter 5 that as the sample thickness decreases, the effect of photomodification becomes more pronounced throughout the sample [70]. The other possibility is that chain orientation, which happens during stretching of the PP strands, decreases  $\beta$ -scission reactions.  $\beta$ -scission reactions are encouraged by PP chain motions, while these motions are prevented when chains are stretched under extensional forces [10].

In order to study the viscoelastic properties in more detail,  $\eta^*$ - $\omega$ ,  $G'$ - $\omega$ ,  $\tan \delta$ - $G^*$  and Cole-Cole plots are shown in Figure 7-3 and Figure 7-4. Figure 7-3 shows these graphs for runs 1 to 4 (runs without coagent), whereas Figure 7-4 shows the corresponding graphs for runs 5, 6, 7 and 8 (runs with coagent).

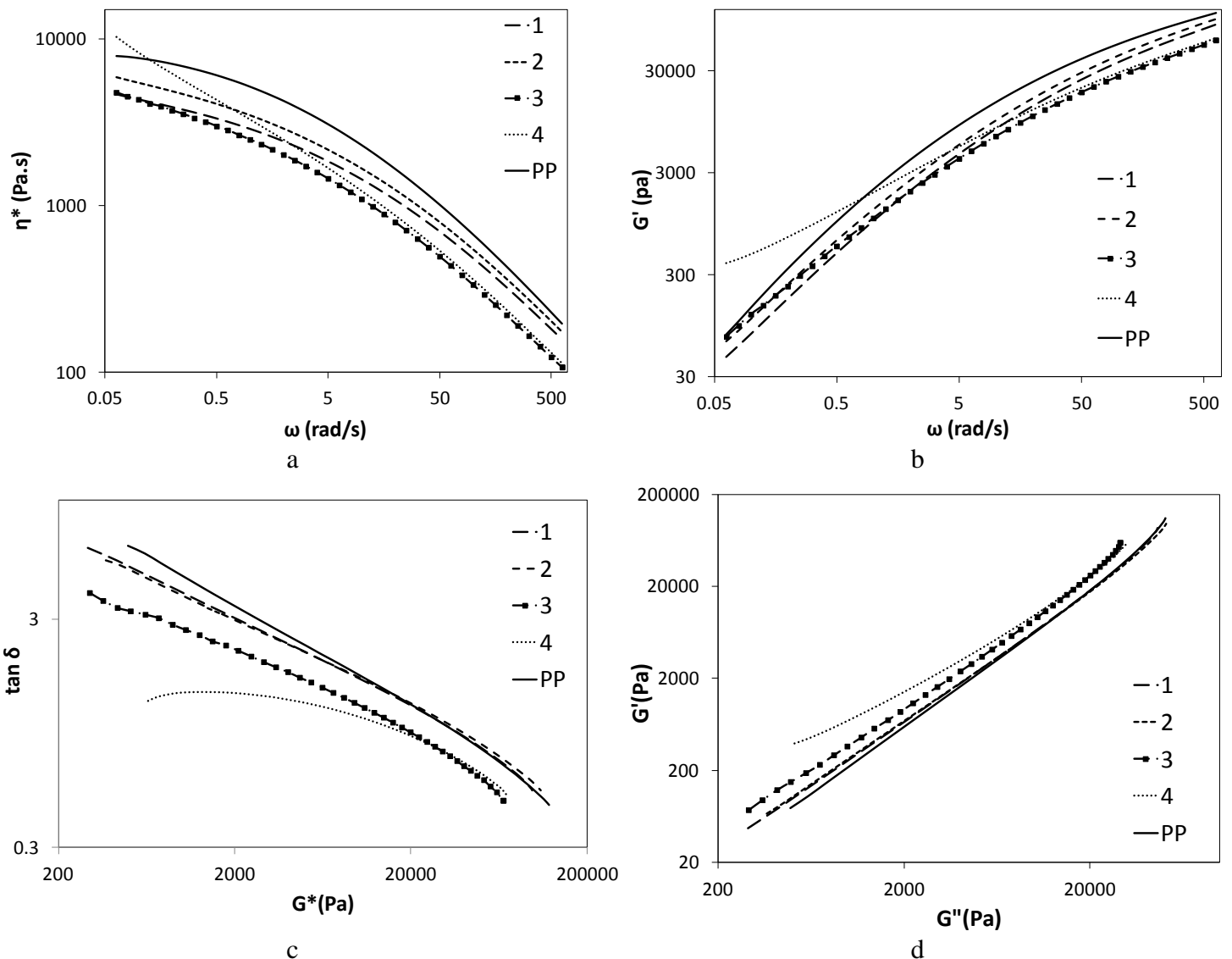


Figure 7-3: Comparison between viscoelastic properties of the runs without coagent a)  $\eta^*$ - $\omega$ , b)  $G'$ - $\omega$ , c)  $\tan \delta$ - $G^*$  and d) Cole-Cole plots

In Figure 7-3 a ( $\eta^*$ - $\omega$ ), run 4 has significantly larger  $\eta^*$  at low frequencies and exhibits more shear thinning behaviour than the parent PP and all other runs. This significant shear thinning behaviour of run 4 resulted in lower viscosity compared to the parent PP at high frequencies, which is an advantage due to easier processing of the modified PP. In Figure 7-3 b ( $G'$ - $\omega$ ), run 4 shows larger  $G'$  values at low frequencies. Larger storage modulus ( $G'$ ) of run 4 once again verifies formation of long chain branches in this run. Moreover, the

slope of the  $G'-\omega$  curve in run 4 is significantly lower than all other runs at low frequencies, which is another indication of formation of branches in this run (LCBPP has a lower  $G'-\omega$  slope at low frequencies). Runs 2 and 3 also show a decrease in  $G'-\omega$  slope, while their storage modulus ( $G'$ ) is not larger than the parent PP (like run 4). It is believed that although LCBs were formed in these runs (more shear thinning behaviour is also observed in runs 2 and 3, Figure 7-3 a), the number of long chain branches was not large enough to compensate for the effect of formation of low MW chains. These low MW chains are formed due to  $\beta$ -scission reactions, which happen in parallel to LCB reactions.

$\tan \delta-G^*$  and Cole-Cole plots (Figure 7-3 c and d) are indicators of the MWD characteristics of the runs. It is shown that all runs have broader distributions than the parent PP. This is in agreement with PI and ModSep values of runs 1 to 4, which are cited in Table 7-2 (larger PI and lower ModSep of runs 1 to 4 compared to the parent PP). Moreover, according to  $\tan \delta-G^*$  and Cole-Cole plots, the distribution becomes broader in the runs radiated for longer time (runs 3 and 4). As radiation time increases, more macroradical combination reactions can happen and chains with different length will be formed, which causes broadening of the MWD.

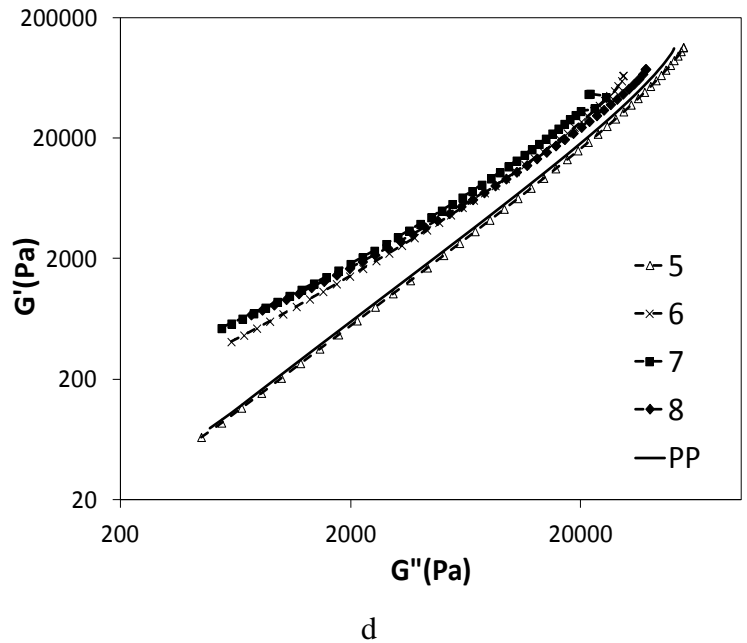
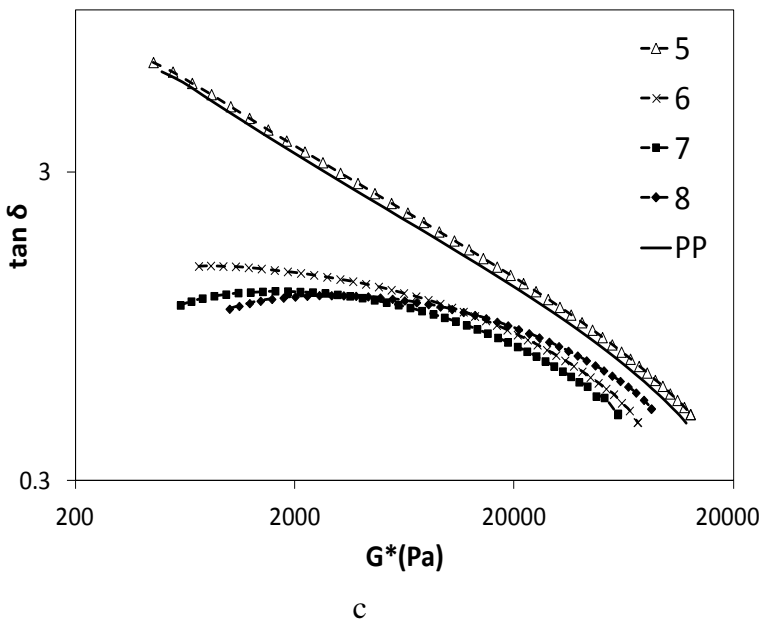
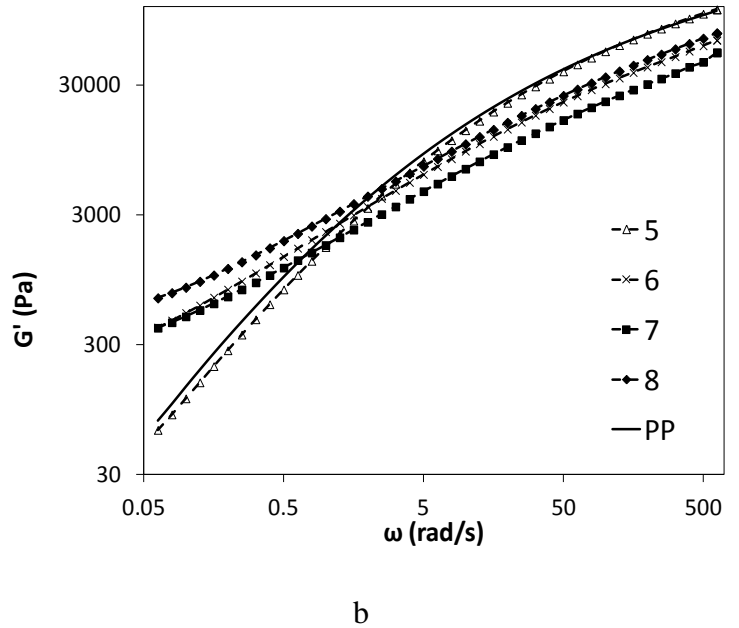
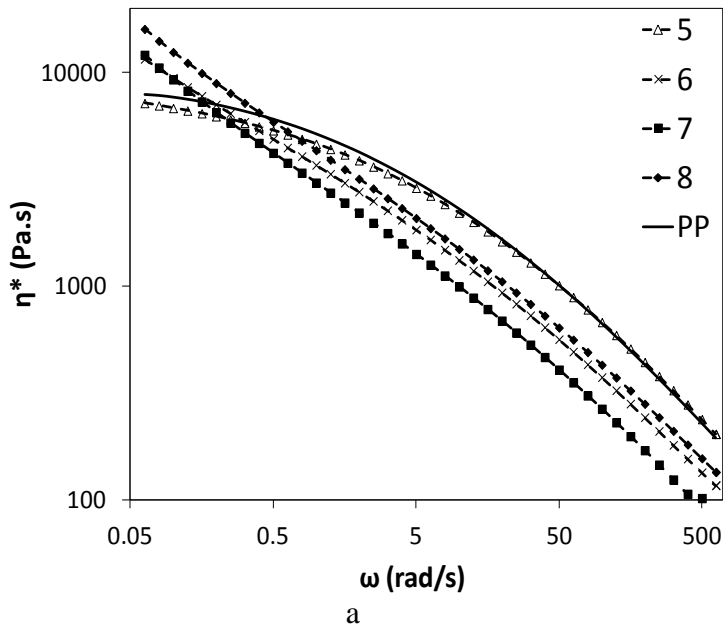


Figure 7-4: Comparison between viscoelastic properties of the runs with coagent a)  $\eta^*$ - $\omega$ , b)  $G'$ - $\omega$ , c)  $\tan \delta$ - $G^*$  and d) Cole-Cole plots

Figure 7-4 compares  $\eta^*$ - $\omega$  (a),  $G'$ - $\omega$  (b),  $\tan \delta$ - $G^*$  (c) and Cole-Cole (d) plots of the runs prepared with 0.25 wt-% of coagent (5 to 8). In Figure 7-4 a, all runs, except run 5 have larger  $\eta^*$  at low frequencies compared to the parent PP, which indicates larger MW of the

modified runs. Due to presence of branches in runs 6, 7 and 8, these runs not only show more shear thinning behavior, but also they have larger elastic modulus compared to the parent PP (Figure 7-4 b). Also, the slope of the  $G'-\omega$  curve is significantly lower at low frequencies, which confirms formation of branches and crosslinks in these runs. In Figure 7-4 c and d, all runs except run 5, which is expected to be degraded, significantly deviate from the parent PP. This shows that the MWD of these modified runs has been significantly changed in comparison to the parent PP.

### 7.3.1.1 EMPIRICAL MODELS AND TRENDS

The data points presented in Table 7-2 were analyzed with Design Expert (statistical software). Empirical models were fit to each response. These models are cited in Table 7-3. The procedure for choosing the significant variables in these models is discussed in Appendix C along with the corresponding  $R^2$  and adjusted  $R^2$  values of each model. The last row in Table 7-3 (gel content) will be discussed later in section 7.3.2.

Table 7-3: Empirical models for viscoelastic properties and gel content based on coded variables

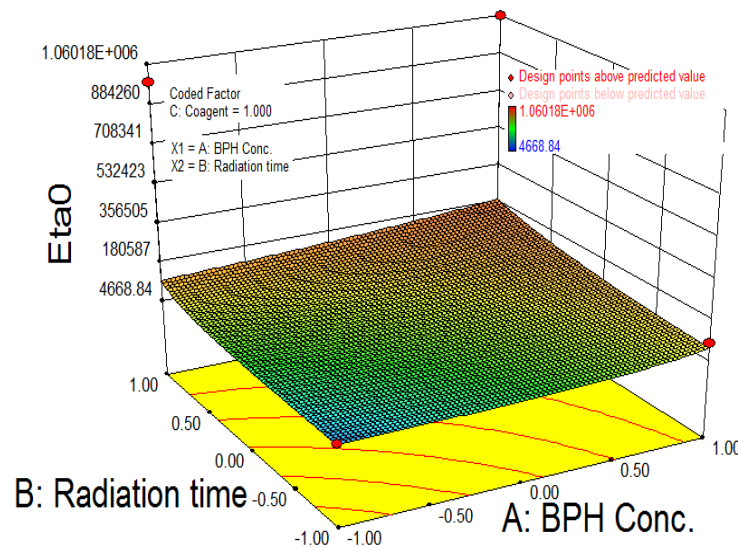
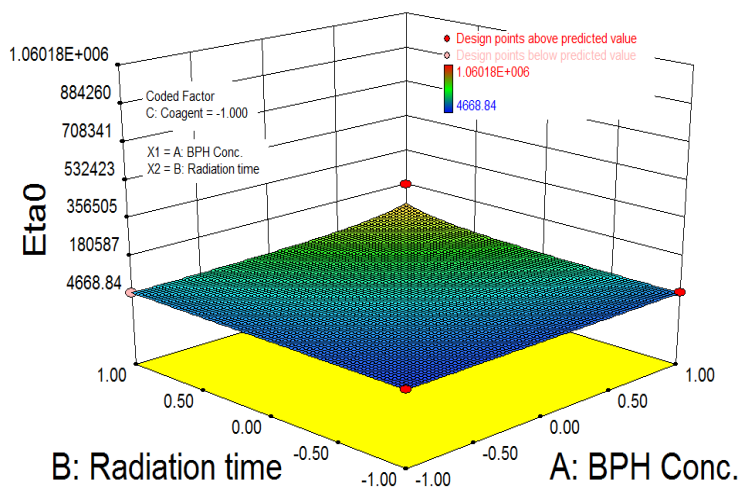
Empirical model	Equation #
$1/\sqrt{\eta_0}=8.15E-3-2.41E-3*A-2.89E-3*B-2.55E-3*C +1.97E-3*ABC$	Equation 7-1
$\text{Log}_{10}(\lambda) =1.79+0.87*A+1.49*B+0.90*C-0.83*ABC$	Equation 7-2
$n=0.49-0.027*A-0.018* B+0.019*ABC$	Equation 7-3
$(\text{ModSep})^{1.45} =3.96-0.84* A-1.51* B-0.83* C+0.87*ABC$	Equation 7-4
$1/\sqrt{ER}=1.6-0.29*A-0.41* B-0.26* C+0.24* ABC$	Equation 7-5
$PI=7.8+2.55*B+2.07*C-1.38*AB-1.79* ABC$	Equation 7-6
$\text{Log}_{10}(\text{Gel}+0.0017)=-1.07+0.83*A+1.03*B+1.04*C-0.86*ABC$	Equation 7-7

In Table 7-3, variables A, B and C are BPH concentration, radiation time and coagent concentration (as per Table 7-1), respectively. AB and ABC denote two factor (BPH concentration-radiation time) and three factor interactions (BPH concentration-radiation time-coagent concentration), respectively. In the equations of Table 7-3, factors and their interactions are shown in terms of coded variables (see Table 7-1 for the coded values of these variables). The equations of Table 7-3 confirm the trends discussed earlier during the analysis of Table 7-2. Zero shear viscosity ( $\eta_0$ ) and relaxation time ( $\lambda$ ) are significantly and

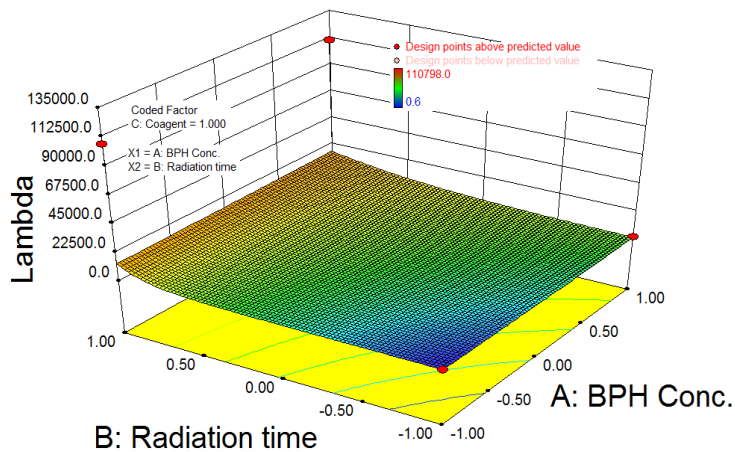
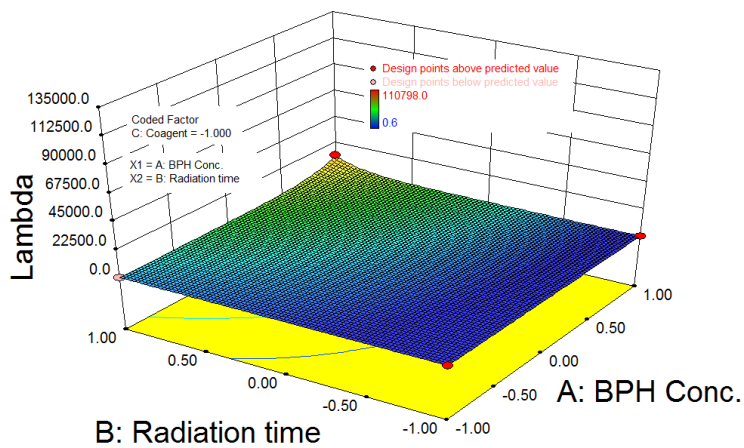
positively affected by BPH concentration (A), radiation time (B) and coagent concentration (C). Also, shear thinning index ( $n$ ) is negatively affected by BPH concentration and radiation time (more shear thinning behaviour due to formation of LCBs). In order to study these factors along with their interactions more closely, 3D interaction plots are shown in Figure 7-5. In Figure 7-5 the graphs on the right show interactions when coagent was used, whereas the ones on the left are without coagent.

A comparison of the graphs on the right with those on the left shows that the trends are the same for runs prepared with and without coagent. However, the maximum of  $\eta_0$ ,  $\lambda$  and the minimum of  $n$  are reached when TMPTA coagent was used in the runs. Also, an increase in  $\eta_0$  and  $\lambda$  and a decrease in  $n$  values are more significant at high BPH concentration compared to low BPH concentration ranges.

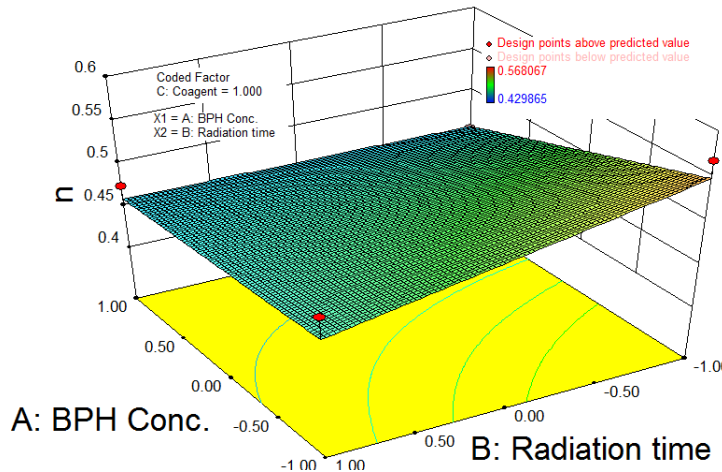
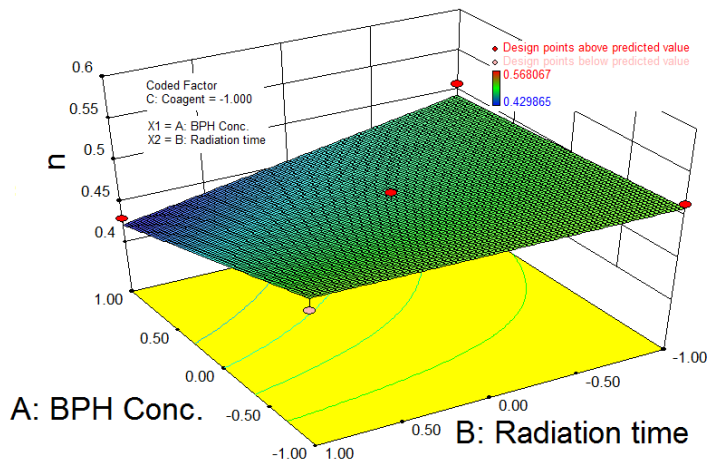
Equation 7-4, Equation 7-5 and Equation 7-6 reflect changes in the MWD, when BPH concentration, radiation time and coagent concentration change. An increase in any of these variables leads to broader MWD with a tail in the high molecular weight ranges (larger ER and lower ModSep). Using the empirical models shown in Table 7-3, ABC interactions plots are constructed for the rheological polydispersity indices. Figure 7-6 a, b and c show ABC interactions for Modsep, ER and PI, respectively. It can be seen that as radiation time increases, ModSep decreases, while ER and PI increase. The reason is broadening of the MWD towards high MW ranges. This is due to formation of long chain branches, which causes formation of a tail in the MWD and broadens the MWD in general. Same as with the other viscoelastic properties, the changes in polydispersity indices are more significant at higher BPH concentrations.



A



B



C

Figure 7-5: 3D interaction plots for  $\eta_0$  (a),  $\lambda$  (b) and  $n$  (c); the plots on the left are without coagent, whereas the plots on the right are with coagent

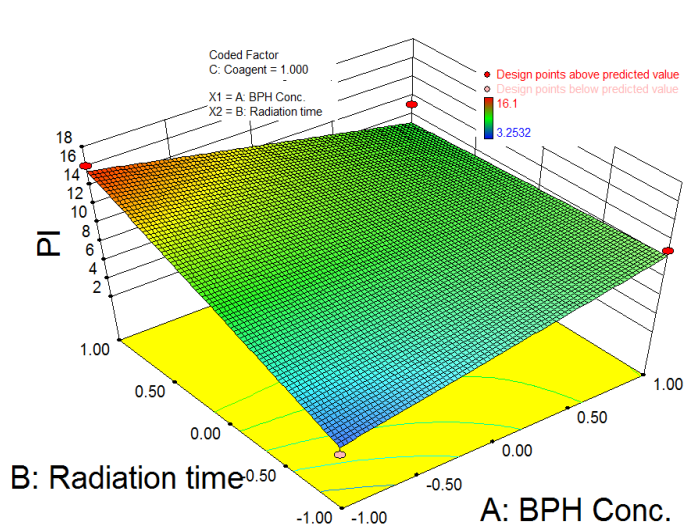
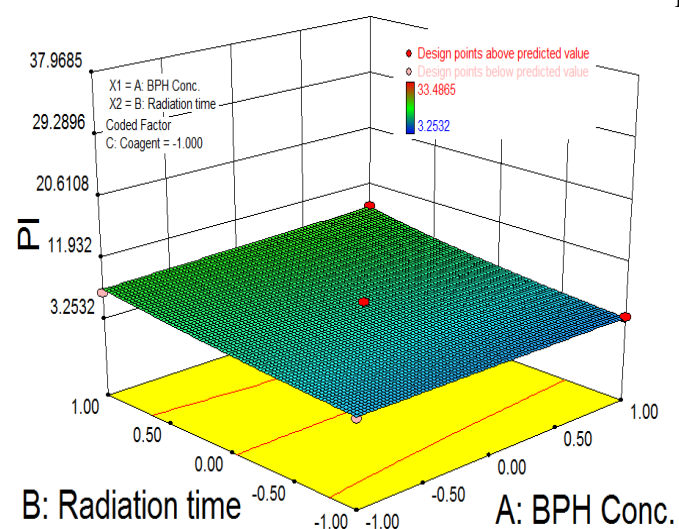
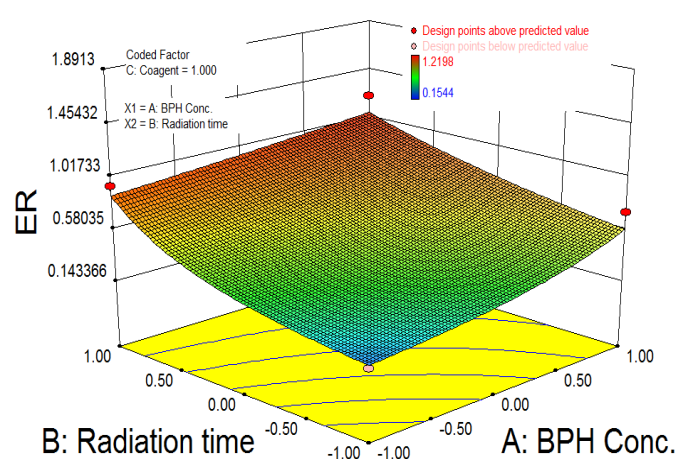
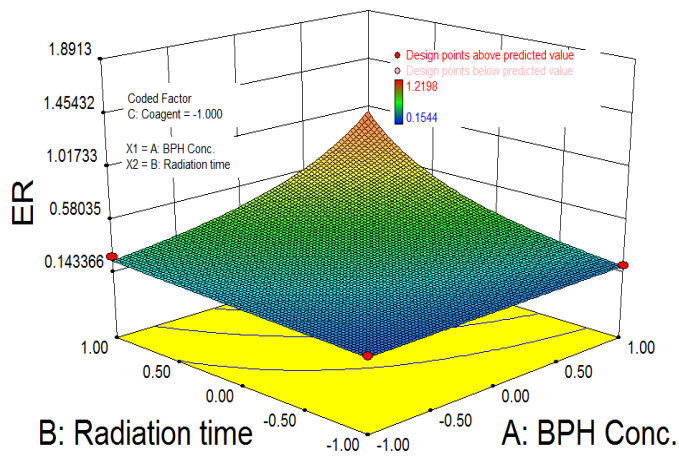
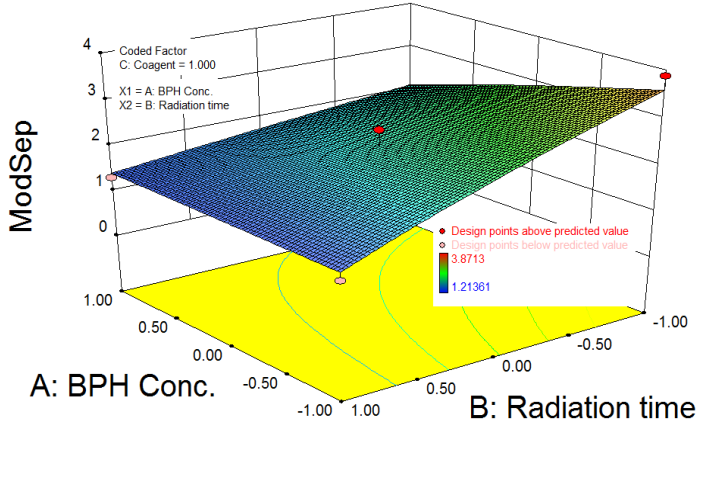
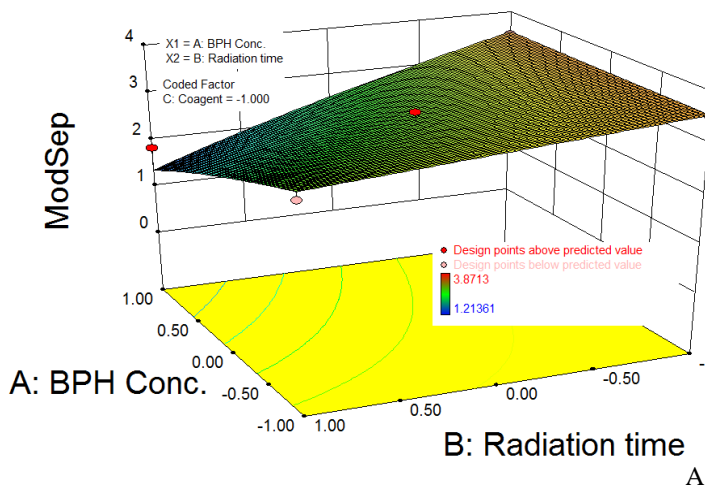


Figure 7-6: 3D interaction plots for ModSep (a), ER (b) and PI (c); the plots on the left are without coagent, whereas the plots on the right are with coagent

### 7.3.2 GEL CONTENT MEASUREMENTS

The percentage of gel for in each run was determined (as per section 7.2), and the values are summarized in Table 7-2. Among runs prepared with no coagent only run 4, which has the highest BPH concentration and radiation time, has crosslinked and insoluble structures.

On the other hand, among runs prepared with coagent, only run 5, which is clearly degraded (see Table 7-2 and the discussions in section 7.3.1), has no gel in its structure. Increasing BPH concentration from run 5 to 6 leads to formation of about 2.5 % gel in the modified PP. Formation of gel in the runs might be undesirable for certain applications. However, considering the significant improvement in rheological properties of run 6, 2.5 % gel is still an acceptable margin. In contrast to runs 5 and 6, increasing BPH concentration at high radiation time (runs with coagent), causes formation of less gel in the samples (see runs 7 and 8). This trend has also been observed in Chapter 6 for batch photomodification at the presence of coagent. When BPH concentration increases, more radicals will be formed; consequently, the number of PP macroradicals that go through degradation ( $\beta$ -scission) increases. Thus, the number of PP macroradicals which do not have TMPTA in their structure increases. The probability of reaction between PP macroradicals (which are protected by TMPTA) and products of  $\beta$ -scission (PP with a double bond at its chain end or secondary PP macroradicals), or tertiary PP macroradicals (PP macroradicals prior to  $\beta$ -scission), increases (see the mechanisms in Figure 6-12 of Chapter 6). These reactions encourage formation of long chain branches rather than crosslinked networks. Hence, although  $\eta_0$  and ER of these runs have significantly increased, the gel content is relatively low. At low radiation time, the concentration of radicals is not large enough due to insufficient progress in the extent of reaction. Thus, as BPH concentration increases, gel content also increases. The mechanisms responsible for these effects (the differing trends at high and low radiation times) are discussed in section 6.3.3.1 of Chapter 6.

Increasing radiation time (see runs 6 and 8, or run 2) causes formation of a significantly larger amount of gel in the runs. This is again in agreement with results from the batch modification and the mechanism responsible for this behaviour is shown in Figure 5-16. As

mentioned in the discussion in Chapter 6, an increase in radiation time increases the probability of hydrogen abstraction from the chains that are already long chain branched. This leads to formation of connected network structures.

It is worth emphasizing here that the changes observed in the rheological properties of the modified runs that have high gel content (see runs 7 and 8 in Figure 7-4 and Table 7-2) are due to formation of both long chain branches and crosslinks. The presence of long chain branches after excluding the gel from the samples has been confirmed using both GPC and rheological tests on the sol fraction of run 8. These experiments are explained in Section 7.3.4 and Appendix D, respectively.

Same as for the rheological indicators, an empirical model was used to show the significant variables and interactions affecting the gel content of the runs (Table 7-3). The model confirms that BPH concentration, radiation time and presence of coagent all have a significant and positive effect on the gel content of the runs. The 3-factor interaction (ABC) was also found to be significant. Figure 7-7 shows representative factor interactions in two 3D surface plots. Figure 7-7a shows the AB interaction when coagent was not used, and Figure 7-7b is for the case when coagent was used. Again, the maximum gel content was reached when coagent was used. The above mentioned trends with coagent can also be observed in Figure 7-7b (at low radiation time, an increase in BPH concentration leads to a higher gel content, while at high radiation time a lower amount of gel results).

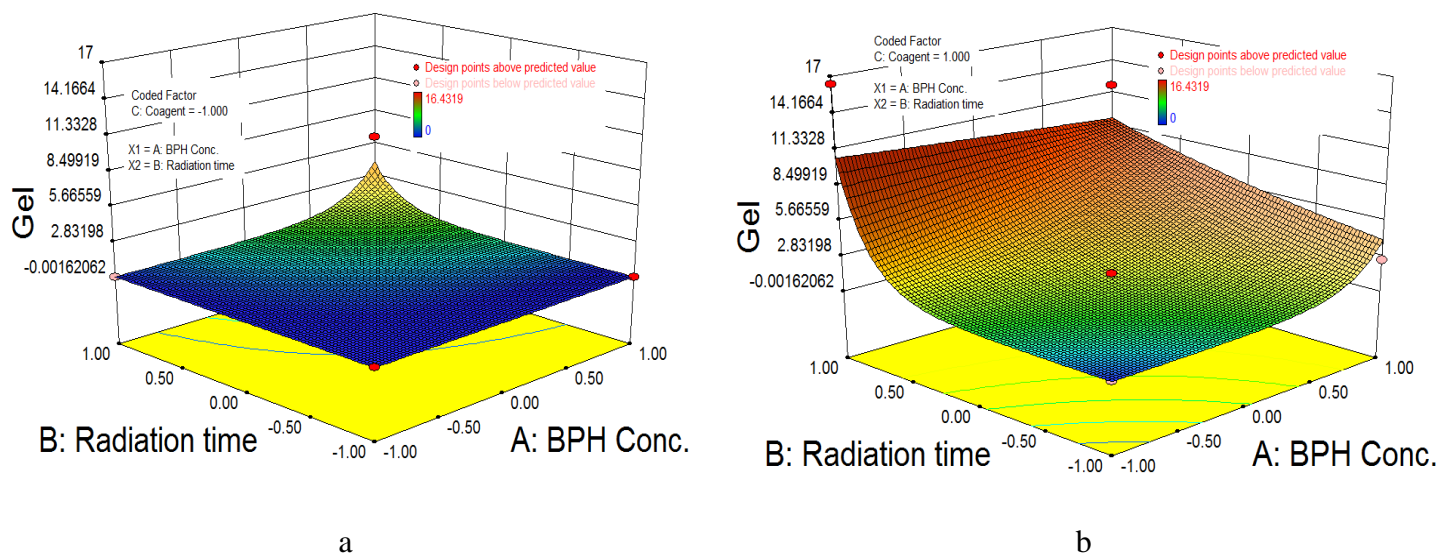


Figure 7-7: 3D interaction plots for gel content a) without coagent b) with coagent

### 7.3.3 CONDITIONS THAT RESULT IN LONG CHAIN BRANCHED PP WITH MINIMUM GEL CONTENT

In order to find the conditions that maximize LCB while having the lowest gel content during the continuous modification of PP, the same steps as in Chapter 6 were followed. The contour plots were constructed for  $\eta_0$ ,  $\lambda$ ,  $n$ , ER, and gel content. Certain specifications were set for each response in order to locate the (optimal) processing window. Table 7-4 shows such specifications that lead to optimal processing conditions.

Table 7-4: Response variables and their specs for locating the optimal processing condition region

Response	Specifications
$n$	< 0.48
$\eta_0$ (Pa.s)	> 10,000
$\lambda$ (s)	> 3
ER	> 0.4
Gel content (%)	< 5

The contour plots corresponding to these processing specs are shown for runs without and with coagent (TMPTA) in Figure 7-8a and b, respectively. The optimal processing window,

which satisfies these limits for the response variables (specs of Table 7-4) is shaded in black.

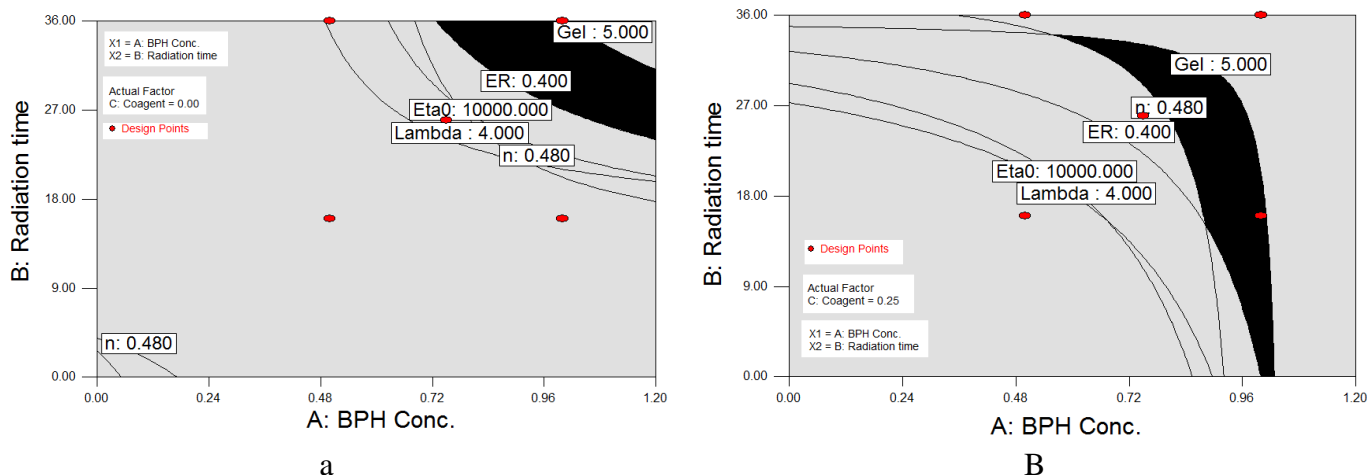


Figure 7-8: Conditions that yield high degree of LCB without significant gel content a) without TMPTA, b) with TMPTA

### 7.3.4 GPC MEASUREMENTS

GPC measurements were selectively conducted on runs 4, 6, 8 and the parent PP. These runs were chosen, since they manifest clear evidence for LCB in their rheological measurements (see Table 7-2 and the discussion in section 7.3.1). Run 4 was the only run prepared without coagent that shows indications of formation of long chain branches. Runs 6 and 8 were both prepared using TMPTA and both show indications of formation of LCBs. The gel content of run 6 was exceptionally low, while its rheological properties confirmed formation of a large amount of LCBs. Run 8 was chosen since it had the largest  $\eta_0$ ,  $\lambda$  and ER, and the lowest  $n$  value among all runs. Figure 7-9a and b show the MWD and  $\log [\eta]$ - $\log M$ , respectively, for these selected runs.

The MWD of all these runs shows presence of a tail at the high MW ranges (Figure 7-9a). For runs 6 and 8, this tail at high molecular weights has almost formed a shoulder, which confirms formation of larger molecules due to LCB.

Figure 7-9b shows  $\log [\eta]$  vs.  $\log M$ . As mentioned in section 3.2 of Chapter 3, deviations of the modified runs from the linear parent PP towards lower  $[\eta]$  values indicate formation of LCBs. All three modified runs deviate from the linear PP at molecular weights above 447 kg/mol ( $10^{5.65}$  g/mol). Since all three modified runs deviate almost equally from the linear PP, the weight average number of long chain branches ( $B_w$ ) in these polymers was found to be the same and around 0.26 branches per molecule. This value was calculated by solving Equation 3-20 and Equation 3-21 (Chapter 3).

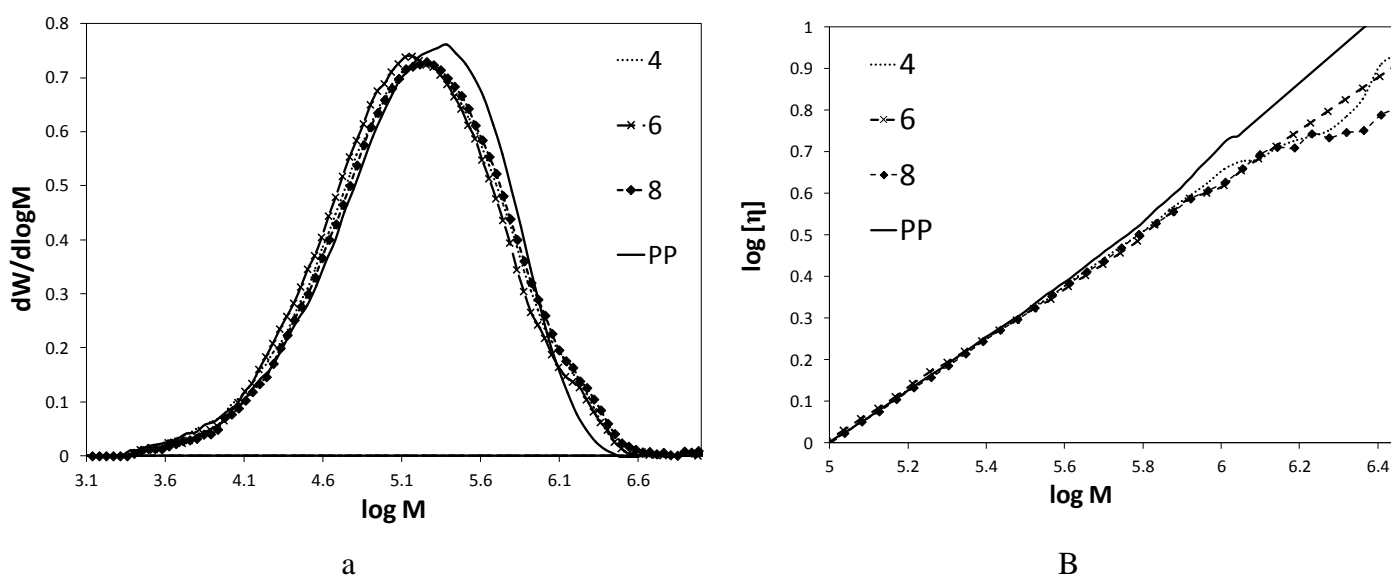


Figure 7-9: MWDs and  $\log [\eta]$  vs.  $\log M$  for runs 4, 6, 8 and the parent PP

Using the MWD, number average molecular weight ( $\bar{M}_n$ ), weight average molecular weight ( $\bar{M}_w$ ), z average molecular weight ( $\bar{M}_z$ ) and polydispersity index (PDI) values were calculated and the results are summarized in Table 7-5. As expected from Figure 7-9a, all modified runs have greater  $\bar{M}_w$  and significantly larger  $\bar{M}_z$  than the parent PP. Also, an increase in the PDI of the samples shows that the MWD has become broader due to the presence of long chain branches. As expected, run 8 has the largest  $\bar{M}_w$ ,  $\bar{M}_z$  and the broadest MWD, which is in agreement with the rheological measurements (Table 7-2).

Table 7-5: Molecular weight averages and PDI of the selected radiated runs along with the parent PP

Sample ID	BPH content (wt-%)	Radiation time (s)	Coagent content (wt-%)	$\bar{M}_n$ (kg/mol)	$\bar{M}_w$ (kg/mol)	$\bar{M}_z$ (kg/mol)	PDI
4	1	36	0	70	288	551	4.1
6	1	16	0.25	69	279	641	4.0
8	1	36	0.25	73	339	1,229	4.7
PP	0	0	0	73	271	274	3.7

## 7.4 CONCLUDING REMARKS

A new design was proposed for the continuous modification of PP using UV radiation. Essentially, the batch modification of Chapters 4 to 6 was scaled up to the continuous processing design of the current chapter. The modification was carried out on PP strands after melt mixing in a twin screw extruder. In order to achieve the radiation time needed for formation of long chain branches (LCBs), the extruded PP strand was folded between two rollers several times. Radiation was carried out between rollers and the modified strand was collected on a winder. The effect of BPH concentration, radiation time and coagent concentration on the rheological behaviour and gel content were studied. Zero shear viscosity  $\eta_0$ , relaxation time  $\lambda$ , shear thinning index  $n$ , rheological polydispersity indices (PI, ER and ModSep) and the gel content were determined, and empirical models (based on a statistical experimental design) were fit to each of these response variables. Using these models, optimal processing conditions that result in long chain branching rather than crosslinking in PP were obtained.

## **8 CHAPTER 8: OVERALL THESIS CONCLUSIONS, MAIN THESIS CONTRIBUTIONS AND RECOMMENDATIONS**

### **8.1 OVERALL THESIS CONCLUSIONS**

1) UV radiation can be utilized to produce both CRPP and LCBPP by manipulating radiation conditions. Both modifications require hydrogen abstraction from PP main chains and excited photoinitiators (BPH in this thesis) are responsible for this hydrogen abstraction. If radiation intensity and process temperature are high,  $\beta$ -scission reactions will be the dominant reactions. In contrast, if radiation intensity and temperature remain low during the photomodification, macroradical combination reactions will dominate over  $\beta$ -scission a few minutes after the beginning of the reaction. Macroradical combination is responsible for formation of LCBs in PP.

2) Changes in PP molecular structure can be evaluated via shear rheology, GPC and gel content measurements. Formation of LCBs results in larger  $\eta_0$ ,  $\lambda$ , ER, shear thinning behavior and broader MWD compared to the parent PP.  $\eta_0$ ,  $\lambda$ , ER and shear thinning behavior of the degraded samples decrease, and their MWD becomes narrower compared to the parent PP. A GPC differential viscometer detector was used to determine the number of LCBs in the long chain branched samples.

3) After analysis of the runs prepared using different combinations of radiation variables, such as lamp intensity, photoinitiator concentration (two different types of photoinitiators), radiation time and temperature, it was found that all these variables or their interactions can significantly affect the molecular properties of PP.

4) Apart from UV radiation conditions, thickness of the samples can also affect the modification. For samples with lower thickness, less radiation time is required to modify the rheological properties via incorporation of LCBs in the sample. This is due to the limited UV penetration depth, which was found to be below 1 mm.

5) As radiation time increases (at low lamp intensity and radiation temperature), both LCB and gel content increase, because chains which are already long chain branched can go through hydrogen abstraction again. Combination of long chain branched macroradicals results in formation of crosslinked networks in the polymer.

6) TMPTA has been used as a coagent along with photoinitiator to modify PP using shorter radiation times (less than 45 s radiation time). Formation of crosslinks are more probable when TMPTA is used since multifunctional TMPTA comonomers incorporated in the PP chains, block  $\beta$ -scission and add extra double bonds to the PP structure. These double bonds can react with another macroradical with TMPTA in its structure and thus form a crosslinked network (insoluble gelled structures).

7) TMPTA concentration, BPH concentration and UV radiation time were found to significantly affect structures (LCBs or crosslinks) formed during PP photomodification. It was found that at high BPH concentration (above 0.5 wt-% BPH) and low TMPTA concentration (below 0.1 wt-%), maximum number of LCBs was formed, while gel content remained at the minimal level.

8) Continuous photomodification of PP was done post-extrusion to scale up PP photomodification. PP strands were continuously provided via a twin screw extruder. The effect of BPH concentration, UV radiation time and TMPTA concentration on the molecular structure of the photomodified PP was studied. LCBs were formed after 36 s radiation at 1 wt-% BPH concentration even without TMPTA use. Addition of TMPTA encourages formation of crosslinks; however, by decreasing radiation time, formation of excessive gel in the samples can be restricted.

9) UV radiation was found to be safe, efficient and a relatively inexpensive technique that can be used for PP modification.

## **8.2 CONTRIBUTIONS**

This thesis has made the following contributions:

- Prior to this work, utilizing UV radiation in post-reactor modification of PP was limited to producing CRPP and crosslinked PP [20, 50]. In this thesis, LCBPP with high melt strength was produced (for the first time) via UV radiation in the solid state with no coagent (Chapters 4, 5 and 7).
- The effects of different radiation variables on the molecular structure of the modified PP were clarified (Chapter 4). Utilizing photoinitiation reactions for PP modification has recently been revisited by researchers. But there was no comprehensive study on the effect of different variables in PP photomodification. Comparisons were made between molecular properties of photomodified PP which was prepared via two types of photoinitiator with different kinetics. The combinations of processing variables that lead to formation of LCBs in PP were found for each photoinitiator.
- The limitations of utilizing UV radiation for PP modification were identified and solutions were suggested to overcome these limitations (Chapter 5 and 6). Limited UV penetration depth and low rate of LCB reactions are two of the photomodification reaction limitations. Determination of critical thickness which UV can penetrate into the samples, and minimum radiation time required to form long chain branched structures rather than degraded PP represent another major contribution of this thesis.
- As mentioned above, one of the drawbacks of using UV radiation to prepare LCBPP is long radiation time. In 2009, a patent was published by BASF [83], which suggested using photoinitiators along with coagents to form LCBs in PP and increase its melt strength. Utilizing coagent can solve the problem with high radiation time and decrease the required radiation time to form long chain branches. However, no in-depth study had been conducted on how photoinitiator concentration, coagent concentration or radiation time can affect the photomodification reactions. In Chapter 6, a detailed study was conducted on the effect of coagent concentration, in combination with other (statistically and practically) significant radiation variables (BPH concentration and radiation time).
- An optimal processing window was obtained for photomodification to maximize long chain branches in PP with minimal gel both in the presence and absence of cogent.

- Finally, process scale up from bench scale (batch) radiation to continuous pilot plant was demonstrated. Since UV radiation has great potential for industrial use and commercialization, a methodology has been developed to continuously modify PP via UV radiation. Using this continuous processing technique, LCBs were successfully formed in PP in the solid state. Radiation time was significantly decreased by manipulating the processing conditions to meet industry standards. Developing a setup for continuous photomodification of PP is essential to scale up the process.

## **8.3 RECOMMENDATIONS FOR FUTURE WORK**

### **8.3.1 SHORT-TERM RECOMMENDATIONS**

1) The focus of this thesis was on modification of PP melt properties; however, these modifications can affect the properties of the modified PP in the solid state as well. Hence, mechanical properties of the photomodified PP should be studied to find how physical and mechanical properties will deviate from those of the parent PP. It is recommended that mechanical tests such as tensile, flexural or impact be conducted on photomodified PP samples. Also, extensional viscosity measurements could be conducted selectively for the samples in Chapters 5 to 7, in order to collect more complementary information.

2) In this thesis, the modification was conducted in the solid state; thus, it is speculated that the crystallinity of the samples can affect the modification process. The cooling procedure was the same for all samples prepared for this thesis (cooling by blowing air under pressure in the hot press), so the crystallinity of the samples prior to radiation was the same for all of them. However, it is not clear if the modification is more successful in the amorphous or crystalline region. In order to study the effect of crystallinity, it is recommended that samples be prepared with different cooling modes, so they grow different crystalline structures. For example, samples can solidify by blowing air, quenching, or cooling slowly at room temperature. Annealing can also be applied on some of the samples to form more

developed crystalline domains. By keeping the radiation conditions constant, the effect of crystallinity of the samples on PP photomodification can be investigated.

3) As mentioned in Chapter 5, since UV penetration depth is limited, the effect of modification decreases through the depth of the samples. As UV penetrates through the sample's thickness, its intensity decreases, so the number of LCBs and the molecular structure changes from the surface to the core of the sample. A GPC test can be conducted on different layers of the same sample (layers from the surface and layers from the core of the sample) and the effect of penetration depth can be studied more closely.

### **8.3.2 LONG-TERM RECOMMENDATIONS**

Aside from long-term studies on photomodification reactions, an area of limited studies in general, and the detailed mathematical modelling of the UV modification of PP, the final step of this research warrants a more detailed look.

The final step was concerned with the continuous photomodification of PP to scale up the process. The effects of three variables were studied; however, there were other variables, which were not studied in this thesis. The variables which are recommended for complementary studies are lamp intensity, extruder output rate, and strand's extension rate (which can be adjusted via the winding machine rpm). Moreover, the effect of temperature can also be studied by cooling the strands during photomodification using pressurized air. It is recommended to study the effects of these variables on the molecular properties of PP and optimize the continuous photomodification process further.

Also, the effect of stretching the PP strand during continuous modification and its consequences for PP photomodification should be studied in more detail. Stretching of PP strands happens while folding the strands back and forth between the two rollers and collecting them via a winding machine. It is believed that the level of stretching and extension of the strand can affect polymer chain orientation, free volume between chains and chain motions. These effects can be in favor or against certain reactions in PP photomodification and promote formation of certain molecular structures (for example,

LCB over degradation of polymer). It is recommended that the effect of chain orientation and chain movements on photomodification be studied in more detail. For these studies, birefringence can be used to assess polymer chain orientation.

## REFERENCES

1. Tzoganakis C, Vlachopoulos J, Hamielec A. Production of controlled-rheology polypropylene resins by peroxide promoted degradation during extrusion. *Polymer Engineering & Science* 1988;28(3):170-180.
2. Mohring PC, Coville NJ. Homogeneous Group 4 metallocene Ziegler-Natta catalysts: the influence of cyclopentadienyl-ring substituents. *Journal of Organometallic Chemistry* 1994;479(1-2):1-29.
3. Scheutz B, Rainer K. Metocene-Metallocene Polypropylene used in the Pharmaceutical and Medical Sector. *Business Briefing: Medical Device Manufacture and Technology* 2005;39: 1-4.
4. Gotsis A, Zeevenhoven B, Hogt A. The effect of long chain branching on the processability of polypropylene in thermoforming. *Polymer Engineering & Science* 2004;44(5):973-982.
5. Graebing D. Synthesis of branched polypropylene by a reactive extrusion process. *Macromolecules* 2002;35(12):4602-4610.
6. Parent JS, Bodsworth A, Sengupta SS, Kontopoulou M, Chaudhary BI, Poche D, Cousteaux S. Structure-rheology relationships of long-chain branched polypropylene: Comparative analysis of acrylic and allylic coagent chemistry. *Polymer* 2009;50(1):85-94.
7. Wong B, Baker W. Melt rheology of graft modified polypropylene. *Polymer* 1997;38(11):2781-2789.
8. Krause B, Voigt D, Häußler L, Auhl D, Münstedt H. Characterization of electron beam irradiated polypropylene: Influence of irradiation temperature on molecular and rheological properties. *J Appl Polym Sci* 2006;100(4):2770-2780.
9. Han SM, Choi CH. Polypropylene resin compositions having high melt tension and method for preparing the same 2012; 20120149845A1, US patent.
10. Rätzsch M, Arnold M, Borsig E, Bucka H, Reichelt N. Radical reactions on polypropylene in the solid state. *Progress in Polymer Science* 2002;27(7):1195-1282.

11. Langston JA, Colby RH, Chung TM, Shimizu F, Suzuki T, Aoki M. Synthesis and characterization of long chain branched isotactic polypropylene via metallocene catalyst and T-reagent. *Macromolecules* 2007;40(8):2712-2720.
12. Tullo AH. Metallocene rise again. *Chem Eng News*, 2010;88(42):10-16.
13. Yu Q, Zhu S. Peroxide crosslinking of isotactic and syndiotactic polypropylene. *Polymer* 1999;40(11):2961-2968.
14. Su F, Huang H. Supercritical carbon dioxide-assisted reactive extrusion for preparation long-chain branching polypropylene and its rheology. *The Journal of Supercritical Fluids* 2010; 56(1):114-116.
15. Auhl D, Stange J, Münstedt H, Krause B, Voigt D, Lederer A, Lappan U, Lunkwitz K. Long-chain branched polypropylenes by electron beam irradiation and their rheological properties. *Macromolecules* 2004;37(25):9465-9472.
16. Krause B, Voigt D, Lederer A, Auhl D, Munstedt H. Determination of low amounts of long-chain branches in polypropylene using a combination of chromatographic and rheological methods. *Journal of Chromatography A* 2004;1056(1-2):217-222.
17. Abbas Mousavi S, Dadbin S, Frounchi M, Venerus DC, Guadarrama Medina T. Comparison of rheological behavior of branched polypropylene prepared by chemical modification and electron beam irradiation under air and N<sub>2</sub>. *Radiat Phys Chem* 2010;79(10):1088-1094.
18. Lugao A, Otaguro H, Parra D, Yoshiga A, Lima L, Artel B, Liberman S. Review on the production process and uses of controlled rheology polypropylene--Gamma radiation versus electron beam processing. *Radiat Phys Chem* 2007;76(11-12):1688-1690.
19. Lugão AB, Hutzler B, Ojeda T, Tokumoto S, Siemens R, Makuuchi K, Villavicencio A-CH. Reaction mechanism and rheological properties of polypropylene irradiated under various atmospheres. *Radiat Phys Chem* 2000;57(3-6):389-392.
20. He G, Tzoganakis C. A UV-initiated reactive extrusion process for production of controlled-rheology polypropylene. *Polymer Engineering and Science* 2011;51(1):151-157.
21. UV-Vis Luminescence Spectroscopy theoretical principal, Home page of: <http://teaching.shu.ac.uk/hwb/chemistry/tutorials/molspec/lumin1.htm>; webpage,[online], [10/11, 2011].

22. Rabek JF. Mechanisms of photophysical processes and photochemical reactions in polymers : theory and applications. Chichester [West Sussex] ; Toronto: Wiley, 1987.
23. Mita I, Hisano T, Horie K, Okamoto A. Photoinitiated thermal degradation of polymers. I. Elementary processes of degradation of polystyrene. *Macromolecules* 1988;21(10):3003-3010.
24. Hingmann R, Marczinke B. Shear and elongation flow properties of polypropylene melts. *J Rheol* 1994;38:573-587.
25. Vega J, Santamaria A, Munoz-Escalona A, Lafuente P. Small-amplitude oscillatory shear flow measurements as a tool to detect very low amounts of long chain branching in polyethylenes. *Macromolecules* 1998;31(11):3639-3647.
26. Ferry JD. Viscoelastic properties of polymers; Toronto: Wiley, 1980.
27. Stange J, Uhl C, Münstedt H. Rheological behavior of blends from a linear and a long-chain branched polypropylene. *J Rheol* 2005;49(5):1059-1079.
28. Sugimoto M, Suzuki Y, Hyun K, Ahn KH, Ushioda T, Nishioka A, Taniguchi T, Koyama K. Melt rheology of long-chain-branched polypropylenes. *Rheologica acta* 2006;46(1):33-44.
29. Nam G, Yoo J, Lee J. Effect of long-chain branches of polypropylene on rheological properties and foam-extrusion performances. *J Appl Polym Sci* 2005;96(5):1793-1800.
30. Tian J, Yu W, Zhou C. The preparation and rheology characterization of long chain branching polypropylene. *Polymer* 2006;47(23):7962-7969.
31. Tzoganakis C. A rheological evaluation of linear and branched controlled-rheology polypropylenes. *The Canadian Journal of Chemical Engineering* 1994;72(4):749-754.
32. Shroff R, Mavridis H. New measures of polydispersity from rheological data on polymer melts. *J Appl Polym Sci* 1995;57(13):1605-1626.
33. Delgadillo-Velázquez O, Hatzikiriakos S, Sentmanat M. Thermorheological properties of LLDPE/LDPE blends. *Rheologica Acta* 2008;47(1):19-31.
34. Meissner J, Hostettler J. A new elongational rheometer for polymer melts and other highly viscoelastic liquids. *Rheologica Acta* 1994;33(1):1-21.

35. Wagner MH, Bastian H, Hachmann P, Meissner J, Kurzbeck S, Münstedt H, Langouche F. The strain-hardening behaviour of linear and long-chain-branched polyolefin melts in extensional flows. *Rheologica acta* 2000;39(2):97-109.
36. Meissner J. Development of a universal extensional rheometer for the uniaxial extension of polymer melts. *Transactions of The Society of Rheology (1957-1977)* 1972;16(3):405-420.
37. Meissner J, Raible T, Stephenson S. Rotary clamp in uniaxial and biaxial extensional rheometry of polymer melts. *Journal of Rheology (1978-present)* 1981;25(1):1-28.
38. Münstedt H. New universal extensional rheometer for polymer melts. Measurements on a polystyrene sample. *Journal of Rheology (1978-present)* 1979;23(4):421-436.
39. Sentmanat ML. Miniature universal testing platform: from extensional melt rheology to solid-state deformation behavior. *Rheologica acta* 2004;43(6):657-669.
40. Sentmanat M, Wang BN, McKinley GH. Measuring the transient extensional rheology of polyethylene melts using the SER universal testing platform. *Journal of Rheology (1978-present)* 2005;49(3):585-606.
41. Wood-Adams PM, Dealy JM, Willem deGroot A, Redwine OD. Effect of molecular structure on the linear viscoelastic behavior of polyethylene. *Macromolecules* 2000;33(20):7489-7499.
42. Scoriah M, Tzoganakis C, Dhib R, Penlidis A. Characterization by dilute solution and rheological methods of polystyrene and poly (methyl methacrylate) produced with a tetrafunctional peroxide initiator. *J Appl Polym Sci* 2007;103(2):1340-1355.
43. Scoriah M, Dhib R, Penlidis A. Branching Level Detection in Polymers. *Encyclopedia of Polymer Processing (ECHP)*, S.Lee, Ed., Taylor and Francis, New York 2005;251-265.
44. Zimm BH, Stockmayer WH. The dimensions of chain molecules containing branches and rings. *J Chem Phys* 1949;17:1301-1314.
45. Weng W, Hu W, Dekmezian AH, Ruff CJ. Long chain branched isotactic polypropylene. *Macromolecules* 2002;35(10):3838-3843.

46. Langston JA, Colby RH, Shimizu F, Suzuki T, Aoki M, Chung T. One-pot Synthesis of Long Chain Branch PP (LCBPP) Using Ziegler-Natta Catalyst and Branching Reagents 2007;260(1):34-41.
47. Zhou W, Zhu S. ESR study on peroxide modification of polypropylene. *Ind Eng Chem Res* 1997;36(4):1130-1135.
48. Qu B, Xu Y, Shi W, Raanby B. Photoinitiated crosslinking of low-density polyethylene. 6. Spin-trapping ESR studies on radical intermediates. *Macromolecules* 1992;25(20):5215-5219.
49. He G, Huang Y, Yang Q. The rheological property and foam morphology of linear polypropylene and long chain branching polypropylene. *Journal of Wuhan University of Technology-Mater.Sci.Ed.* 2013;28(4):798-803.
50. Zamotaev P, Shibirin E, Nogellova Z. Photocrosslinking of polypropylene: the effect of different photo-initiators and coagents. *Polym Degrad Stab* 1995;47(1):93-107.
51. Kukaleva N, Stoll K, Santi M. Modified olefin polymers 2011;20110136931, US Patent Application.
52. Amintowlieh Y, Tzoganakis C, Penlidis A. Polypropylene with improved strain hardening characteristics 2014; 61/995,627 US provisional patent application.
53. Montgomery DC. *Applied statistics and probability for engineers*. New York: New York : Wiley, 2003.
54. Jain S, Goossens H, van Duin M, Lemstra P. Effect of in situ prepared silica nanoparticles on non-isothermal crystallization of polypropylene. *Polymer* 2005;46(20):8805-8818.
55. Kurzbeck S, Oster F, Münstedt H, Nguyen T, Gensler R. Rheological properties of two polypropylenes with different molecular structure. *J Rheol* 1999;43(2):359-374.
56. Auhl D, Stadler FJ, Münstedt H. Rheological properties of electron beam-irradiated polypropylenes with different molar masses. *Rheologica Acta* 2012:1-11.
57. Lugaõ AB, Cardoso ECL, Lima LFCP, Hustzler B, Tokumoto S. Characterization study of gamma-irradiated, high melt-strength polypropylene. *Nuclear Instruments and Methods*

in Physics Research Section B: Beam Interactions with Materials and Atoms 2003;208:252-255.

58. Amintowlieh Y, Tzoganakis C, Hatzikiriakos SG, Penlidis A. Effects of processing variables on Polypropylene degradation and long chain branching with UV irradiation, *Polymer Degradation and Stability*. 2014; 104:1-10.

59. Wu Q, Qu B. Photoinitiating characteristics of benzophenone derivatives as new initiators in the photocrosslinking of polyethylene. *Polymer Engineering & Science* 2001;41(7):1220-1226.

60. Chen YL, Rånby B. Photocrosslinking of polyethylene. II. Properties of photocrosslinked polyethylene. *Journal of Polymer Science Part A: Polymer Chemistry* 1989;27(12):4077-4086.

61. Rånby B. Photoinitiated modifications of polymers: photocrosslinking, surface photografting and photolamination. *Mat Res Innovat* 1998;2(2):64-71.

62. Honerkamp J, Weese J. A nonlinear regularization method for the calculation of relaxation spectra. *Rheologica Acta* 1993;32(1):65-73.

63. Wood-Adams PM, Dealy JM. Using rheological data to determine the branching level in metallocene polyethylenes. *Macromolecules* 2000;33(20):7481-7488.

64. Lau H, Bhattacharya S, Field G. Melt strength of polypropylene: Its relevance to thermoforming. *Polymer Engineering & Science* 1998;38(11):1915-1923.

65. Gotsis A, Zeevenhoven B, Tsenoglou C. Effect of long branches on the rheology of polypropylene. *J Rheol* 2004;48(4):895-914.

66. Yamaguchi M, Suzuki K. Enhanced strain hardening in elongational viscosity for HDPE/crosslinked HDPE blend. II. Processability of thermoforming. *J Appl Polym Sci* 2002;86(1):79-83.

67. Bernnat, A. Polymer melt rheology and the rheotens test. PhD Thesis, University of Stuttgart, Germany, 2001.

68. Kim B, Kim K. Cross-Linking of polypropylene by peroxide and multifunctional monomer during reactive extrusion. *Adv Polym Technol* 2003;12(3):263-269.

69. Borsig E, Van Duin M, Gotsis A, Picchioni F. Long chain branching on linear polypropylene by solid state reactions. *European Polymer Journal* 2008;44(1):200-212.
70. Amintowlieh Y, Tzoganakis C, Penlidis A. The effect of depth and duration of UV radiation on polypropylene modification via photoinitiation . *J Appl Polym Sci*. 2014: 131, 41021-41032.
71. Rudin A. *The elements of polymer science and engineering : an introductory text and reference for engineers and chemists*. Academic Press, 1999.
72. Gabriel C, Münstedt H. Influence of long-chain branches in polyethylenes on linear viscoelastic flow properties in shear. *Rheologica Acta* 2002;41(3):232-244.
73. Socrates G. *Infrared and Raman characteristic group frequencies: tables and charts*. Wiley, 2001.
74. Tzoganakis C. Reactive extrusion of polymers: A review. *Adv Polym Technol* 1989;9(4):321-330.
75. Moad G. The synthesis of polyolefin graft copolymers by reactive extrusion. *Progress in Polymer Science* 1999;24(1):81-142.
76. Bettini S, Agnelli J. Grafting of maleic anhydride onto polypropylene by reactive extrusion. *J Appl Polym Sci* 2002;85(13):2706-2717.
77. Prut EV, Zelenetskii AN. Chemical modification and blending of polymers in an extruder reactor. *Russian Chemical Reviews* 2001;70(1):65-79.
78. Azizi H, Ghasemi I. Reactive extrusion of polypropylene: production of controlled-rheology polypropylene (CRPP) by peroxide-promoted degradation. *Polym Test* 2004;23(2):137-143.
79. Lagendijk R, Hogt A, Buijtenhuijs A, Gotsis A. Peroxydicarbonate modification of polypropylene and extensional flow properties. *Polymer* 2001;42(25):10035-10043.
80. Wang X, Tzoganakis C, Rempel GL. Chemical modification of polypropylene with peroxide/pentaerythritol triacrylate by reactive extrusion. *J Appl Polym Sci* 1996;61(8):1395-1404.

81. Sardashti P, Tzoganakis C, Polak MA, Penlidis A. Radiation Induced Long Chain Branching in High-Density Polyethylene through a Reactive Extrusion Process. *Macromolecular Reaction Engineering* 2014;8(2):100-111.
82. Amintowlieh Y, Tzoganakis C, Penlidis A. Preparation and characterization of long chain branched polypropylene through UV irradiation and coagent. Under review: *Polymer-Plastics Technology and Engineering* 2014: manuscript length 45.
83. Kukaleva N, Stoll K, Santi M. Modified olefin polymers 2009; WO/2009/090126, World Intellectual Property Organization.
84. Shroff R, Mavridis H. Long-chain-branching index for essentially linear polyethylenes. *Macromolecules* 1999;32(25):8454-8464.

## APPENDICES

### APPENDIX A: JUSTIFICATION FOR USING RHEOLOGICAL POLYDISPERSITY INDICES

In this appendix, we briefly discuss the theoretical background related to rheological polydispersity indices and their use, as first discussed in section 3.1.1 of Chapter 3. More details can be found in Reference [32] of this thesis.

It is expected that ER correlates with the distribution of high MW chains. The following explains the reasons for this correlation.

At  $G''=500$  Pa (low frequencies, terminal region),  $G'$  relates to the  $J_e^0$  via the following equation:

$$G'(\omega) = \int J_e^0 (G''(\omega))^2 \quad \omega \rightarrow 0$$

In the equation above,  $J_e^0$  (steady state compliance) relates to the MWD using the following justifications.

$J_e^0$  relates to polydispersity of the relaxation spectrum according to the following equation:

$$\frac{\tau_w}{\tau_n} = J_e^0 * G_N^0$$

$\tau_w$  and  $\tau_n$  are the weight average and number average relaxation times, respectively, and can be defined using the following equations:

$$\tau_w = \frac{\int_{-\infty}^{+\infty} H(\tau)\tau^2 d\ln\tau}{\int_{-\infty}^{+\infty} H(\tau)\tau d\ln\tau} = \eta_0 J_e^0 \quad \tau_n = \frac{\int_{-\infty}^{+\infty} H(\tau)\tau d\ln\tau}{\int_{-\infty}^{+\infty} H(\tau) d\ln\tau} = \frac{\eta_0}{G_N^0}$$

Many examples of using these rheological polydispersity indices can be found in references [20, 31, 32, 84].

In order to justify using ModSep as an indication of the molecular weight distribution, the following equation can be used. Since  $j_e^0$  is directly related to the molecular weight distribution of the polymer, ModSep can be used to compare different samples MWDs.

$$ModSep = (G_{ref} * j_e^0)^{0.5}$$

The equation above can easily be derived from the following well known relations at the terminal region and Equation 3-14 of this thesis.

$$G' = \eta_0^2 j_0^e \omega^2 \quad \omega \rightarrow 0 \quad \omega' = \left(\frac{G'}{\eta_0^2 j_0^e}\right)^{0.5}$$

$$G'' = \eta_0 \omega \quad \omega \rightarrow 0 \quad \omega'' = \frac{G''}{\eta_0}$$

Correlation between PI and the MWD of PP has mostly been proven empirically rather than theoretically. However, since it has been found that PI correlates very well with the molecular weight distribution, it has been used extensively in the literature as well as industry [32].

## **APPENDIX B: PROCEDURES FOR CHOOSING SIGNIFICANT TERMS IN EMPIRICAL MODELS**

The measured response values in Table 4-3 were analyzed using Design Expert software and the following steps were followed for each response:

- 1) Model fitting: Empirical models were fitted with linear, two factor interaction and quadratic model terms.
- 2) Analysis of variance (ANOVA) was subsequently employed to identify the model significant parameters. The number of terms in the model was reduced by using backward elimination methods. For each photoinitiator, a different empirical model was obtained.
- 3) Model diagnostics: Model diagnostic tests were carried out to check if the model is well behaved. If the responses were not well behaved, the Box-Cox transformation was applied

to modify the fitted model. This transformation was used with response variables  $\lambda$ , PI and ER.

4) Response surface graphs: The conditions that minimize or maximize a certain response were found in order to determine the process window for an optimized response.

These empirical models for all responses considered are summarized in Table B for each photoinitiator.

Table B: Best empirical models for each response variable

Ini. <sup>1</sup> type	Model	R <sup>2</sup>	Adj. <sup>2</sup> R <sup>2</sup>
BPH	$n=0.488+5.1E-4*C+5.0*AC-4.9E-4*AD+8.8E-7*BC-8.1E-8*B^2$	0.88	0.84
DEBPH	$n=0.613-9.0E-4*C+5.0E-4*AC-4.9E-4*AD+9.9E-7*BC-8.0E-8*B^2$		
BPH	$\eta_0=4370+9587*A+17*B+15*D-85*AC+115*AD+0.01*BC-0.14*CD-0.02*B^2$	0.84	0.73
DEBPH	$\eta_0=2063+172*A+17*B-32*D-85*AC+115*AD+0.01*BC-0.14*CD-0.02*B^2$		
BPH	$1/\sqrt{\lambda}=0.856-1.121*A+2.91E-3*AC-3.349E-3*AD-1.199E-7*B^2$	0.82	0.76
DEBPH	$1/\sqrt{\lambda}=2.102-0.537*A+2.91E-3*AC-3.350E-3*AD-1.20E-7*B^2$		
BPH	$PI-3=0.022-0.044*A-1.439E-5*AB-1.156E-4*AD+0.063*A^2+4.194E-7*D^2$	0.64	0.5
DEBPH	$PI-3=0.0167-0.024*A-1.439E-5*AB-1.156E-4*AD+0.063*A^2+4.194E-7*D^2$		
BPH	$ModSep=3.749-0.617*A-6.362E-4*B-1.294E-3*AB-1.742E-3*AD-9.151E-6*C^2$	0.85	0.75
DEBPH	$ModSep=3.64529+0.71248*A+2.06406E-4*B-1.29358E-3*AB-1.742E-3*AD-9.151E-6*C^2$		
BPH	$ER^{-1.82}=0.686-4.594E-4*B-4.194E-3*AD+2.036E-3*CD+0.327*A^2$	0.75	0.69
DEBPH	$ER^{-1.82}=0.686-4.593E-4*B-4.194E-3*AD+2.036E-3*CD+0.327*A^2$		

1:Ini.=initiator

2:Adj.= Adjusted

3:Eq.=Equation

In Table B variables A, B, C and D are concentration of the photoinitiator, duration of radiation, lamp intensity, and air pressure used for cooling, respectively.

Equations in Table B were used to generate contour plots in Chapter 4 in order to locate the optimal conditions for LCB rather than degradation.

## **APPENDIX C: CRITERIA TO CHOOSE FACTORS IN EMPIRICAL MODELS**

The data points presented in Table 7-2 were analyzed with Design Expert (statistical software). Empirical models were fit to each response. The significant variables were chosen based on the Shapiro-Wilk test. The significance of the final model and the significance of the lack of fit of the final model were considered, so the model with minimum lack of fit was chosen. The Shapiro-Wilk test examines the unselected main factors and interactions to determine if they follow normality. It is worth noting that the lack of fit was insignificant for all models shown in Table 7-3. Table C includes these models (models in Table 7-3) along with the corresponding  $R^2$  and adjusted  $R^2$  values for each model.

Table C: Empirical models for viscoelastic properties and gel content based on coded variables

Empirical model	$R^2$	Adj. $R^2$
$1/\sqrt{\eta_0}=8.15E-3-2.41E-3*A-2.89E-3*B-2.55E-3*C +1.97E-3*ABC$	0.72	0.57
$\text{Log}_{10}(\lambda) =1.79+0.87*A+1.49*B+0.90*C-0.83*ABC$	0.86	0.78
$n=0.49-0.027*A-0.018* B+0.019*ABC$	0.74	0.64
$(\text{ModSep})^{1.45} =3.96-0.84* A-1.51* B-0.83* C+0.87*ABC$	0.92	0.87
$1/\sqrt{ER}=1.6-0.29*A-0.41* B-0.26* C+0.24* ABC$	0.92	0.88
$PI=7.8+2.55*B+2.07*C-1.38*AB-1.79* ABC$	0.95	0.92
$\text{Log}_{10}(\text{Gel}+0.0017)=-1.07+0.83*A+1.03*B+1.04*C-0.86*ABC$	0.85	0.77

## **APPENDIX D: CONFIRMING FORMATION OF LONG CHAIN BRANCHES IN A SAMPLE WITH HIGH GEL CONTENT**

The aim of this appendix is to confirm independently the formation of long chain branches by separating their effect from that of the crosslinked gel in a sample. It is known from the literature (and shown in previous chapters of this thesis) that changes in the rheological behavior of the modified runs with high gel content are due to formation of both long chain branches and crosslinks. For this reason, run 8 (of Chapter 7, see Table 7-1) was chosen for extra confirmation experiments, in order to check whether we could separate the effect of LCBs from that of the crosslinked gel. Run 8 exhibits greater  $\eta_0$ ,  $\lambda$  and smaller shear thinning index ( $n$ ) compared to the parent PP. However, since it has 12 % of gel, one might argue that the changes in the rheological properties are only due to crosslinking rather than the presence of LCBs. In order to investigate further the observed rheological behaviour of the samples and runs of Figure 7-4, the gel fraction of this run was excluded via solvent extraction. The same procedure described in Section 6.2.4.1 for the extraction of gel from runs for GPC measurements was applied to run 8 and the parent PP. After excluding the gel content of run 8, the sol fraction was used to make discs for further rheological measurements (parallel plate rheometer). The same experimental procedure was applied to the parent PP and then its rheological properties were measured via the parallel plate rheometer as well for the sake of comparison. Figure D shows  $\eta^*$  versus  $\omega$  for run 8 and the parent PP, before and after the gel exclusion procedure. Figure D clarifies that run 8 exhibits the rheological properties of a long chain branched polymer even after removing its gel content (larger  $\eta_0$  and  $\lambda$ , and smaller shear thinning index). This confirms that the rheological behavior of the whole sample is not due to the presence of crosslinked gel only, since the sol fraction does exhibit similar rheological behavior, as seen in Figure D below (due to the presence of long chain branches). In parallel, this separates clearly the effect of LCBs from the effect of the crosslinked gel and reinforces further the observed evidence from the GPC measurements (Section 7.2.5).

A decrease in  $\eta_0$  of run 8 and of the parent PP after the gel exclusion procedure is due to degradation (samples were immersed in boiling xylene for 4 hours followed by drying in the oven).

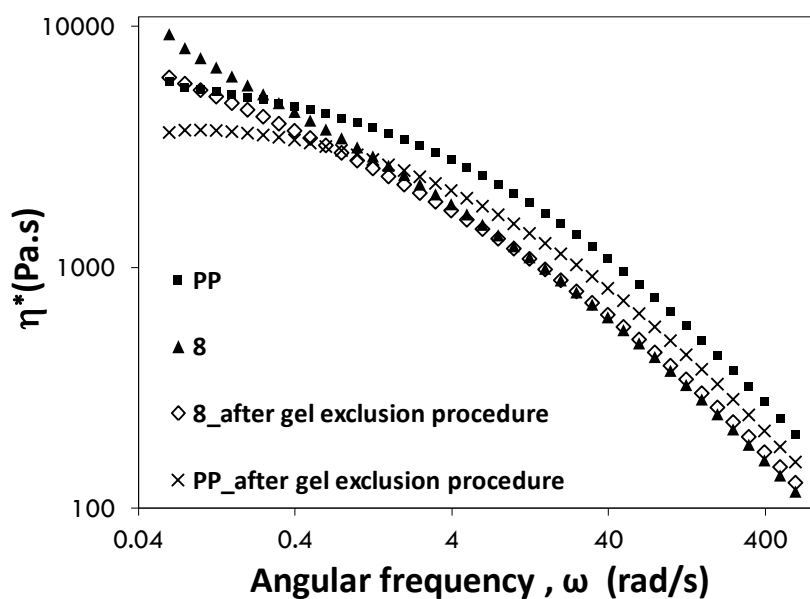


Figure D: Comparison between  $\eta^*$ - $\omega$  plots of run 8 and parent PP, before and after gel exclusion